PERFOMANCE TESTS OF A THREE-ELEMENT THIN FILM DETECTOR WITH AN ANALYSIS OF LARGE SCATTERING ANGLE CHARGE STATE CHARACTERISTICS OF GERMANIUM AND SELENIUM IONS

By

ZORAN MILOSEVICH

A DISSERTATION PRESENTED TO THE GRADUATE SCHOOL
OF THE UNIVERSITY OF FLORIDA IN PARTIAL FULFILLMENT
OF THE REQUIREMENTS FOR THE DEGREE OF
DOCTOR OF PHILOSOPHY

UNIVERSITY OF FLORIDA

1991

ACKNOWLEDGMENTS

The author gratefully acknowledges the help and support he has received from a number of people that he has had the pleasure of knowing. Many thanks go to Dr. M. L. Muga for his patience, help and advice that he has given in his role as chairman of the supervisory committee and research advisor. Also many thanks go out to the other personnel in the nuclear chemistry group at the University of Florida, D. J. Burnsed and S. D. Thompson.

The much appreciated help of Dr. R. L. Coldwell that he has given in setting up computer accounts, writing codes for data analysis and his help and advise is very gratefully acknowledged.

Many thanks also go out to the people who were associated with the Space Astronomy Laboratory for their help and support in the experimental work and data analysis. This group includes Dr. F. E. Dunnam, Dr. P. S. Haskins, Dr. R. B. Piercey, Dr. M. A. Herath-Banda, Dr. A. C. Rester and A. D. Weisenberger. Also thanks go to Dr. G. J. Bamford for his help in advice concerning ROBFIT.

Thanks go to Dr. R. J. Hanrahan for his advise and for the use of his computers and ^{60}Co source. Also thanks go out to Dr. A. K. Gupta for his advice and support throughout the years. Thanks also go out to the other committee members for their advice and support, Dr. W. B. Person and Dr. Z. R. Pop Stojanovic.

Many thanks go out to the staff at the Holifield Heavy Ion Research Facility for their help in carrying out the experiments described in this text. This group includes R. L. Robinson, W. Milner,

R. Miles and R. Auble. Also many thanks go to Oak Ridge Associated Universities for their support. Also providing support throughout the years have been the UF Department of Sponsored Research and the Department of Chemistry. Also thanks go to IBM for computing funds through the Research Computing Initiative.

Most of all the author wishes to express his appreciation for the patience and help he has received from his mother and sister and late father while he was in graduate school.

TABLE OF CONTENTS

ACKNOWLEDGMENTS ii

ABSTRACT vi

CHAPTERS

1 REVIEW OF CHARGED PARTICLE DETECTORS 1

Introduction 1
Theory 11
Thin Film Detectors 15

2 DETECTOR RESPONSE TO SELECTED ACCELERATED HEAVY IONS 23

Introduction 23
Experimental Apparatus 26
Results and Discussion 30

3 THIN FILM DETECTOR RESPONSE TO ^{252}Cf FISSION FRAGMENTS 113

Introduction 113
Experimental 119
Results and Discussion 123

4 CHARGE STATE CHARACTERISTICS OF Ge AND Se IONS INVOLVED IN SMALL IMPACT PARAMETER COLLISIONS WITH A GOLD TARGET 137

Introduction 137
Theory 142
Experimental 144
Results and Discussion 145

5 SUMMARY 157

APPENDIX A GUIDE TO THE USER OF A TFD 163

APPENDIX B PERTINENT CODES 169

REFERENCES 187

BIOGRAPHICAL SKETCH 195

Abstract of Dissertation Presented to the Graduate School
of the University of Florida in Partial Fulfillment of the
Requirements for the Degree of Doctor of Philosophy

PERFORMANCE TESTS OF A THREE-ELEMENT THIN FILM DETECTOR WITH AN ANALYSIS OF LARGE SCATTERING ANGLE CHARGE STATE CHARACTERISTICS OF GERMANIUM AND SELENIUM IONS

By

Zoran Milosevich

May 1991

Chairman: M. Luis Muga
Major Department: Chemistry

Two experiments have been carried out with the purpose of testing the three-element thin film detector with a surface barrier detector (3TFD-SBD) for use as a nuclear charged particle identifier. The detector consists of a stack of three sequential thin film detectors (TFD's) for measuring the specific luminescence ($\Delta L/\Delta x$) of a transiting ion, and a terminal surface barrier detector for measuring the ion residual energy (E_r) after energy losses in traversing the TFD's. The purpose of the two experiments was to develop a better understanding of the advantages of having a three element design and to try to quantitatively relate the performance of a TFD in comparison to other particle detectors.

The first experiment tested the detector assembly response to accelerated Ge and Se ions, in the 53 to 169 MeV range, that were

scattered 30^{o} off a gold foil target. Various detector characteristics are presented including the $\Delta L/\Delta x$ response of a single detector as a function of the ion velocity and the time resolution of the detector assembly. It is also possible to improve the detector response by taking advantage of the three successive $\Delta L/\Delta x$ measurements of a transiting ion.

The second experiment measured the TFD response to ^{252}Cf fission fragments in coincidence with the prompt gamma rays. The nuclear charge resolving power $(Z/\Delta Z)$ was determined for a single TFD and the result compared to other nuclear charged particle detectors.

In the data analysis of the first experiment, information concerning certain characteristics of the charge states of the scattered ions was revealed. The results were compared to calculated values obtained from two different models that have been used to predict the average charge state of ions after electronic stripping from small impact parameter collisions with neutral targets. The results from this experiment might add some information to the scarce data dealing with charge state distributions of heavy mass ions involved in small impact parameter collisions.

CHAPTER 1
REVIEW OF CHARGED PARTICLE DETECTORS

Introduction

Charged particle detectors can be divided into five major groups: (1) track detectors, (2) gas ionization detectors, (3) solid state detectors, (4) secondary electron emission detectors and (5) scintillation detectors. All these detectors work on the principle of coulomb interaction between the electrons in the detector material and the highly charged nuclear particle. Here, charged particles will be restricted to positively charged heavy nuclei and therefore will not include betas, mesons or any other high energy particles.

The first group of detectors, nuclear track detectors, have been used since the very first studies of radioactivity. In 1896, Henri Becquerel reported the blackening of photographic plates when in the presence of a double sulfate of uranium and potassium [1]. Since this phenomenon did not depend on whether the uranium salt was or was not in the presence of light, Becquerel realized that the radiations were being emitted by the salt itself. Thus was born the first method of detecting nuclear radiation.

Nuclear emulsions consist of grains of silver bromide suspended in a gelatin matrix, with the grains being typically about 0.25 µm in diameter. As a charged particle passes through the emulsion, certain grains are struck by it. These grains are "sensitized" and are able to catalyze the reduction of silver ions to metallic silver. When the silver bromide grains are immersed in a suitable developing solution, all the silver ions are eventually converted to metallic silver. But the sensitized grains which were struck by a passing charged particle develop faster. Thus a visual track is left which occupies the site of the path of the charged particle.

The early photographic emulsions used were of large grain size which made it difficult to recognize the individual tracks of the particles. It was not until the 1930s that the use of fine grain, low density nuclear emulsions allowed for the observation of clear tracks. These tracks are usually examined under a microscope where by the length of the track one is able to determine the particle range or energy and by the density of the track one can distinguish between different particles having different values of dE/dx.

The mid-1950s saw the development of large high precision mass spectrometers. This inspired a further development of nuclear emulsions since they were used at the focal plane of the early spectrometers. By measuring the position that the ions would strike the emulsions at the focal plane, a very accurate determination of particle energy was made.

An advantage to using nuclear emulsions is that one has a permanent record of the tracks made by the ions. Other advantages are that track detectors are relatively inexpensive to use and one can choose an emulsion to suit one's experimental needs. Certain emulsions allow one to develop the tracks of more ionizing particles leaving tracks of weakly ionizing particles undeveloped, thus allowing an experimentalist to select according to his/her needs. A big disadvantage is that it is a long and tedious task to scan the tracks at high magnification and analyze them. This is especially true for emulsions used at the focal plane of a mass spectrometer, since it is not unusual to have focal planes that are several meters in length.

Along with these solid nuclear track detectors, there are also gas and liquid versions in the form of cloud chambers and bubble chambers. Cloud chambers were first used by Wilson in 1911 to detect tracks made by alpha particles in an expansion type cloud chamber [2]. An expansion cloud chamber is a chamber filled with gas, which can be almost any gas. As a charged particle passes through the chamber, the volume is adiabatically expanded. The vapors become supersaturated and condense on the ions formed by the passing charged particle. These droplets are visible under illumination and are usually recorded photographically. The bubble chamber operates similarly to the cloud chamber. Both the cloud chamber and bubble chamber are used more frequently in high energy physics applications.

While Becquerel was using photographic plates to look at radiation emitted by radioactive substances, Marie Curie noted that the air between two metal plates became electrically conducting when in the presence of radioactive substances [3]. This was an early version of a gas ionization chamber, which is the second, and most common, group of charged particle detectors. All gas ion chambers operate by using an electric field to collect all the charges created by direct ionization of gas molecules caused by a passing charged particle. As the charged particle collides with the neutral gas molecules, the gas is either excited to a higher energy state or it is ionized, where the cation and electron drift toward their respective electrodes. The measurement of the ionization current is an accurate measure of the rate of ion pair formation.

With a weak applied electric field, it is possible for the ions to recombine with the electrons, so a low current is measured. As the applied voltage is increased, the current increases which means that the amount of original charge that is lost is reduced. With further increase in voltage, ion recombination is suppressed to a negligible level, and a region of ion saturation is reached where all the original charges are collected at the electrodes. In this saturation region, if the applied voltage is increased, no current increase is seen.

The electrons that drift toward the anode will collide with other neutral gas molecules. But due to the relatively low applied electric field, the electrons have low mobility and thus little kinetic energy between collisions. With a further increase in voltage, the electrons' average energy between collisions increases until eventually the kinetic energy is greater than the ionization potential of the neutral gas molecules. At this threshold value, secondary ionization occurs, i.e. with each collision between the charged particle and one neutral gas molecule, more than one ion pair is created. Each additional electron that is created can further ionize other neutral gas molecules and a cascade, known as a Townsend avalanche, is created. This cascade terminates when all the electrons are collected at the anode. This process is the principle under which proportional counters operate. Under the right conditions, the number of secondary ionizations is proportional to the number of primary ion pairs formed. Proportional counters were developed in the 1930s, slightly after the first use of the Geiger-Muller tube.

In 1908, Rutherford and Geiger used a glass tube filled with gas at low pressures to detect single alpha particles emitted from a source [4]. By 1928, the Geiger-Muller (GM) tube was developed. This tube consisted of a gas-filled tube with a long thin wire in the middle. The GM tube operates in a similar manner as the proportional counter in that it employs gas multiplication from the original ion pair. In the proportional counter, each electron creates an avalanche which is independent of any other avalanche associated with the original ionizing event. As the electric field is increased, the intensity of the avalanches are enhanced where each avalanche creates a second avalanche. As the electric field is increased further, an exponential number of avalanches are created and a region known as the Geiger discharge is reached where all pulses from the GM tube are the same regardless of the number of original ionizing pairs. Thus the GM tube can operate only as a counter and no energy information about the detected ion can be obtained. However, the pulses are relatively large so the associated electronics are simple, but the GM tube also suffers from a long dead time.

In 1959, McKenzie and Bromley showed that it was possible to measure the energy of alpha particles, with excellent resolution, using a solid state detector [5]. They used a germanium crystal that had a layer of gold evaporated onto one of the surfaces. The disadvantage of this detector was that it had to be cooled to liquid nitrogen temperature. This inspired the development of the silicon-gold surface barrier detector (SBD) [6]. One was able to operate this detector at room temperature and achieve better resolution than the early germanium-gold detectors. By 1961, the first fission fragment spectrum of ^{252}Cf by a solid state detector was reported [7]. Also the first dE/dx measurement by a solid state detector was made using a 50µm thick Si-Au detector [8].

It was realized early in the development of solid state detectors that they had the advantage of having excellent energy resolution as well as a linear response in energy. The stopping power of the solid state detectors was greater than that of the gas detectors, thus the effective thickness needed for charged particle energy measurements was less. The other advantage was that only 3 eV of energy was needed to create an electron-hole pair as compared to 30 eV needed to create an electron-charged particle pair in a gas. Thus the statistical fluctuation in the number of charge carriers per pulse was a smaller fraction of the total with the solid state detectors as compared with a gas ionization detector and therefore better energy resolution was obtained. Another advantage that was realized was that there was no spatial dependence of the charge pulse on the ionization track as there was in a gas. But despite these advantages there was also seen some disadvantages of solid state detectors such as pulse-height defect, plasma time jitter, degradation of performance and high cost of fabricating large area detectors, and thus further interest in gas detectors arose.

In 1968, Charpak invented the multiwire proportional chamber (MWPC) [9]. Basically this was a gas filled chamber which had a plane of independent wires placed between two plane electrodes. The wires were thin and placed 2 mm. apart, which gave the detector a position sensitivity of about 2 mm. This design minimized the spatial dependence seen in earlier gas detectors. Another development included a parallel plate avalanche counter (PPAC) [10,11], which was basically a gas proportional detector with large parallel plates spaced closely together acting as electrodes. The close spacing allowed for the fast collection of electrons at the anode with timing resolutions as good as 120 ps [10].

There have been many other designs of the PPAC and MWPC for various low energy applications. One example is the Mammoth Twin Ion Chamber [12] which consists of two halves, an upper and lower half, separated by a massive cathode plate in the middle. The outer structure contains the anode plates, each of which is separated in half lengthwise. There are also five segments, the first four being used for measuring the energy loss of a particle, ΔE, and the fifth, the largest of the five, to measure the residual energy of the particle.

Another method used in gas detectors, which was developed by Breskin and others [13,14,15,16], is that of low pressure MWPC in identifying charged particles. The low pressure creates a higher value of E/P, the electric field per unit pressure, which also increases time resolution. Time resolutions of 135 ps for 120 MeV ^{58}Ni ions have been reported [16]. Another fairly recent technique in use is Bragg Curve Spectroscopy. This involves collecting at the anode plate all the electrons that a charged particle creates in a gas volume, thus measuring all the energy lost by the charged particle. From the measured energy lost in a given path length, one is able to determine the nuclear charge from an energy-loss versus atomic number curve.

The fourth group of detectors are the secondary electron emission detectors. It had been known for a long time that electrons are emitted from a material struck by an energetic charged particle. The number of electrons emitted is dependent upon the Z of the ion and upon the type of material being struck. Since the electrons are emitted near the surface of the material, it would be possible to have a thin sample of material to act as a transmission detector without reducing the yield of electrons emitted. Thus Stein and Leachman were able to use a thin metal foil to detect fission fragments from the neutron induced fission of ^{235}U [17]. The emitted electrons were electrostatically focused on a scintillator coupled to a photomultiplier tube. The use of other types of foils followed and these included VYNS [18] and the more commonly used carbon foil [19]. Carbon foils are preferred today because of the smooth surface they possess and because they are convenient.

Different methods have been used to collect the electrons emitted from a thin foil. One method makes use of the first dynode of a PM tube to collect the electrons [20] while another makes use of a SBD [21]. The method giving the best results uses electrostatic mirrors to deflect the electrons to a microchannel plate detector [22]. Today these detectors are used mainly for their fast timing characteristics.

In 1903, Crookes reported the use of a ZnS scintillator in detecting radiation from uranium [23]. This was quite a laborious task for that time period which was made much easier by the development of the photomultiplier (PM) tube. In general, inorganic scintillators having high Z material are used for the detection of photons while organic scintillators are used for detecting particle radiations.

An ideal scintillator will have the following characteristics : (1) the kinetic energy of the charged particle will be converted into light with high efficiency, (2) the conversion is linear over a wide energy range and the light output is proportional to the total energy deposited by the particle, (3) the detector material should be transparent to its own light, i.e. have negligible self absorption, (4) the decay time should be fast, (5) the scintillator should be of good optical quality which can be manufactured in large dimensions, (6) the index of refraction should be close to that of glass to insure efficient optical coupling to the PM tube. Naturally, it is hard to find a scintillator that has all of these properties, so an experimentalist needs to compromise on some properties to have characteristics needed for a specific purpose.

Organic scintillators, in general, have most of these properties, except that the light yield is lower than that of the inorganic scintillators, but unlike inorganic scintillators, the organic scintillators tend to have much faster decay times, on the order of nanoseconds.

The chemical composition of organic scintillators typically consists of molecules containing phenyl groups, giving the π-electron structure needed for the fluorescence process used in detecting charged particles. The kinetic energy of the charged particle is absorbed by the π-electrons, which are then excited into a higher energy state. If the excited state is a singlet state above the first excited singlet state, S_1, the electrons de-excite to S_1 through radiationless internal conversion. From S_1, they eventually de-excite to the ground state giving off light. The time involved in the de-excitation to S_1 is on the order of picoseconds while the de-excitation from S_1 takes place on the order of nanoseconds. The difference in energy between S_1 and the ground state is around 3 to 4 eV.

Useful organic scintillators are also transparent to their own light, or in other words there is very little overlap between the absorption and emission spectra. A typical organic scintillator consists of a small concentration of a very efficient primary scintillator which is dissolved in a solvent, either liquid or solid. The charged particle kinetic energy is absorbed by the solvent and the emitted energy is transferred to the primary scintillator. Sometimes there is further transfer to another scintillator, the waveshifter, which matches the wavelength of the emitted light to the optimal response of a PM tube. With all the transfer of energy, the light tends to be at lower energy than the absorption energy of the scintillator.

This was a brief review of the various types of particle detectors and emphasis here will be placed on scintillator detectors. Reference to the other types of detectors will be made for comparison.

Theory

The experimental techniques used for identifying charged particles are all based upon the theoretical treatment of the energy loss a charged particle experiences when passing through matter. Bethe first developed the theoretical treatment using the Born approximation and assuming a high particle velocity, small charge and an ion fully stripped of its electrons [24]. The specific energy loss, dE/dx was derived as

$$-\frac{dE}{dx}=\frac{4\pi e^4 z^2 \rho \; N_o \; Z}{mv^2 A} \ln\left(\frac{2mv^2}{I}\right) \qquad (1)$$

where m is the electron rest mass, e is the charge, N_o is Avogadro's number, z is the full charge of the particle with velocity v, A is the atomic weight of the detector material having atomic number Z and density ρ and I is the average excitation potential of these atoms. This can be rewritten as

$$-\frac{dE}{dx} = B \frac{Mz^2}{E} \ln\left(\frac{CE}{M}\right) \qquad (2)$$

where B and C are constants given as

$$B = 2\pi\rho e^4 N_o Z/mA \qquad (3)$$

$$C = 4m/I. \qquad (4)$$

Upon integrating equation 2 with respect to dE and dx over a detector thickness T, and by rearranging terms, the particle identification formula becomes

$$TMz^2 = K[\Delta E(E_t + k_o + k_1 \Delta E)] \qquad (5)$$

where K is a proportionality constant, k_o is a constant, $k_1 = -0.5$ and E_t is the total incident energy. Thus in the simplest particle identification scheme, a thin transmission detector is used to measure the the energy lost by a particle, ΔE, and a second detector is used to stop the particle and record the total residual energy E_r. The total energy, E_t, is therefore the sum of ΔE and E_r.

One experimental method used is to measure ΔE and E_r and by using equation 5 obtain the product Mz^2. Then by using a table to look up values of the product Mz^2 for various ions, one is then able to identify the particle. This scheme is however limited to ions with $z<10$ since the values of Mz^2 begin to overlap at that point. To overcome this problem for heavier ions, the time of flight of the ion is measured by taking the timing signal from the ΔE detector as the start signal and the timing signal from the E_r detector as the stop signal. With the time of flight t, and total energy E_t, one is able to determine the mass M of the particle since M is proportional to $E_t t^2$ and from knowing the mass, one is then able determine z from the ΔE measurement.

While the nuclear charge resolution ΔZ is determined by direct measurement, the mass resolution is dependent upon three measured parameters. With two detectors separated by a distance ℓ, the time of flight $t = t_2 - t_1$ for an ion travelling with velocity $v = \ell/t$ and with energy E_t, the mass can be determined since $M = 2E_t t^2/\ell^2$. The mass resolution is then given by

$$\frac{\Delta M}{M} = \left[\left(\frac{\Delta E}{E}\right)^2 + \left(\frac{2\Delta t}{t}\right)^2 + \left(\frac{2\Delta l}{l}\right)^2\right]^{\frac{1}{2}} \tag{6}$$

where ΔE_t is the uncertainty in the measured total energy, Δt is the time resolution and Δl is the difference between the axial and oblique ion trajectories between the two detectors.

Another method of particle identification uses the range energy relationship

$$R = aE^b + c \qquad (7)$$

where E is the energy, R the range and a, b, c are constants and b is energy dependent for ions less than about 10 MeV/amu. Using this equation, Goulding [25] developed the relationship

$$TMz^2 = K(E_t)^b - (E_r)^b \qquad (8)$$

where K is a proportionality constant and this method has been shown to be effective in identifying ions with $z<11$.

All of these methods have been shown to be effective in identifying ions of low Z value moving at high nonrelativistic velocity using any of the detectors discussed previously, especially using solid state detectors. Silicon detectors can be fabricated with a small thickness so that they could be used as a ΔE detector and a thick surface barrier detector is usually used as a E_r detector. But as mentioned previously, the assumption used to derive equation 1 was that the ion transiting the detector had a low Z value and high velocity.

In a theoretical calculation for the non-relativistic energy loss of a charged particle which was first derived by Bloch [26], the energy loss was determined to be

$$-\frac{dE}{dx} = \frac{4\pi e^4 z^2 \rho N_\circ Z}{mv^2 A}\left\{\ln\left(\frac{2mv^2}{I}\right) + \psi(1) - R\psi\left(1 + i\frac{ze^2}{\hbar v}\right)\right\} \qquad (9)$$

where Ψ is the logarithmic derivative of the gamma function with real part $R\Psi$. When $z<Z$, this equation is reduced to equation 1, which means equation 1 is valid for light ions having z value less than the Z value of the detector material. For any higher particle z value, equation 1 breaks down and equation 9 is the one that needs to be considered.

For scintillation detectors to be used as ΔE detectors, it was necessary to know the relationship between the specific luminescence and the specific energy loss. This relationship was given by Birks [27] as

$$\frac{dL}{dx} = \frac{dL}{dE}\,\frac{dE}{dx} = \frac{S\ dE/dx}{1 + kB\ dE/dx} \qquad (10)$$

where S is the scintillation efficiency, kB the scintillation quenching factor which accounts for the nonradiative de-excitation of the portion of excited scintillating centers along the path of an ionizing particle. When plotting experimentally measured light output of organic scintillators as a function of incident ion energy, it was found that the light output increased fairly linearly with increasing energy and decreased with the Z of the particle [28]. However, when the light output is plotted as a function of ion velocity, the output increases with the Z of the ion [29]. Most of the work performed using scintillators to identify charged particles has involved thin film detectors (TFD). This particular detector will be now considered in detail.

Thin Film Detectors

From the very earliest studies of heavy ions, the detector of choice had been the nuclear track detectors due to their accuracy in determining the characteristics or the ions being studied. Then the various types of gas detectors were being favored, mainly due to their ease of use as compared to the nuclear emulsions, which required a long time to analyze the tracks. With the development of the solid state detectors, experimentalists had what seemed to be an ideal particle detector.

The solid state detectors used for heavy ion study have been shown to have superior energy resolution and better timing than the early gas detectors. With better methods of fabrication, thin solid state detectors were possible for use as ΔE detectors. But with all these advantages the two big disadvantages were that the solid state detectors deteriorated after a period of time from the damage from particle radiations adding to the high cost of using these detectors. Thus new developments in gas detectors took place as was previously discussed.

While the energy resolution was not quite that of the solid state detectors, these detectors have been shown to be useful in heavy ion studies, and they did not experience the degradation that the solid state detectors experienced. While there was no expense associated with replacing a deteriorated gas detector, there was the high cost in building the complex detectors, as the one described earlier. There is also the cost and sometimes troublesome gas handling equipment associated with the gas ionization chambers.

Therefore these detectors are limited to a few laboratories around the world.

About the same time that these gas ionization chambers were being developed, a new low cost detector was invented [30], the thin film detector (TFD). A TFD is any plastic scintillator with thickness as low as 20 $\mu g/cm^2$ or as high as several hundred $\mu g/cm^2$. They are usually made from NE-102A plastic scintillator because of its relatively high light yield and excellent timing characteristics. The light output of NE-102A is 65% of anthracene [31], which is among the best of the plastic scintillators, and it has a decay time of 2.3 ns, which is second only to NE-111 in the Nuclear Enterprises products. The light output is usually detected by one or two PM tubes, usually RCA 8850 or a similar tube due to its ability in detecting low intensity light [32].

There are two different methods in fabricating thin films. One method [33] involves dissolving the NE-102A in a solvent such as ethyl acetate. A few drops of this solution are placed on the surface of a glass plate which is partially submerged in water which is contained in a ceramic coated photographic developing pan. The glass plate is inclined to allow for the solution to run onto the water surface, where the solvent dissolves leaving a floating thin film. This film is then removed and mounted on a frame. The frame is usually a square acetate frame but in the past the TFD had been mounted on the flat surface of a hemicylindrical lucite frame. This film is then placed perpendicular to the face of one or two opposing PM tubes.

The second method of fabricating the TFD [34] again involves making a solution by dissolving the NE-102A in a solvent but the solvent is usually something with a higher vapor pressure such as benzene. A portion of this solution is then placed on the face of a PM tube and the solvent allowed to evaporate leaving a thin film on the face. This method has an advantage over the other method in that there is optimal optical coupling to the PM tube, but the disadvantage is that the TFD cannot be used as a transmission detector.

The TFD was invented in 1970 by M. L. Muga and it was first used as a time pickoff in a time-of-flight (TOF) detector system. It was soon realized [35] that by measuring the specific luminescence $\Delta L/\Delta x$ of the TFD, it could also serve as a ΔE detector, measuring the energy loss of heavy charged particles. The detector response to ^{252}Cf fission fragments, which experienced only a 10% energy loss through the detector, showed a clear separation between the light and heavy fragment groups. With only a 10% reduction in energy, it was demonstrated that the TFD could be effectively used as a transmission detector without significantly impeding the flight of the ion. The TFD also showed the different energy losses experienced by ^3He and ^4He as well as ^{127}I, showing that it is ideally suited for detecting light ions as well as heavy ions [36].

Thus further investigations into TFD response led to qualitative experiments looking at the specific luminescence of the TFD to various ions [29] including ^{84}Kr, ^{40}Ar, ^{16}O, ^{35}Cl, ^{37}Cl, ^{79}Br, ^{81}Br. In these experiments, there was an observed difference between the measured and the calculated values of energy loss and it was also observed that the response of the TFD was dependent on the atomic number of the ion as well as its velocity. But most of these experiments concentrated on the response of the TFD to high energy ions, generally greater than 2 MeV/amu, and it was determined that the TFD could distinguish between heavy ions differing by two charge units in the energy range above 4 MeV/amu. In another experiment [37] looking at the response of the TFD to degraded alpha particles from ^{228}Th, a plot of the specific luminescence vs. dE/dx showed a double valued curve, and thus no clear relationship of $\Delta L/\Delta x$ to dE/dx, at least for light ions over a wide energy range.

With the establishment of the TFD as a useful detector of heavy ions, several investigations of various aspects of fission were performed using the TFD [38,39,40,41]. Since the fission fragments in general have energies in the range of 1 MeV/amu, the TFD has shown to be a useful low energy heavy ion detector. But the characteristics of the TFD with respect to its response to low energy heavy ions has not been closely examined until recently.

Batra and Shotter measured the energy loss of the primary light and heavy fragments from the spontaneous fission of ^{252}Cf passing through various thicknesses of NE-102A scintillator [40]. They observed that that the measured stopping power of the fragments were larger than the theoretical values obtained from Lindhard's theory. A difference was also noted by Muga, as previously mentioned, and Batra and Shotter point out that such observations have been previously reported for ions passing through various other light materials such as carbon.

It had been determined early in the study of the TFD that one could improve the charge resolution with thicker foils. Muga [42] noted an improved resolution by a factor of about 2 with 400 μg/cm^2 foils compared to 100 μg/cm^2 foils for ^{40}Ar ions in the energy range of 3 MeV/amu. Manduchi et al. [43] looked at the luminescence and timing properties of the TFD with varied thicknesses. They observed that the timing properties of the TFD to ^{252}Cf fission fragments did not vary significantly with varying thicknesses. They also concluded that the luminescence did not carry definite physical information with respect to the use of the TFD as a ΔE detector. But it has been determined by other workers [44, 45] that the luminescence response of the TFD did vary with atomic number and velocity of the charged particle, so it does carry important physical information.

Brooks et al. [44] also investigated the TFD response to ^{252}Cf fission fragments with various thicknesses of foils. They report a sharp increase in the pulse height between thicknesses of 4μm and 5μm with no pulse height increase in foils thicker than 8μm. The steep increase was attributed to surface effects in the NE-102A. Franklyn [45], however, observed no sharp increase in pulse height with varying thicknesses of scintillators in a similar study looking at the TFD response to thermal neutron induced fission of ^{235}U, again illustrating the effectiveness of the TFD as a ΔE detector.

In an attempt to understand the scintillation process of the TFD, several theoretical models have been developed. The first model was by Muga and Griffith [46] which was later refined by Muga and Diksic [47]. This model was based upon the assumption that a heavy ion passing through a thin scintillator produces luminescence through scattered electrons and that the interaction of the heavy ion with the π-electrons is negligible. The ion, as it passes through the scintillator, creates a cylindrical region of radiation damage about its path. About this cylinder is an annular disk whose volume is created by the scattered electrons. The number of electrons per unit area that penetrate the disk at radius r is denoted by ρ^A with ρ_c^A being a critical value of this number density above which all luminescence centers are excited. This is termed a saturation of luminescence centers. At distances where $\rho^A < \rho_c^A$, the fraction of luminescence centers that are excited are proportional to ρ^A. For a particular ion having a particular velocity, there exists a saturation radius r_{sat} for which $\rho^A = \rho_c^A$. In a cylindrical volume bound by r_{sat}, the luminescence production is proportional to $\rho_c^A \pi r_{sat}$. Beyond r_{sat}, the luminescence production is proportional to $\rho^A(r)$ and is given as

$$I(r_{sat}) = \int_{r_{sat}}^{r_{max}} \rho(r)\ 2\pi r\ dr \tag{11}$$

Thus the specific luminescence can be written as

$$\frac{\Delta L}{\Delta x} = C\ \left[\pi r_{sat}\, \rho_c^A + I(r_{sat})\right] \tag{12}$$

where C is a constant proportional to the thickness of the detector.

A more empirical model of specific luminescence was developed by Ajitinand [48] where the specific luminescence is given as

$$\frac{dL}{dx} = aN\left[\left(\frac{E}{M}\right)^3 + \left(\frac{E}{M} - r\right)^3\right] \tag{13}$$

where $r=bN^c$, and N is the total number of scattered electrons given as

$$N = Z^2_{eff}/(E/M^2) \qquad (14)$$

and where E is the ion energy, M the mass and Z_{eff} is the effective ion charge given as

$$Z_{eff}=Z(1-e^{-x}) \qquad (15)$$

where Z is the ion atomic number and x is given as

$$x=d(E/M)^{0.5/Zg} \qquad (16)$$

where a, b, c, d, g are all empirical constants.

More recently, Kanno and Nakagome [49] developed a theory which assumes three steps in the TFD scintillation process: (1) free electrons in the scintillator are recoiled by heavy ion impact; (2) the recoil electrons excite π-electrons; (3) photons are emitted when the electrons de-excite. In step 1, the energy of the recoiled electrons are calculated by a simple Rutherford scattering formula. It is also assumed that the electrons are scattered radially outward and in the forward direction (relative to the direction of heavy ion travel) from a point. In the second step, one of the assumptions made is that the primary recoil electrons transit toward the recoil direction statistically and they are less likely to excite at the beginning of their range due to their high energy. Thus there is an effective range R_e beyond which it is possible for the recoil electrons to excite the π-electrons. The region where the excitation occurs is denoted as $P_{eff}(R_o,x)$ and is a function of R_o, the primary electron range and x, the position of the heavy fragment in the film. The total number of emitted photons, or the luminescence, is then given as

$$L = \int_0^T \rho \sigma P_{eff} (R_o, x) \, dx \tag{17}$$

where r is the density of π-electrons in the TFD of thickness T and s is the recoiling cross section of an electron. This theoretical treatment has shown good agreement with experimental observations.

With all these studies of the TFD, there still was no clear indication of the limits of detection these detectors possess or in general how well scintillators will perform in their response to heavy ions at low energies. Knowledge of the TFD resolution would be useful in determining what types of detectors to choose for use as a particle identifier for a particular experiment.

CHAPTER 2
DETECTOR RESPONSE TO SELECTED ACCELERATED HEAVY IONS

Introduction

There is much current interest in nuclear physics in studying the properties of nuclei far from the line of stability. About 2000 species have been studied, of which about 270 are stable, and theory predicts that the total number of nuclides that can be produced with sufficiently long half lives for physical study is around 8000. There is also continued interest in the search for superheavy elements, where a region of stability is predicted near Z=116 and N=184. The nuclear reactions proposed to produce these exotic nuclei, fusion-evaporation, fusion-fission and deep inelastic reactions, will transfer many units of charge and mass between projectile and target as well as create strong energy dissipation and a large number and variety of residual fragments. Thus due to the short predicted half lives of these exotic nuclei as well as weak reaction channels needed to produce them, new experimental techniques as well as instruments are needed for greater selectivity in separating the desired nuclei from the other residual fragments.

New on-line isotope separators have been constructed at a number of facilities to help in the search for exotic nuclei [50]. The definition of an on-line isotope separator is a target, ion source and electromagnetic mass analyzer coupled in series. The on-line material that is analyzed is the target of a bombardment where the reaction products of interest that are formed during irradiation are slowed down and stopped in the system. Chemical and physical methods are then used continuously to separate the various species and transfer them to the ion source.

New recoil mass separators have been and are being constructed which will filter out undesired reaction products [51]. In many fusion-evaporation reactions, the product of interest is emitted in the direction of the beam and therefore must be separated from the beam, which may have up to 10^{12} higher intensity. These mass separators make use of electric and magnetic fields to separate reaction products. An ion with mass m, charge state q, kinetic energy E_k and moving with velocity v perpendicular to an electric field E, will travel on a curved path through the field and the radius of curvature will be proportional to E_k/q; if traveling through a magnetic field $\underline{B}$, the ion will have a radius of curvature proportional to mv/q. Since v and the ratio m/q common in these two expressions, all recoil mass separators will separate ions according to their values of either v or m/q, but most recoil separators will separate in m/q. The reaction products in a typical heavy ion experiment will be multiply charged with a gaussian distribution about a mean charge state $\bar{q}$ which may lie in a range $\bar{q}$=20-40, for example. The intensities of the principle charge state tend to be about 20% of the total distribution. Therefore with dispersion in m/q, knowledge of mass, charge state or nuclear charge Z is needed to identify the ion of interest to be able to gate with other detectors being used on a particular experiment.

Since most mass separators disperse in m/q, the expression $m/q = B\rho t/d$ is used for mass determination where $B\rho$ is the magnetic rigidity, t the time of flight over a distance d. A detector of the types described in chapter 1 is used at the focal plane to determine q. These detectors tend to be of complex multi-detector design and are typically made up of several different types of detectors. For example, it is very common to have a gas detector for use as a ΔE detector and for determining ion position. Position determination is important since a distribution of separated ions with various m/q values will be focused on the detector plane. There are also start and stop detectors used for time of flight determination with the start detector located in front of the ΔE detector and the stop detector after. The start detectors are usually either a thin scintillator foil or a carbon foil, the former being more durable and the latter having slightly better timing characteristics.

An example of a focal plane detector system is the SHIP at the GSI in Darmstadt, Germany [52]. The start detector is a carbon foil having a time resolution of 200 ps. The ΔE detector is a gas ionization detector which has a position sensitivity of 1.2 mm. The stop detector is a TFD of 150 $\mu g/cm^2$ thickness with a time resolution of 400 ps. While not all focal plane detectors are this complex, most do use the advantages of the various types of detectors to achieve optimal performance for a specific purpose or experiment.

With the design of a three element thin film detector-surface barrier detector (3TFD-SBD) assembly, it was desirable to test it as an on-line detector for future use as a detector for in-beam experiments. Of interest was testing the response of the detector assembly to typical heavy ions that might be encountered at a very low energy range by looking at the light output as well as the timing response of the TFD scintillators.

Experimental Apparatus

The 3TFD-SBD assembly consists of 3TFD's, one SBD and the associated detector chamber and PM tubes, as shown in figure 1. The assembly consists of four separate aluminum chambers, one for the SBD and three identical chambers, one for each TFD. Several connecting chambers have been designed for connecting the assembly to various scatter chambers or chambers housing fission sources.

Each TFD was made from NE-102A plastic scintillator and was fabricated as described by the recipe of Muga, et al. [33] but with the modification used by Thompson [53]. A solution was made which consisted of 12.0 g of NE-102A dissolved in 50.0 ml ethyl acetate and 4.0 ml amyl acetate. This solution was allowed to sit for about two weeks to ensure complete dissolution of the NE-102A. This solution was then irradiated for 4 hours in a 600 Curie ^{60}Co source at a distance of about 2 cm. This allowed for the cross-linking of the polymer chains which produced a thicer and more durable film.

After irradiation, a few drops of this soution were poured onto a glass plate, which leaned on the side of a porcelain coated photographic developing pan half filled with distilled water. The

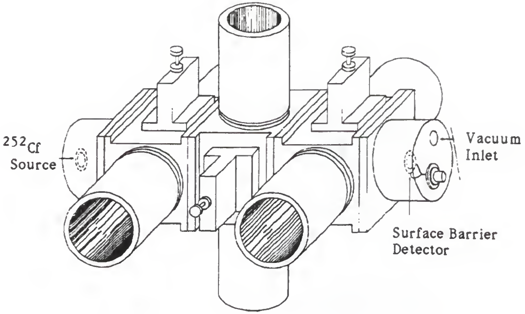

Figure 1. This diagram shows the Three Element Thin Film Detector-Surface Barrier Detector Assembly chamber as set up with a ^{252}Cf source chamber.

glass plate sat on its edge at an angle and was partly submerged in the water. As the solution slowly ran down the glass plate and touched the water surface, the solvent dissolved in the water and the NE-102A film was left floating on the surface. The film was lifted from the water by using a metal ring of about 5" in diameter with an attached handle. An area of film which was visibly free from imperfections was selected and the ring placed gently on top containing the chosen film region. The remainder of the film was wrapped around the ring and the film was then lifted off the surface. It was mounted on a square acetate frame which had an outside edge of length 29 mm and an inner edge length of 22 mm. The frame was then clamped by two brass plates attached to a plunger which allowed the film to be removed from the path of transiting ions inside the detector chamber.

The chamber that houses the TFD, shown in figure 2, has six faces of almost equal dimensions including one pair of faces that have an extended 1/4" thick edge to connect to the adjacent chamber with the use of nuts and bolts. This face is 3" x 3" and is perpendicular to the path of incoming ions. The opening in the center of this face is 3/4" in diameter Two other faces are each 2 3/4" x 2 1/2" and has a 1 1/2" diameter circular opening with a small ledge onto which sits a 3/16" thick quartz window. Around the edge of each quartz window is a rubber O-ring which is used to seal the chamber. The face of each PM tube rests on the quartz window and an aluminum sleeve attaches onto the chamber and houses the PM tube. One of the two 2 3/4" x 3" faces, the top as seen in figure

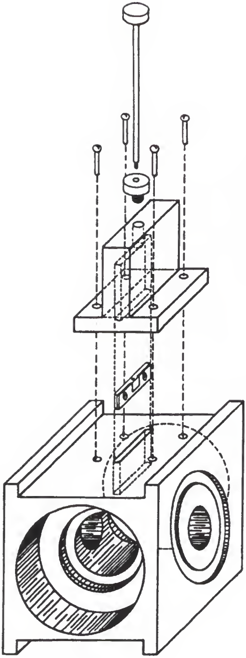

Figure 2. Diagram of a chamber housing a single Thin Film Detector (TFD). The side of the chamber facing the page would have the face of a photomultiplier tube against it. On top of the chamber is a smaller chamber for housing a retracted TFD. The ion path would be left to right or vice versa.

2, has a small chamber which is used to house the TFD when retracted from the ion path.

The SBD is housed in a cylindrical chamber which includes a BNC-microdot vacuum feedthrough to connect to the SBD and a vacuum inlet for pumping down the entire detector assembly with a mechanical vacuum pump. The PM tubes used are RCA 8850 tubes chosen for their low dark current and ability to detect low intensity light. Details of the 3TFD-SBD have been provided elsewhere [54].

Results and Discussion

An experiment looking at the response of the 3 TFD-SBD assembly to varying nuclear charge and mass was performed at the HHIRF at the Oak Ridge National Laboratory. Various isotopes of germanium and selenium were accelerated at the Tandem Van deGraaff and scattered off a thin target. The ions that were deflected into the 3TFD-SBD assembly were detected and the response of the detector was recorded event-by-event on magnetic tape for subsequent analysis at the University of Florida.

A diagram of the experimental arrangement is shown in figure 3. A 1.6 m scatter chamber was mounted onto the beam line and had several different ports on which to mount various detectors. The 3TFD-SBD detector was mounted at a 150° angle from the entrance port of the beam. This angle was selected to ensure that an adequate distribution of ions would scatter into the detector as determined by Rutherford scattering considerations. A gold (Au) foil with approximate thickness of 1.0 mg/cm^2 was mounted onto a target

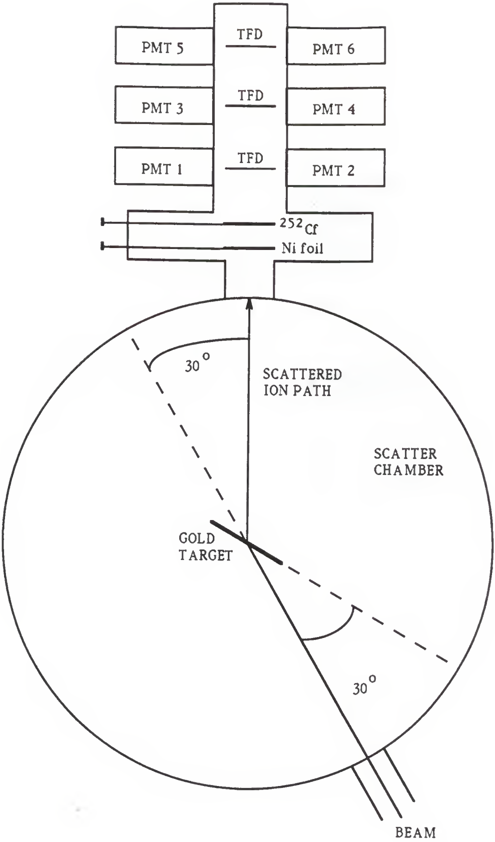

Figure 3. 3TFD-SBD assembly attached to scatter chamber.

frame and placed on a foil ladder which was located in the center of the chamber. The target ladder was able to slide vertically and rotate inside the chamber allowing for the removal of the Au target from the beam path and for the insertion of a quartz target (also located on the target ladder) in the path of the beam to allow for beam focusing. When the Au target was placed in the beam path, the frame was positioned so that the face of the target was 60° off the line of the beam (refer to figure 3).

A connecting chamber, attached to the 3TFD-SBD detector, was used to mount the detector assembly onto the scatter chamber. This chamber housed a ^{252}Cf source and a thin nickel foil. The nickel foil was positioned in the path of the scattered ions during experimental runs to shield the photomultiplier (PM) tubes from low energy photons from the scatter chamber. Between runs, the ^{252}Cf source was positioned so that the spontaneous fission fragments entered the 3TFD-SBD detector to calibrate and check for long term gain shifts in the electronics as well as any gain changes made in between experimental runs.

The set-up of the electronics is shown in figure 4. The analog signal from each PM tube was matched to the signal from the opposing PM tube and then fed into an ORTEC 572 amplifier (AMP) which then went into a LeCroy 3511 ADC. A gate was generated by requiring the timing signal from PM tube 5 to be in coincidence with a delayed signal from PM tube 1 (see figure 4 for labels of PM tubes). Each timing signal from these two PM tubes was amplified by an ORTEC 535 quad fast amp (FA) which then went into an ORTEC 584

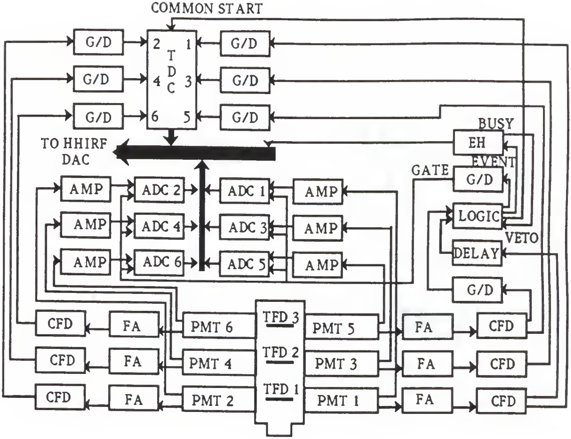

ADC = Analog to Digital Converter
AMP = Amlifier
CFD = Constant Fraction Discr.
DAC = Data Acquisition Computer
EH = Event Handler

FA = Fast Amplifier
G/D = Gate and Delay Generator
PMT = Photomultiplier Tube
TDC = Time to Digital Converter
TFD = Thin Film Detector

Figure 4. Electronic set-up of the experiment as described in the text.

constant fraction discriminator (CFD). The signal then went into an LRS 364 AL four fold coincidence unit (LOGIC) and the output signal went to an ORTEC 416A gate and delay generator (G/D) which then produced the gate. Thus each event that was recorded was due to an ion passing through all three TFD's producing a signal in the first and fifth PM tubes. The same output signal from the LRS 364 AL four fold coincidence unit also provided the common start signal that went into the LeCroy 2228A 8 channel TDC unit. The stop signals were provided by the delayed timing signals from each of the six PM tubes. A seventh LeCroy 3511 ADC was used for the energy signal from the SBD. Unfortunately, the SBD was damaged after the first few experimental runs so the data from the SBD was not analyzed. All digitized data were recorded on magnetic tape and controlled by the HHIRF data acquisition computer.

The ions that were scattered off the Au target were ^{70}Ge, ^{74}Ge, ^{76}Ge, ^{74}Se and ^{76}Se. These ions were delivered at energies ranging from 53.24 MeV to 168.7 MeV. The energies were chosen so that after scattering, the ions entered the detector at 0.65, 0.75, 1.00 and 2.00 MeV/amu (see table 1). Each of the Ge isotopes was analyzed at 2.00, 1.00 and 0.75 MeV/amu and each Se isotope was analyzed at 2.00, 1.50, 1.00, 0.75 and 0.65 MeV/amu. Each experimental run consisted of collecting approximately 10^6 events of a particular scattered ion at a particular energy. The order of the experimental runs is also shown in table 1. The second column shows the isotope that was analyzed and the third shows the energy of the beam before scattering. The fourth column shows the energy of the scattered ion calculated by using the Rutherford scattering

Table 1. The experimental runs are listed in the order that they were performed and with the ion species, the beam energy of the species delivered to the target, the calculated mean energy of the scattered ion and the ion charge state before scattering.

Run Number	Ion	Beam Energy (MeV)	Scattered Ion Energy (MeV)	Charge State
1	^{70}Ge	154.1	140.0	11
2	^{74}Ge	163.8	148.0	11
3	^{76}Ge	168.7	152.0	11
4	^{70}Ge	77.05	70.0	5
5	^{74}Ge	81.90	74.0	5
6	^{76}Ge	84.40	76.0	5
7	^{70}Ge	57.80	52.5	4
8	^{74}Ge	61.43	55.5	4
9	^{76}Ge	63.26	57.0	4
10	^{74}Se	163.8	148.0	11
11	^{76}Se	168.7	153.0	11
12	^{74}Se	81.90	74.0	5
13	^{76}Se	84.40	76.0	5
14	^{74}Se	61.43	55.5	4
15	^{76}Se	63.26	57.0	4
16	^{74}Se	122.86	111.0	7
17	^{76}Se	126.53	114.0	7
18	^{74}Se	53.24	48.1	4
19	^{76}Se	54.83	49.4	4

equation. The fifth column lists the charge state of the ion as it passes the bending magnets of the accelerator. All ion species will have the same charge state at a given initial energy. This is important to remember for the subsequent analysis. A final calibration was performed by adding a measured amount of delay to the timing signals to determine a time of flight calibration as well as to check the timing resolution of the LeCroy 2228A TDC.

For each experimental run, twelve parameters of data were collected: six specific luminescence measurements, one from each PM tube, one timing measurement and five time-of-flight (TOF) measurements between the three TFD's as measured by the six PM tubes. The twelve parameters of raw data are shown for a ^{252}Cf calibration run in figures 5-16. The PM tubes were labeled such that PM tubes one and two collected the light output of TFD one (the first one struck by the transiting ion), PM tubes three and four measured the light output of TFD two and PM tubes five and six measured from TFD three. PM tubes one and five were positioned on the same side of the TFD assembly while PM tubes three and four were at 90^{o} angles to them.

Figures 17-19 show the summed pulse height spectra of the PM tubes with the pulse heights from the pair of PM tubes opposing the common TFD being summed to each other. A noticeable improvement is seen in the peak to valley ratios of the ^{252}Cf fission fragment spectrum after summing with the light and heavy mass fragment groups clearly distinguished. The peak to valley ratio is seen to decrease in each subsequent TFD spectrum due to the fragments picking up electrons from the TFD as it passes through and

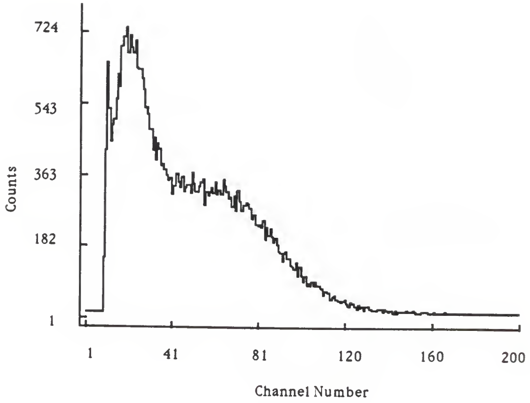

Figure 5. Response of the first TFD to ^{252}Cf fission fragments as measured by PM one.

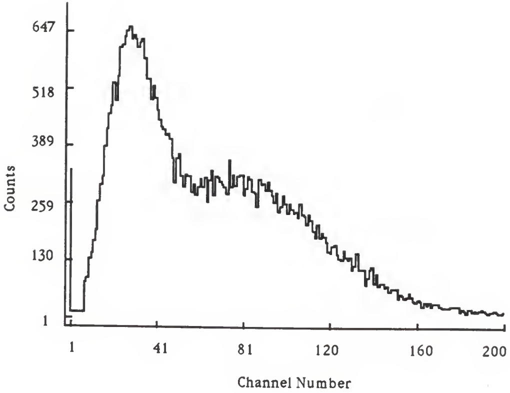

Figure 6. Response of the first TFD to ^{252}Cf fission fragments as measured by PM tube two.

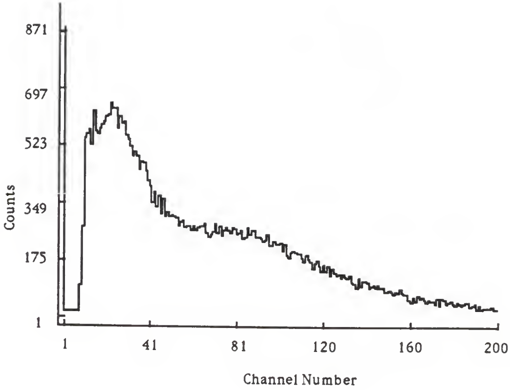

Figure 7. Response of the second TFD to ^{252}Cf fission fragments as measured by PM tube 3.

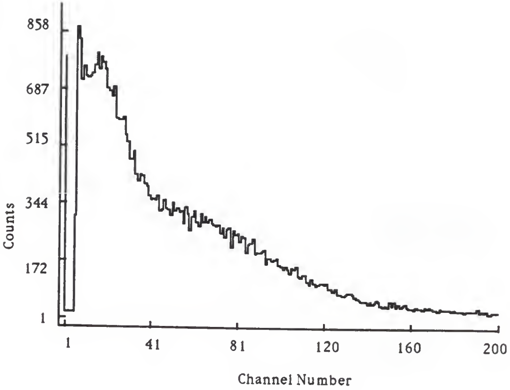

Figure 8. Response of the second TFD to ^{252}Cf fission fragments as measured by PM tube 4.

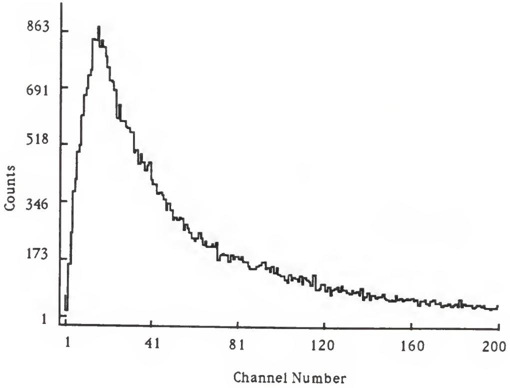

Figure 9. Response of the third TFD to ^{252}Cf fission fragments as measured by PM tube 5.

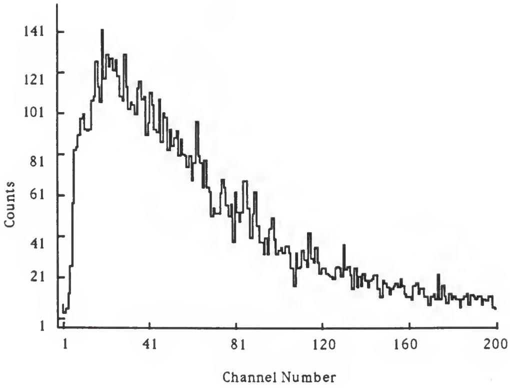

Figure 10. Response of the third TFD to ^{252}Cf fission fragments as measured by PM tube 6.

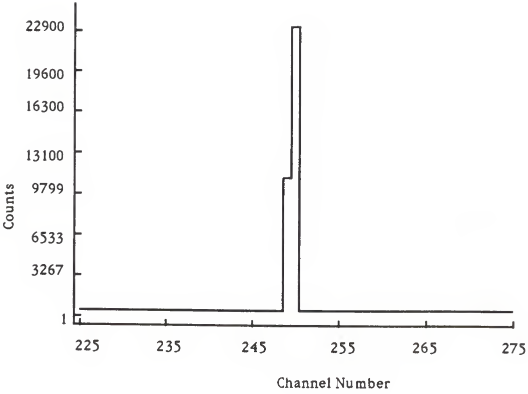

Figure 11. Timing response of PM tube 1 to ^{252}Cf fission fragments. In this spectrum and any other spectum showing time response, each channel corresponds to approximately 200 ps.

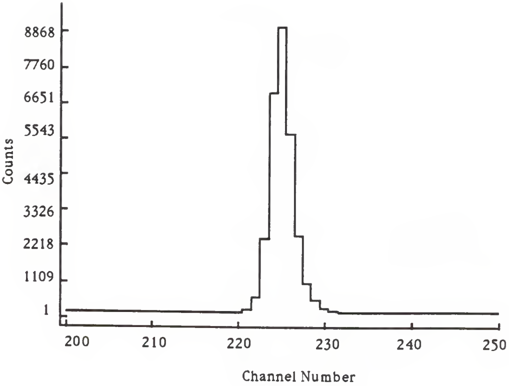

Figure 12. Time response between PM tubes 1 and 2 to ^{252}Cf fission fragments.

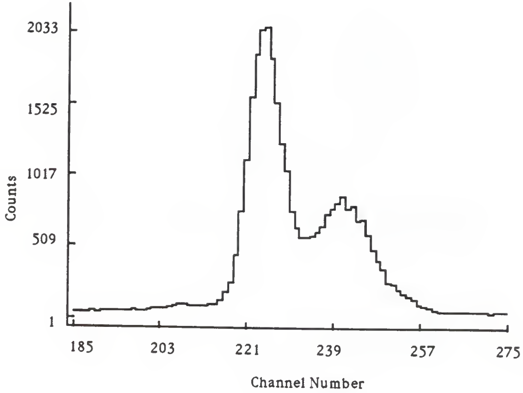

Figure 13. Time response between PM tubes 1 and 3 to ^{252}Cf fission fragments. The spectrum represents the TOF of the fragments between TFD 1 and TFD 2.

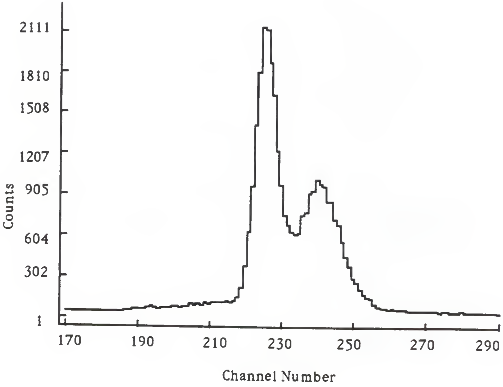

Figure 14. Time response between PM tubes 1 and 4 to ^{252}Cf fission fragments. The spectrum represents the TOF of the fragments between TFD 1 and TFD 2.

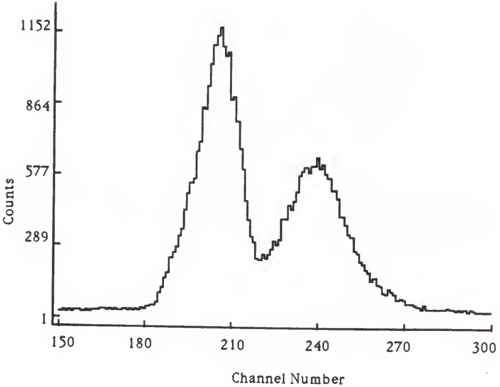

Figure 15. Time response between PM tubes 1 and 5 to ^{252}Cf fission fragments. The spectrum represents the TOF of the fragments between TFD 1 and TFD 3.

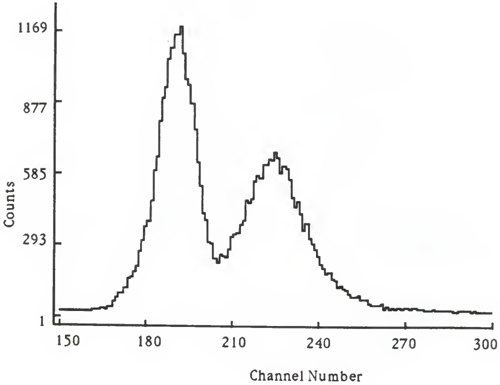

Figure 16. Time response between PM tubes 1 and 6 to ^{252}Cf fission fragments. The spectrum represents the TOF of the fragments between TFD 1 and TFD 3. This response differs from the one shown previously in that the PM tubes here are located on the opposite side of the detector assembly from each other.

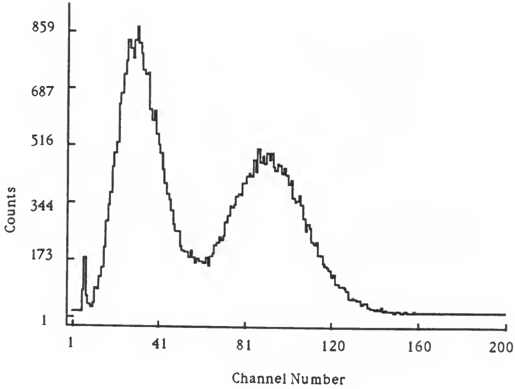

Figure 17. Summed luminescence response of TFD 1 to ^{252}Cf fission fragments. The pulse heights of the two opposing PM tubes (1 and 2) were summed giving the resulting spectrum.

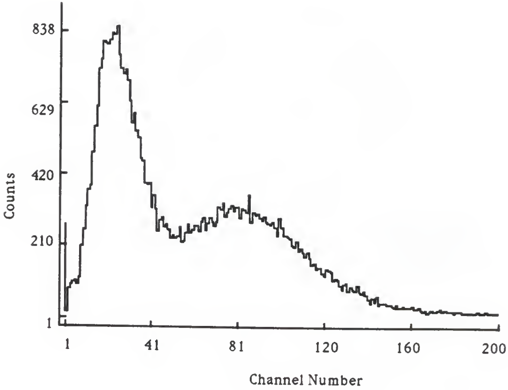

Figure 18. Summed luminescence response of the second TFD to ^{252}Cf fission fragments. The pulse heights of the two opposing PM tubes (3 and 4) were summed to give the above spectrum.

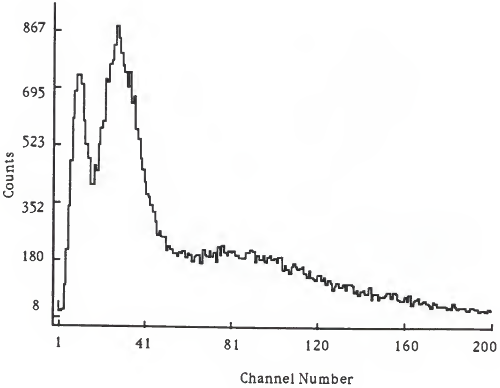

Figure 19. Summed luminescence response of the third TFD to ^{252}Cf fission fragments. The pulse heights of the two opposing PM tubes (5 and 6) were summed to give the above spectrum.

thus being slowed down. In the subsequent analysis, the TFD spectra were all summed in the same manner unless otherwise noted. The 8K spectra of the specific luminosity measurements were condensed to 512 channels and the 2K spectra of the TOF measurements were also condensed to 512 channels for easier computer storage. All data analysis was performed on the IBM 3090-600 operating VM/CMS and MVS located at the Northeast Regional Data Center at the University of Florida. All data were adjusted for any changes in gain made before each experimental run by matching the location of the light and heavy mass peaks in the ^{252}Cf fission fragment calibration summed spectra which were taken before and after the experimental runs of interest.

Figures 20-31 show the 12 parameter data taken from the first experimental run with ^{70}Ge at 154.1 MeV before scattering off the gold target. A wide distribution is seen in the TFD response which can be attributed to the wide distribution in charge states that the scattered ions possess. The first time spectrum (figure 26) is a very narrow peak due to the fact that it is basically measuring the time jitter in the electronics of the first PM tube and the subsequent modules. By the setup of the electronics, this spectrum represents the time response between the first PM tube and itself. The time distribution increases for the signal between PM tube one and two (figure 27) and the other spectra, which are actually measuring ion TOF, also show an increase in the time distribution. Figures 28 and 29 represent flight times that occur in half the distance compared to the ones recorded in figures 30 and 31, i.e. between TFD 1 and TFD 2 as compared to the distance between TFD 1 and TFD 3.

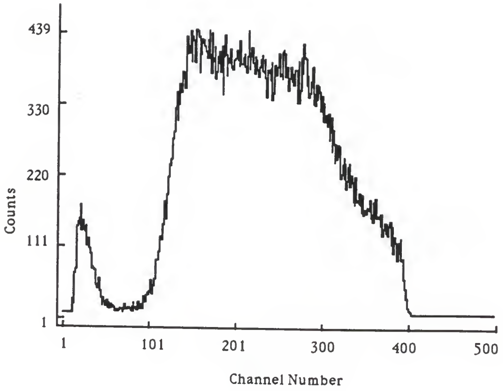

Figure 20. Response of the first TFD to ^{70}Ge ions at 2.0 MeV/amu as measured by PM tube 1.

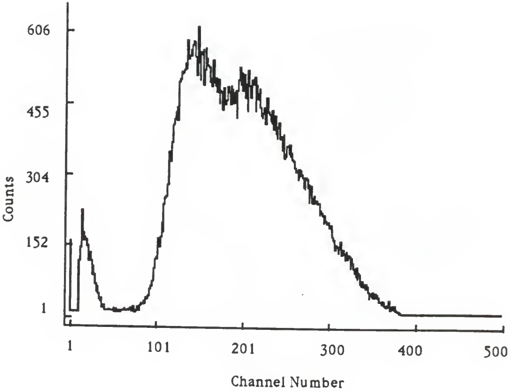

Figure 21. Response of the first TFD to ^{70}Ge ions at 2.0 MeV/amu as measured by PM tube 2.

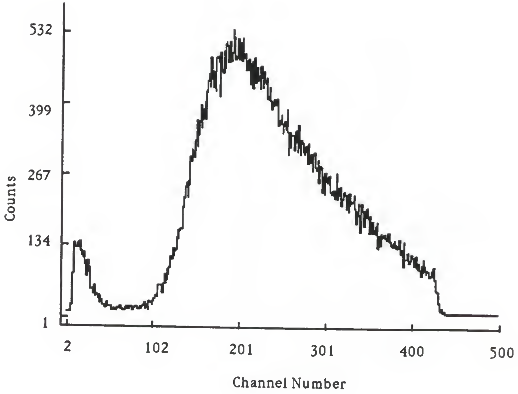

Figure 22. Response of the second TFD to ^{70}Ge ions at 2.0 MeV/amu as measured by PM tube 3.

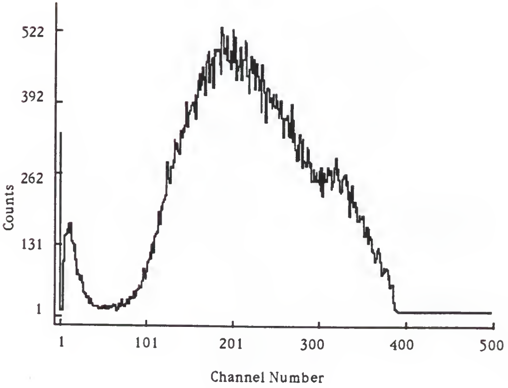

Figure 23. Response of the second TFD to ^{70}Ge ions at 2.0 MeV/amu as measured by PM tube 4.

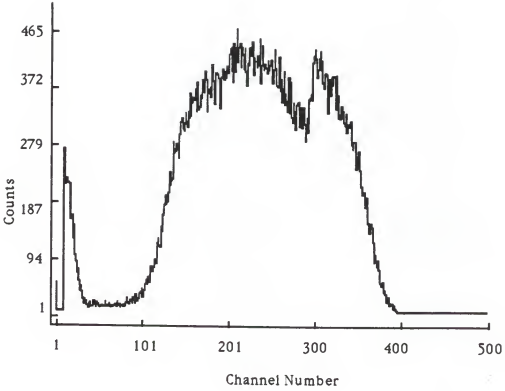

Figure 24. Response of the third TFD to ^{70}Ge ions at 2.0 MeV/amu as measured by PM tube 5.

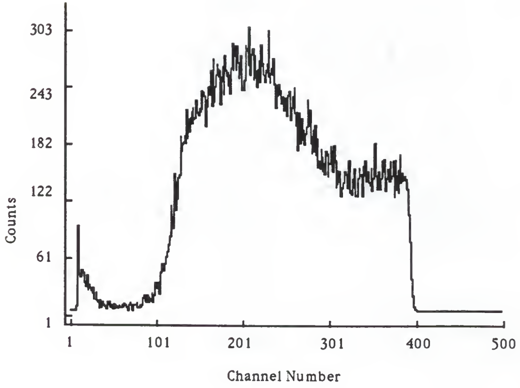

Figure 25. Response of the third TFD to ^{70}Ge ions at 2.0 MeV/amu as measured by PM tube 6.

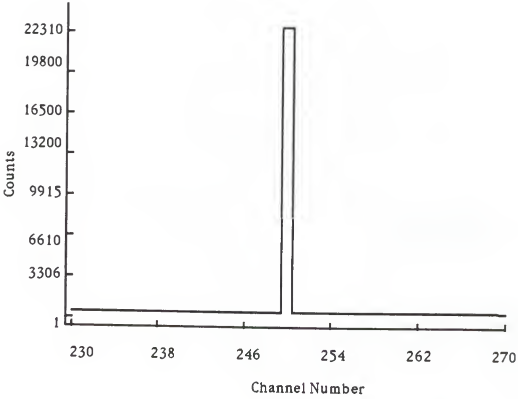

Figure 26. Time response with PM tube 1 providing both the start and stop signals.

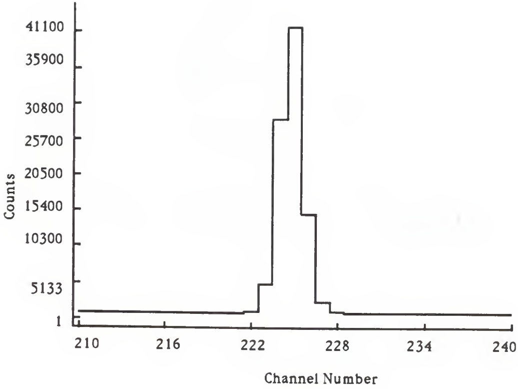

Figure 27. Time response between PM tubes 1 and 2. The start signal was provided by PM tube 1 and the stop signal came from PM tube 2.

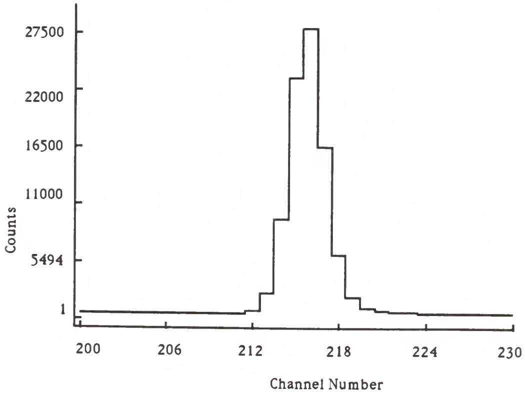

Figure 28. Time of flight of 2.0 MeV/amu ^{70}Ge ions travelling between TFD 1 and TFD 2 as measured with PM tubes 1 and 3.

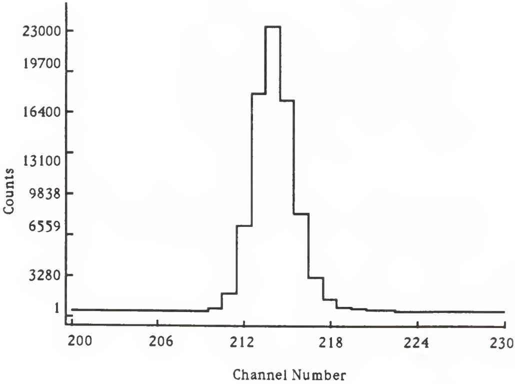

Figure 29. Time of flight of 2.0 MeV/amu ^{70}Ge ions travelling between TFD 1 and TFD 2 as measured by PM tubes 1 and 4.

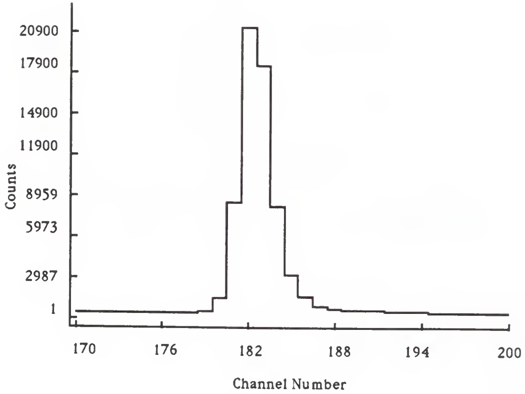

Figure 30. Time of flight of 2.0 MeV/amu ^{70}Ge ions travelling between TFD 1 and TFD 3 as measured by PM tubes 1 and 5.

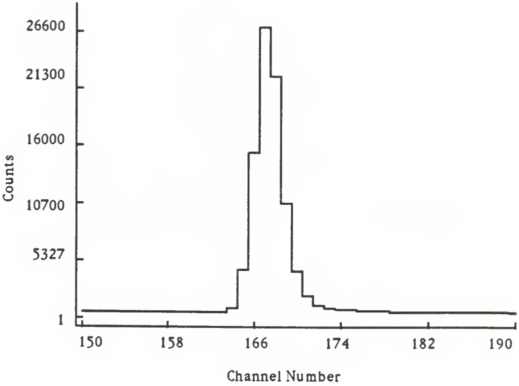

Figure 31. Time of flight of 2.0 MeV/amu ^{70}Ge ions travelling between TFD 1 and TFD 3 as measured by PM tubes 1 and 6.

Figures 32-34 show the summed TFD response summed in the same manner as described above. What is noticeable is a small peak in the lower portion of each spectrum to the right of the small noise peak located in the far lower channels. The size of the peak increases going from TFD one to three and most probably represents a second distribution of charge states that the ion possesses as it picks up electrons from passing through a TFD. This would explain why the peak increases in size going from TFD one to three. This second peak is seen with all the ion species but only at the high energy (2.0 MeV/amu for each ion) and not at any of the lower energies. One possible explanation for this is that the ions are in a much higher charge state before scattering (+11 at 2.0 MeV/amu) at the higher energy and thus are more likely to pick up electrons than the ions possessing less charge at the lower energies. Another explanation would be that the small peak was due to recoiling carbon atoms from the scintillator which were knocked out by the energetic heavy ions.

The pulse height response of the first TFD to ^{70}Ge was analyzed in the following manner. The TFD response to an ion whose TOF was recorded between channels 181 and 183 in the spectrum in figure 30, which was the TOF between PM tubes one and five, was selected, read off tape and plotted. Figure 35 shows the result after reading the first 10^5 data points recorded in the experimental run. The distribution is slightly narrower than the total distribution (figure 32) since the corresponding TOF has a narrower distribution. The peak position and the full width at half maximum (FWHM) were measured for comparison with similar plots of ^{70}Ge at the other

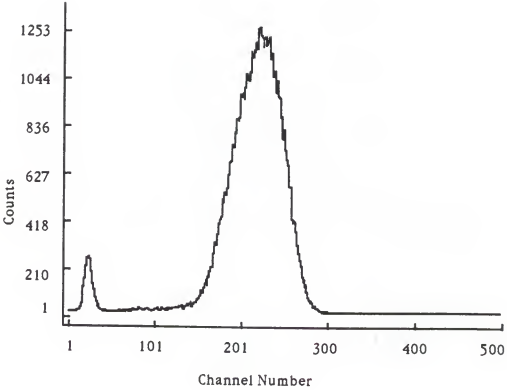

Figure 32. Summed response from PM tubes 1 and 2 measuring the specific luminescence of the first TFD responding to 2.0 MeV/amu ^{70}Ge ions.

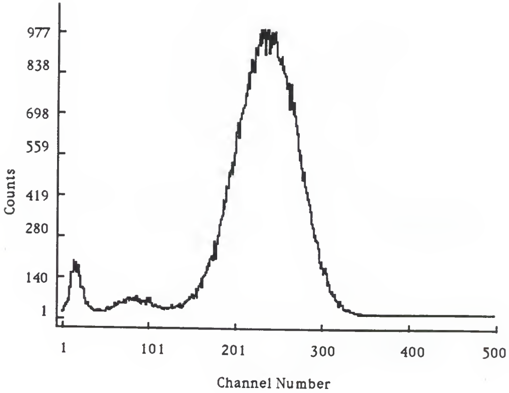

Figure 33. Summed response from PM tubes 3 and 4 measuring the specific luminescence of the second TFD responding to 2.0 MeV/amu ^{70}Ge ions.

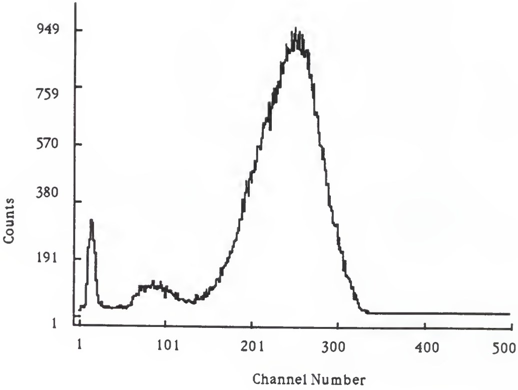

Figure 34. Summed response from PM tubes 5 and 6 measuring the specific luminescence of the third TFD as it responds to 2.0 MeV/amu ^{70}Ge ions.

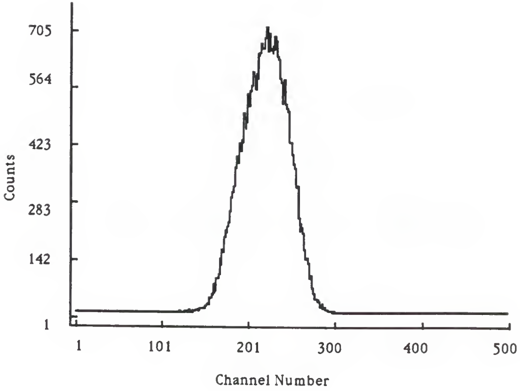

Figure 35. This spectrum shows the response of the first TFD (with summed signals from PM tubes 1 and 2) as was plotted in figure 32. The exception in this plot is that the events that were plotted here were events that were coincident with events occurring between channels 181 and 183 in the plot in figure 30 (time of flight spectrum between TFD 1 and TFD 3).

energies analyzed as well as with the other ions at all their energies. Thus this procedure of taking a time cut was repeated for all the other ions at all the other energies. Since the ions were all of similar mass and thus possessing almost equal time distributions at a given energy, it was possible to take time cuts at the same channel number for each ion. Because of the wider TOF distributions at the lower energies, more cuts in time were possible. A plot for ^{70}Ge was generated from all these time cuts and the result is shown in figure 36 where the TFD response is plotted against the various channel numbers of the time cuts. What is desired however is to see the TFD response to the varying ion velocity, so a simple calculation was performed to determine the incident ion velocity from the measured ion TOF as recorded between PM tubes one and five.

It was observed that the timing signals taken during the calibration runs throughout the experiment did not vary throughout the course of the experiment. This made the calculation of ion velocity an easy task. The timing calibration made at the very end of the experiment was used to determine the resolution of the TDC. The peak positions of the light and heavy mass group of the ^{252}Cf fission spectrum recorded in the TOF between PM tubes one and three was found to lie in channels 228 and 243 respectively. It is known that the most probable assignment to these peaks are ^{106}Mo and ^{142}Ba. A 63.0 cm delay cable was added to the line originating from PM tube three and going into the stop input of the TDC. Since there is 4.907×10^{-2} ns delay per cm of cable, this corresponds to 23.1 ns delay added. This delay resulted in a shift of 114 channels for both ^{252}Cf

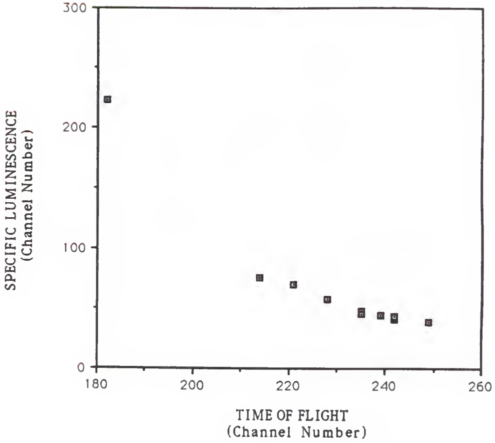

Figure 36. Response of the first TFD to ^{70}Ge ions plotted as a function of the time of flight as measured between TFD 1 and TFD 3. All the points on the graph represent all the runs done in this particular experiment.

peaks in the 512 channel TOF spectrum recorded by PM tubes one and three giving a TDC resolution of 0.203 ns/channel.

Since the velocities of ^{106}Mo and ^{142}Ba from the spontaneous fission of ^{252}Cf are known to be 1.165 and 0.7870 cm/ns respectively [55], the thickness of the first TFD was able to be calculated by a trial and error method with the assumption that the energy loss of the fragments could be calculated from the data in the stopping power tables of Northcliffe and Schilling [56]. The energy loss of the ions were calculated using the Bragg additivity rule and assuming that the molecular weight of the NE-102A scintillator could be approximated as being the same as the molecular weight of polyvinyl toluene, its solvent. Thus the equation for the energy loss of any ion passing through NE-102A could be given as

$$\left(\frac{dE}{dx}\right)_{CMPD} = \frac{1}{MW} \sum_i N_i A_i \left(\frac{dE}{dx}\right)_i \tag{18}$$

where CMPD stands for compound of molecular weight MW and the sum is over all the different elements i of atomic weight A and N is the number of atoms of element i in the compound. The axial distance d between the first two foils was measured to be 8.255 cm and the thickness of the first TFD was first assumed to be 0.400 mg/cm^2. This assumption will later be revised as will be seen in the following calculations.

The ^{106}Mo energy from the ^{252}Cf source before entering the first film is known to be 103.77 MeV. By interpolation of the Northcliffe and Schilling data, the energy loss was found to be 29.24 MeV leaving 74.53 MeV (1.194×10^{-11} J) of energy for the ion going between the first and second TFD. Taking the velocity $v=(2E/m)^{1/2}$, where E is the energy just calculated and the mass m is 1.76×10^{-25} kg for ^{106}Mo, the velocity was found to be 1.164 cm/ns and since the TOF t=d/v, the TOF was found to be 7.09 ns. The TOF of the ^{142}Ba was calculated in the same manner and found to be 10.496 ns, again assuming a 0.400 mg/cm^2 thick foil.

Now taking the calculated ^{106}Mo flight time of 7.09 and the ^{106}Mo peak position in the TFD luminescence response spectrum from figure 17, and assuming a linear fit between flight time t and channel number C as t=mC+b where m is the resolution calculated earlier as .203 ns/channel, b was determined to be -39.2 ns. Using this value a flight time was calculated for ^{142}Ba with respect to its spectral peak position and found to be 10.1 ns. This value differed from the previously calculated value of 10.5 ns which suggested that the original assumption of the TFD thickness was incorrect and that a new value for the thickness needed to be used. These calculations were then repeated until a match was found in the flight times. In this manner, the first TFD thickness was found to be 0.337 mg/cm^2.

A similar procedure was used to calculate the film thickness of the second TFD, but this time the spectrum of the TOF as measured by PM tubes one and five was used for the calculation. The TDC resolution was found to be 0.204 ns/channel. The foil thickness was eventually found again by trial and error to be 0.367 mg/cm^2 and the procedure to calculate this was as follows. After passing through the first TFD ^{106}Mo has energy of 79.13 MeV and ^{142}Ba has an energy of 50.87 MeV. By interpolation of the Northcliffe and Schilling data, the energy loss through the second film was found to be 13.25 MeV for ^{106}Mo leaving 65.88 MeV after passing through the foil and the energy loss of ^{142}Ba was 12.36 MeV leaving 38.51 MeV in energy. After calculating the velocity v_2 of the ions as they pass from film 2 to film 3 (which is different from the velocity v_1 from above between film 1 and 2 due to the energy loss of the ions passing through film 2), the TOF was calculated as $t = d(1/v_1 + 1/v_2)$ and found to be 14.4 ns and 21.3 ns for ^{106}Mo and ^{142}Ba respectively. Again assuming a linear relationship in the TDC response between the TOF and the TDC channel number, the TOF was found to be the same as calculated above for a 0.367 mg/cm^2 thick foil.

From the calculated values of the film thicknesses and from the calculated energy loss values obtained from the stopping power data for Ge and Se ions in the Northcliffe and Schilling tables, the ion velocity incident on the first TFD could be calculated. For this purpose, a series of FORTRAN codes were written each of which calls for two user inputs and generates the incoming ion velocity. The user would enter the channel number C of the time cut desired from a particular TOF spectrum recorded by PM tubes 1 and 5. From previous calibration, the TOF $t = 0.204C - 27.4$ could be calculated. The user would then input a tolerance value, or the minimum error value between the calculated t_{calc} and the "measured" time t. Then an initial guess t_2 of the TOF between TFD 2 and TFD 3 is made by $t_2=t/2$. This then gives a velocity $v_2=d/t_2$ and energy

$$E = \frac{1}{2} mv_2^2. \qquad (19)$$

The energy E_1 of the ion in flight between TFD 1 and TFD 2 is then calculated by interpolation of a function of E_1 vs. $(E_1-\Delta E_2)$ where

E_1-ΔE_2=E_2 and ΔE_2 is the energy loss of the particular ion through the 0.367 mg/cm^2 thick film located in the second position. The function was generated by fitting a seventh degree polynomial to the data points from the Northcliffe and Schilling tables for the particular energy range of interest. Each different ion had a different function and all the fits were done to better than 1% accuracy. Once E_1 was calculated, v_1 could be calculated and then t_1. Then the value for t_{calc} was determined by the equation $t_{calc} = t_1 + t_2$. The percentage difference between t_{calc} and t was the error which was compared to the user supplied tolerance value. If the error was greater than the tolerance value, a new guess to t_2 was generated and the calculation repeated. If the error was less than the tolerance value, the initial energy E_{in} was calculated in a similar manner as was E_1 but with the use of a function E vs. (E-ΔE_1), where ΔE_1 is the energy loss through the first TFD. From this the incident velocity was calculated.

Figures 37-41 show the TFD response to the various ions used in this experiment at various incident velocities. All these plots were generated as described above where the velocities were calculated from the cuts in the TOF spectra recorded by PM tubes one and five. The error bars that are shown in each plot represent the FWHM of the peak in the TFD response. The width of the distribution increases in each plot as the ion velocity increases which again could be explained by the larger distribution in charge states for the higher energy ions. The plot for ^{74}Se (figure 40) indicates the various charge states of the various ions before scattering. All the plots show an almost linear response of the TFD with respect to ion velocity at these low energies.

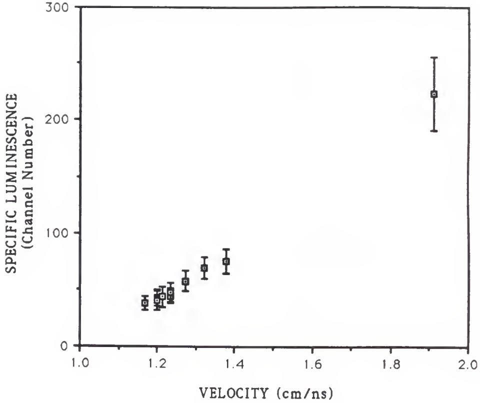

Figure 37. Response of the first TFD to ^{70}Ge ions as a function of the incoming velocity calculated from the measured time of flight. The error bars in this and the subsequent figures indicate full width at half maximum of the peaks generated from the time cuts. all time cuts were three channels wide (approximately 600 ps.).

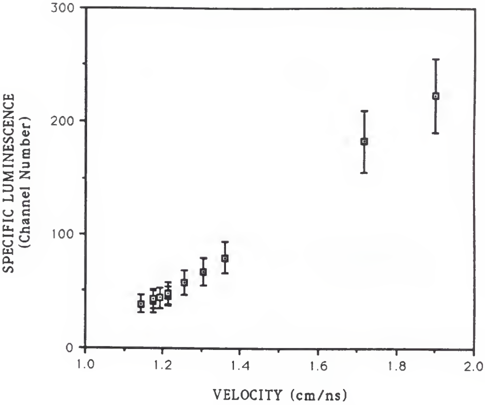

Figure 38. Response of the first TFD to ^{74}Ge ions plotted as a function of incoming velocity calculated from the measured time of flight.

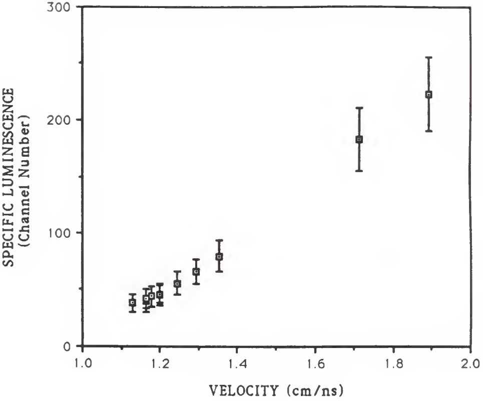

Figure 39. Response of the first TFD to ^{76}Ge ions plotted as a function of incoming velocity calculated from the measured time of flight.

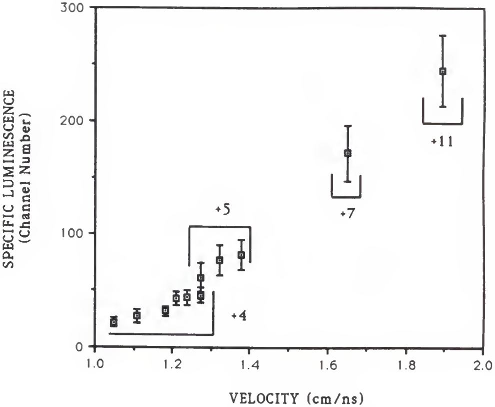

Figure 40. Response of the first TFD to ^{74}Se ions plotted as a function of incoming velocity calculated from the measured time of flight. The indicated charge states are ionic charge states before scattering, the differences arising because the plotted points represent different experimental runs. From left to right, the first three points are due to run 18 (refer to table 1), the next three from run 14, the next three from run 12, the next one from run 16 and the last one from run 10.

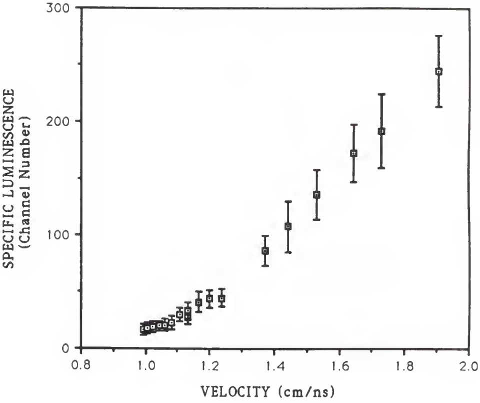

Figure 41. Response of the first TFD to ^{76}Se ions plotted as a function of incoming velocity calculated from the measured time of flight.

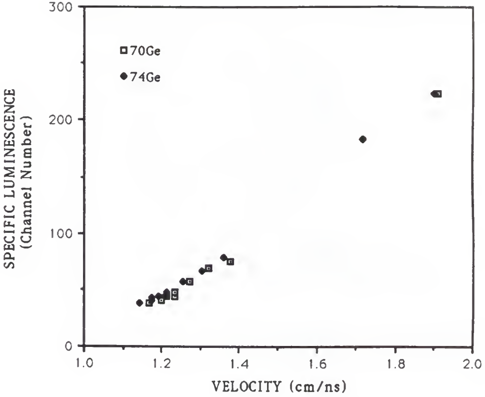

Figure 42. Comparison of the TFD response to ^{70}Ge and ^{74}Ge (same nuclear charge but different mass). As can be seen in this figure and the next three, there is no significant variation in the comparative responses.

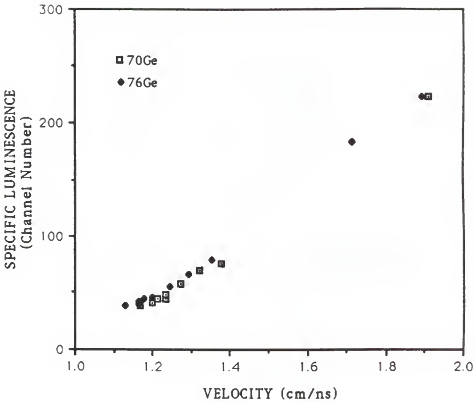

Figure 43. Comparison of the TFD response to ^{70}Ge and ^{76}Ge.

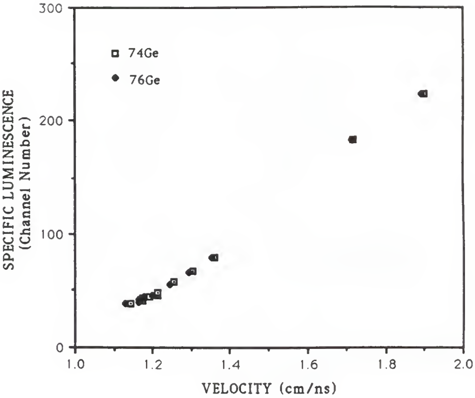

Figure 44. Comparison of the TFD response to ^{74}Ge and ^{76}Ge.

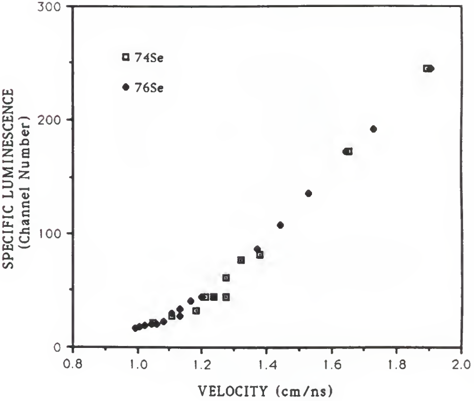

Figure 45. Comparison of the TFD response to ^{74}Se and ^{76}Se.

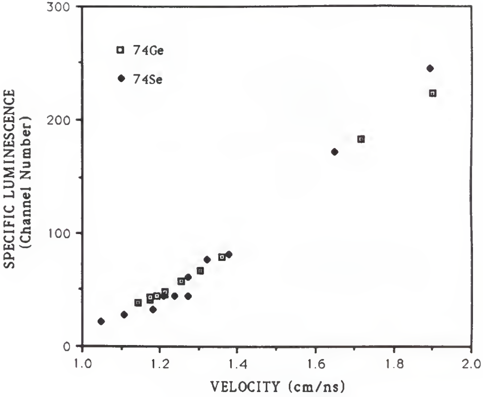

Figure 46. Comparison of the TFD response to ^{74}Ge and ^{74}Se ions (same mass but different nuclear charge). As is shown in this figure and the next, there is little variation in the comparative responses except at the higher energy.

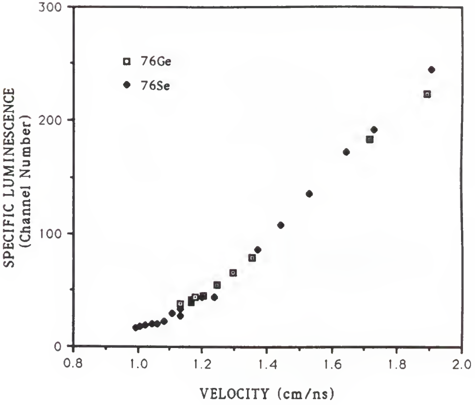

Figure 47. Comparison of the TFD response to ^{76}Ge and ^{76}Se.

The response of the TFD to the various pairs of ions with constant Z value are plotted in figures 42-45. The plots show the invariance of the response to differing ion mass where the mass varied by as much as six units. Figures 46 and 47 show the response of the TFD to the two pairs of ions having the same mass but differing in Z by two charge units. There does not seem to be much variation in the response to the two different ions except at the higher energy. This is mostly due to the low charge states at the lower energies as well as the still relatively low charge state at the higher energies. At the higher energies there also exists the problem of a distribution of charge states from the scattered ions. There is also the added difficulty in the similar values of the energy loss for the two ions at the low energies. This is illustrated in figures 48 and 49 which show the specific energy loss of the Ge and Se ions passing through the TFD at a wide range of energies (figure 48) and at energies less than 1.5 MeV/amu (figure 49). The values of the specific energy loss were again calculated from the tables of Northcliffe and Schilling. The specific energy losses of Mo and Ba ions corresponding to the peak positions of the light and heavy mass fragments from the spontaneous fission of ^{252}Cf were added to the two figures for comparison. From these graphs, it was also possible to plot the specific luminescence values of the TFD against the calculated energy loss of both Se and Ge ions. Figures 50 and 51 show the now familiar double valued curves [37] for $\Delta L/\Delta x$ vs. dE/dx.

The time response of the 3TFD-SBD assembly was also examined from the data. Successively smaller time cuts were taken

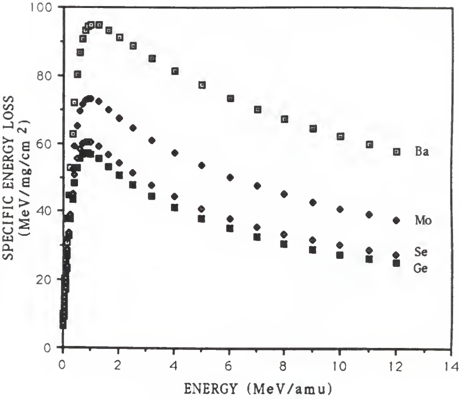

Figure 48. Stopping power curves as plotted from the data found in the tables of Northcliffe and Schilling [56]. The curves plotted are for the ions used in this experiment (Ge and Se) and for the ions in the peaks of the fission fragment spectrum for ^{252}Cf (Mo and Ba).

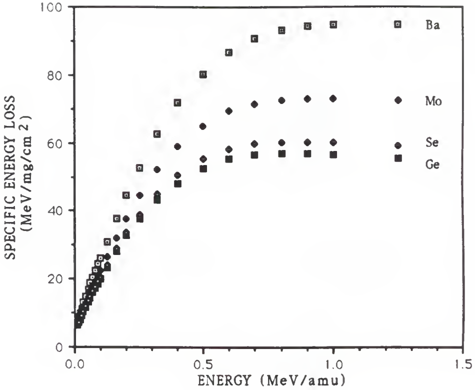

Figure 49. Same plot as found in the previous figure but plotted for the energy range of interest in this experiment.

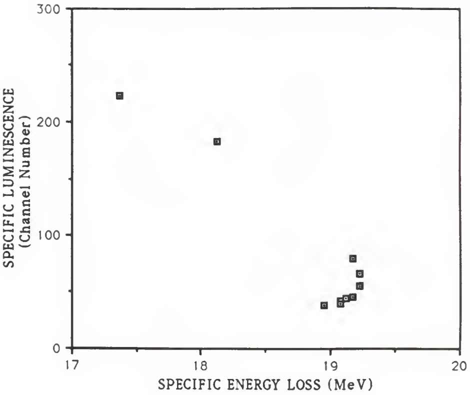

Figure 50. Plot of the measured response of the first TFD to Ge ions as a function of the calculated energy loss of the ion as it passes through the film.

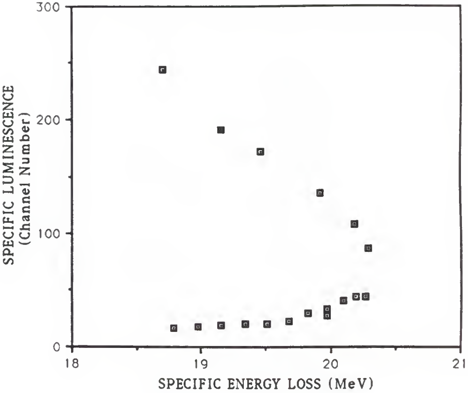

Figure 51. Plot of the measured response of the first TFD to Se ions as a function of the calculated energy loss of the ion as it passes through the film.

in the spectrum of the response between PM tubes 1 and 6 to ^{74}Se ions at 80 MeV. The time response between PM tubes 1 and 5 as well as between PM tubes 1 and 3 to these various cuts was observed. The purpose of these cuts was to successively narrow the time response in the latter two spectra until a constant value was achieved corresponding to a zero width in the response between PM tube 1 and 6. This will give the timing variation in the other two responses. Figure 52 shows the time response between PM tubes 1 and 5 with the various cuts. The wide peak shows the full response with no cuts from the response from PM tubes 1 and 6. The other peaks correspond to cuts of 10, 4 and 1 channels and as can be seen, a constant width was achieved. Figure 53 shows the response with the one channel wide cut as fitted using the spectral fitting code ROBFIT [57]. The width of the peak corresponds to 807 ps. Figure 54 shows the result of these cuts for the response between PM tubes 1 and 3. The peak again was fitted as shown in figure 55 and the width of the fit at FWHM corresponds to 984 ps.

An attempt to improve the width of the luminescence response of the first TFD was made by using the successive luminescence measurements made by the second TFD and the third TFD. The response to ^{70}Ge at 150 MeV as plotted in figure 35, with the time cut mentioned earlier, was used as a test. Figure 56 shows the corresponding response of the second TFD and figure 57 shows the corresponding response of the third TFD, both with the same time cut used for the first TFD. The latter two peaks were normalized to the peak in figure 35 by overlapping the peak position as well as the position of the peaks at their FWHM. Each event in all three TFD

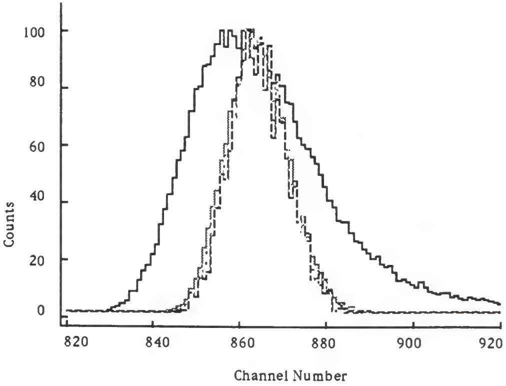

Figure 52. Time response to 80 MeV ^{74}Se ions travelling between TFD 1 and TFD 3 as measured by PM tubes 1 and 5. The outer peak is the full response of the scattered ions and the inner peaks correspond to the same events in coincidence with 10, 4 and 1 channel wide cuts from the same time response as measured between PM tubes 1 and 6. All peak heights are normalized to the same value.

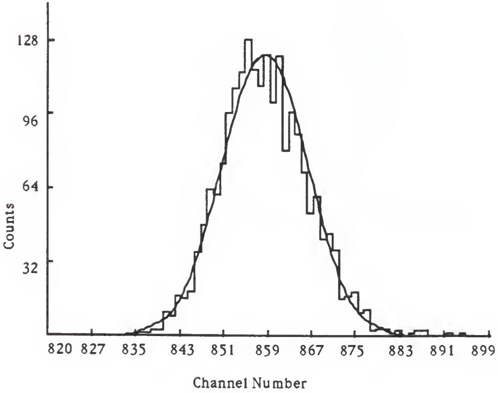

Figure 53. Time response from the previous figure which corresponds to the events in the time response measured between PM tubes 1 and 5 which are in coincidence with events in a one channel wide cut in the response between PM tubes 1 and 6. The fit to the peak gives a value for the full width at half maximum of 807 ps.

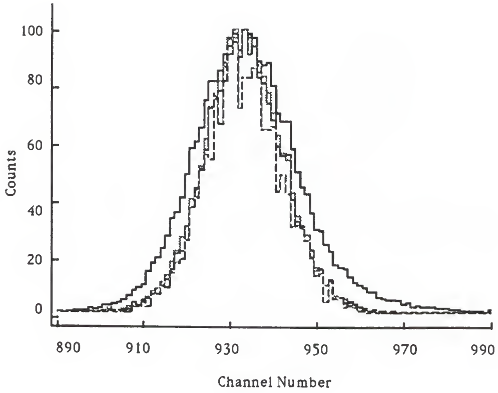

Figure 54. Time response to 80 MeV ^{74}Se ions travelling between TFD 1 and TFD 2 as measured by PM tubes 1 and 3. The outer peak corresponds to the full response and the inner peaks correspond to the same events but which are in coincidence with 10, 4 and 1 channel wide cuts in the response between PM tubes 1 and 6. Peak heights again are normalized to the same value.

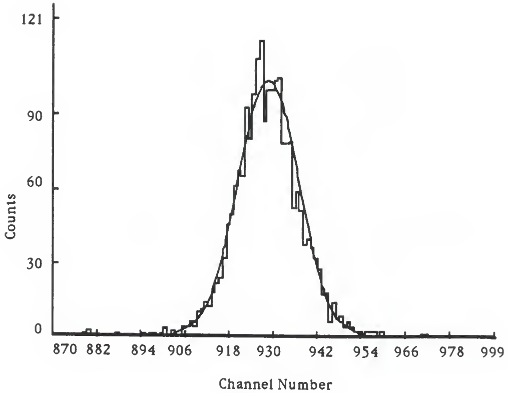

Figure 55. Time response from the previous figure which corresponds to the events in the time response measured between PM tubes 1 and 3 which are in coincidence with events in a one channel wide cut in the response between PM tubes 1 and 6. The fit to the peak gives a value for the full width at half maximum of 984 ps.

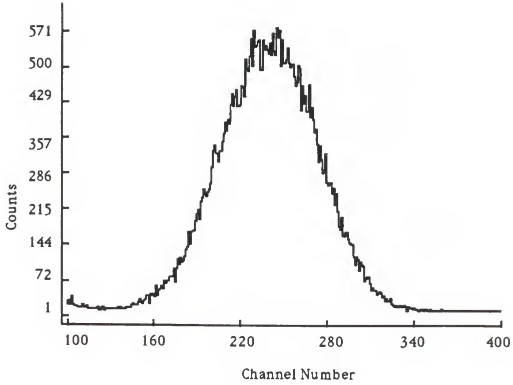

Figure 56. Specific luminescence response of the second TFD to 154 MeV ^{70}Ge ions. The events plotted are ones that were in coincidence with events that occurred between channels 181 and 183 in the time response between PM tubes 1 and 5 (figure 30).

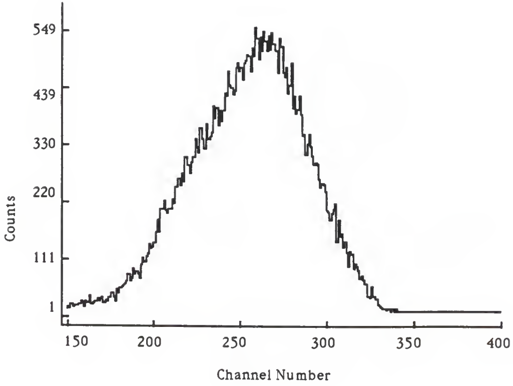

Figure 57. Specific luminescence response of the third TFD to 154 MeV ^{70}Ge ions. The events plotted are ones that were in coincidence with events that occurred between channels 181 and 183 in the time response between PM tubes 1 and 5 (figure 30).

responses was also normalized so that an event which occurred in the lowest channel of the peak was given a value of 0 and an event in the highest channel was given a value of 1. An event occurring in the first TFD was plotted if the corresponding event in the second TFD occurred at the same normalized position or within a 10% width. Figure 58 shows the result of the narrowing of the response of the first TFD.

The process was repeated but a 5% requirement was made. The result is shown in figure 59, where not much of a difference is seen compared to the 10% width requirement. A greater effect of the narrowing of the peak can be seen in figure 60, where along with the 10% requirement made for the second TFD, a corresponding requirement was made for the third TFD where events occurring at a certain position in the response distribution of the first TFD were plotted if the corresponding event occurred within a 10% width in the position in the response distribution of the second TFD and the third TFD. Figure 61 shows a plot of the response of the first TFD with a 5% requirement for the second and third TFD. Again not much of a difference is seen when going from a 10% requirement to a 5% requirement.

All these figures were plotted with the original response (figure 35) and all the heights of the peaks were normalized to show the decreased width. The disadvantage of the selectivity used is the omission of a significant number of events. This can be seen in figure 62 where the successively decreasing peak heights correspond to the original (figure 35) response, the 10% requirement in one TFD, the 5% requirement in one TFD, the 10% requirement in two and the 5%

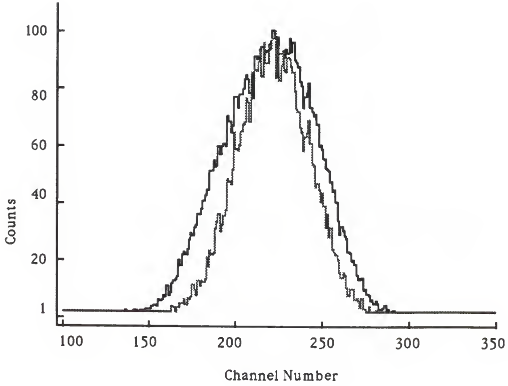

Figure 58. The reduction of the width of the response of the first TFD to 150 MeV ^{70}Ge ions is shown when events are eliminated if they do not fall within a 10% width of the corresponding peak position of the same response in the second film.

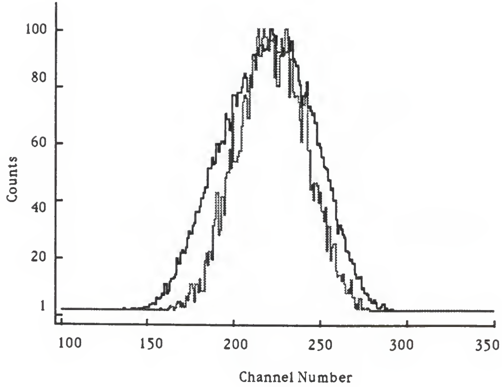

Figure 59. The reduction of the width of the response of the first TFD to 150 MeV ^{70}Ge ions is shown when events are eliminated if they do not fall within a 5% width of the corresponding peak position of the same response in the second film.

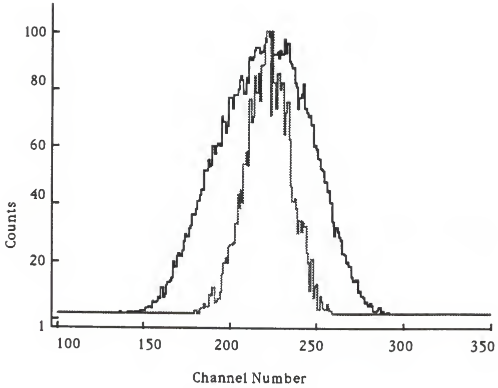

Figure 60. The reduction of the width of the response of the first TFD to 150 MeV ^{70}Ge ions is shown when events are eliminated if they do not fall within a 10% width of the corresponding peak position of the same response in the second and third films.

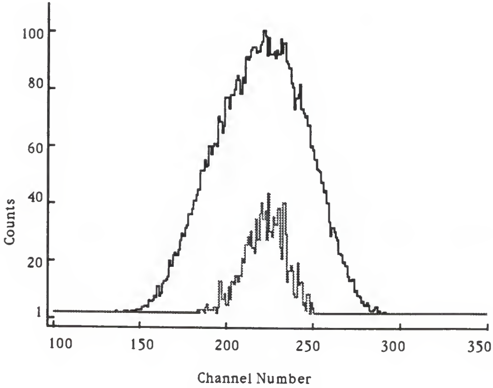

Figure 61. The reduction of the width of the response of the first TFD to 150 MeV ^{70}Ge ions is shown when events are eliminated if they do not fall within a 5% width of the corresponding peak position of the same response in the second and third films.

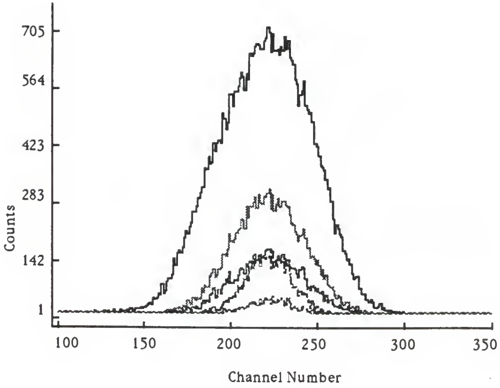

Figure 62. The disadvantage of reducing peak widths as described in the text is shown in this plot where the number of events plotted decreases in the same order as plotted in the previous four figures (where the peak heights had been normalized to emphasize decreasing widths).

requirement in two TFD's. The advantage of course is the better resolution of the luminescence response. The peaks that are plotted in figures 35 and 60 were fitted to determine the FWHM and to determine how much of an effect the narrowing had on the original peak. The fits are shown in figures 63 and 64 and the FWHM of each fit corresponds to 68.479 channels and 31.324 channels respectively thus giving a 54% reduction in the width of the TFD response.

All these peaks were generated from the scattering data of ^{70}Ge at 2.0 MeV/amu. The same analysis was performed for the ^{74}Se scattering data at 1.0 MeV to see if the same type of effect was observed at the lower energy. Figure 65 shows the TFD response from the three TFD's with the corresponding 3 channel wide time cut in the time response between PM tube 1 and PM tube 5. These peak positions were again matched to that of the one corresponding to the first TFD and the peak widths were normalized as described above.

Figure 66 shows all the successive reductions as was described above and this plot corresponds to the plot shown in figure 62 for ^{70}Ge, with the exception that all the peak heights are normalized. The original response from the first TFD is the widest peak in figure 65 and as seen in the plot, the other peaks are approximately the same width. The original wide peak was fitted and the resulting fit is shown in figure 67. The FWHM of the fit corresponds to 22.846 channels. The response of the first TFD which was plotted if the response was within a 5% variance of the other two TFD's, was also fitted. The result is shown in figure 68 where the FWHM corresponds to 13.404 channels. Thus a 41% reduction in width is

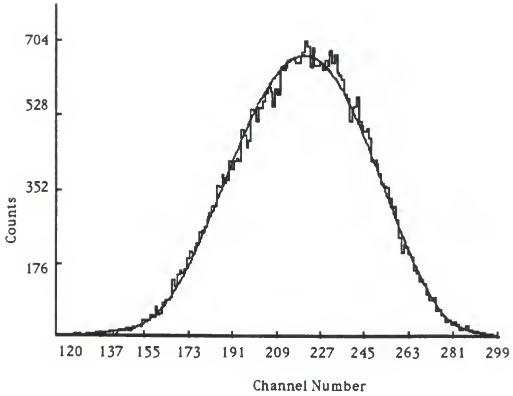

Figure 63. This plot shows the fit to the data which was plotted in figure 35. The spectral fitting code ROBFIT [57] was used and the value of the full width at half maximum was determined to be 68.479 channels.

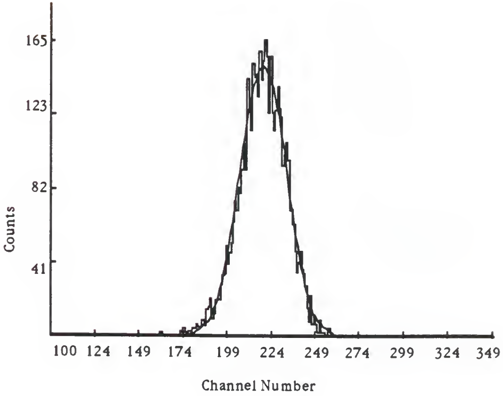

Figure 64. This plot shows the fit to the data which was plotted in figure 60 (the inner peak). The spectral fitting code ROBFIT [57] was used and the value of the full width at half maximum was determined to be 31.324 channels.

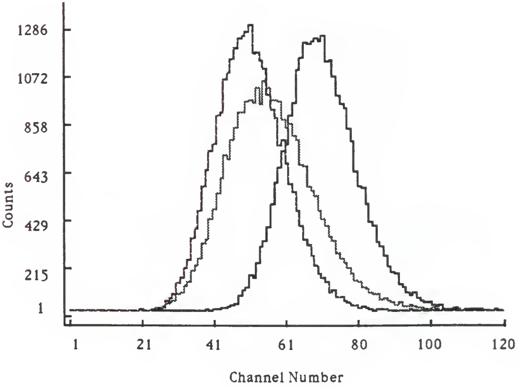

Figure 65. Specific luminescence response of all three films to ^{74}Se ions scattered at 1.0 MeV/amu. The plots correspond to (going from left to right in the figure) the second, the third and the first TFD. All three peaks are shown with the corresponding time cut mentioned in the text. The above figure shows raw data before the heights and widths were normalized for comparing the responses of each TFD for each event.

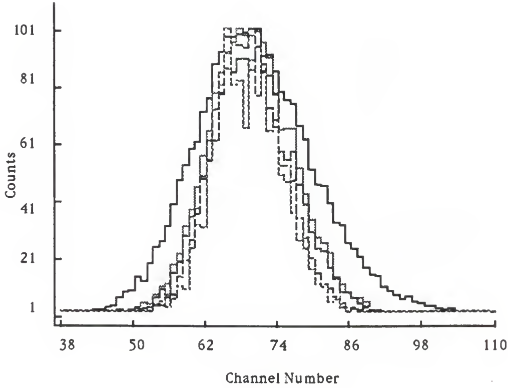

Figure 66. Specific luminescence response of the first TFD to ^{74}Se ions at 1.0 MeV/amu showing the reduced widths that were generated when coincidence criteria were applied in the same manner as described previously for ^{70}Ge at the higher energy.

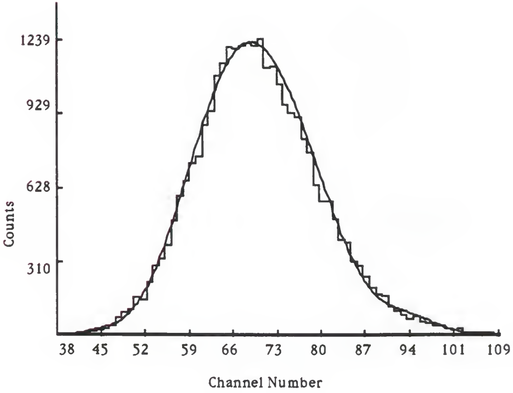

Figure 67. Response of the first TFD to ^{74}Se ions at 1.0 MeV/amu as was plotted in figure 65 with the corresponding peak fit which was generated using the code ROBFIT [57]. The full width at half maximum was found to be 22.846 channels.

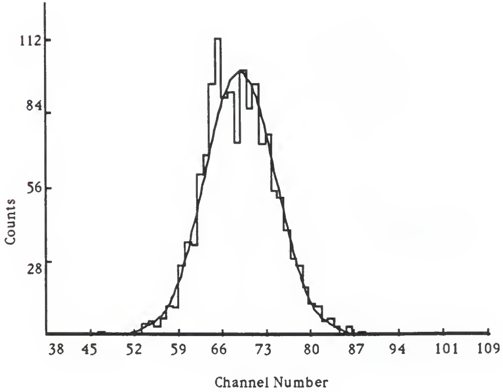

Figure 68. Response of the first TFD to ^{74}Se ions as was plotted in figure 66 (the narrowest peak). This plot shows the events which occurred in a 5% width of the corresponding peak position in the response of the second and third films. The FWHM gives 13.404 channels.

observed in the TFD response to ^{74}Se ions at the lower energy of 1.0 MeV/amu.

The results of this experiment will be again summarized in the final chapter. They will also be further discussed in the same chapter along with the experiment described in the next chapter which observed the response of a TFD to ^{252}Cf fission fragments.

CHAPTER 3
THIN FILM DETECTOR RESPONSE TO ^{252}Cf FISSION FRAGMENTS

Introduction

Since the interpretation that a uranium nucleus can fragment into smaller nuclei, the fission process has been one of the most studied phenomena in all of science. Much is known today about fission barriers, mass yields, etc. since Hahn and Strassman reported the presence of barium and lanthanum in the neutron induced fission of uranium in 1939 [58].

Fission occurs when a heavy nucleus receives enough excitation energy to overcome the fission barrier in the potential energy well, and a release of around 200 MeV (as in the case of ^{240}Pu) in energy occurs. The potential energy as a function of nuclear deformation can be estimated with good approximation by using the liquid drop model [59], which looks at the distortions of a spherical nucleus and its effects on the surface and coulomb energies. For a distorted nucleus having volume $V=(4/3)\pi a b^2$ where the major axis $a=R(1 + \varepsilon)$ and the minor axis $B=(1 + \varepsilon)^{-1/2}$ are described with respect to the original spherical radius R and distortion ε, the total energy change is given as the change in the surface and coulomb energies as

$$\Delta E = \Delta E_s + \Delta E_c = \varepsilon^2 [\, (2/5)\ 17.2\ A^{2/3} - (1/5)\ 0.70\ Z^2\ A^{-1/3} \,] \qquad (20).$$

In 1962, several Soviet workers discovered an isomeric state of ^{242}Am which showed an unusually short spontaneous fission half life [60]. An isomeric state would indicate a second ground state on the potential energy curve, so thus a refinement was made to account for this fission isomer. Using a shell correction as well as a pairing correction, Strutinsky modified the liquid drop model and came up with a potential energy curve that showed a two humped barrier with two ground states [61]. This accounted for the isomeric states which by this time were being identified for numerous species.

Fission barriers were found to decrease with increasing mass for nuclei having mass greater than about 90 amu [62]. For nuclei with $Z > 92$, the barrier height is sufficiently close to the nuclear ground state to allow for a significant probability of tunneling through the barrier. This spontaneous fission mode of decay is small compared to the α decay mode for the lighter fissionable nuclei but it shows a branching ratio of 0.03 for ^{252}Cf and for ^{254}Cf it becomes the main method of decay. For ^{235}U, the fission barrier height is about 5.8 MeV and for ^{252}Cf it is about 2 MeV [63]. It has been shown that the parameter Z^2/A serves as a rough indicator of the ability of a nucleus to fission spontaneously [64]. For larger values of Z^2/A, the spontaneous fission half life will be shorter and for values of $Z^2/A >$ 47, instantaneous breakup of the nucleus would occur upon formation.

One of the most widely studied aspects of fission has been the mass yield. Much experimental data exists on mass distribution of fission, but there is no suitable theory explaining all aspects of the experimental results. In general the mass division in fission has been found to be asymmetric with an increase in symmetric fission with increasing mass and Z. The median mass number for the heavy group shows little increase with increasing Z, but the median mass for the light group does increase. For example, looking at the thermal neutron induced fission of ^{227}Th, ^{235}U, ^{249}Cf, the median mass of the light group increases 89, 95, 106, respectively while the median mass of the heavy group increases only slightly, 138.5, 138.5, 139, respectively. There is also an increase in symmetric yield as the energy of the fission inducing neutron increases. Peak to valley ratios in asymmetric fission have been found to decrease with increasing mass, where ^{252}Cf spontaneous fission peak to valley ratio is 750, ^{254}Fm is 60. Looking at the fermium isotopes peak to valley ratios, ^{255}Fm is about 12, ^{257}Fm is about 1.5 and ^{258}Fm and ^{259}Fm show symmetric mass distributions.

Charge distribution in fission has been much harder to determine. The early work in determining charge distribution of fission products has been primarily from radiochemical analysis. The problem with this method is that the fission products tend to be neutron rich and thus have very short β decay half lives, thus making it impossible to determine independent yields.

Another method in determining charge distributions has been measuring the K x-ray yield from the fission fragments [65,66,67,68,69]. This has the advantage over radiochemical methods in that the high yield primary products are the ones which are sampled. The disadvantage is that the K x-rays do not reflect the independent yields of fission fragments, where the yields have shown differences as large as a factor of two between adjacent elements. Smaller yields occur near closed shells due to higher transition energies between low lying states.

A third method used to determine charge distribution is by looking at the prompt gamma de-excitation emitted by the fission products prior to β decay [70,71,72]. In the fission process, neutrons are emitted from the primary fragments approximately 10^{-11} seconds after the scission point, with γ-rays, x-rays and internal conversion electrons emitted between 10^{-12} to 10^{-6} seconds after scission. More than half the γ-rays emitted come from states having half lives less than $2x10^{-19}$ seconds. There are an average of eight γ-ray photons emitted per fission with an average energy of 1 MeV per photon giving a total of 8 MeV of energy given off by the photons. In the case of ^{252}Cf, there are about 10 photons per fission with 8.6 MeV total energy per fission from the γ-rays.

If one assumes that γ-ray emission should not occur when it is energetically possible to emit a neutron, then the γ-ray yield is found to be higher than expected. After scission, each fragment will have a high excitation energy and will liberate neutrons to dissipate this excitation energy by 5-6 MeV (the average neutron binding energy) for each neutron emitted. After all the neutrons are emitted, the residual energy should be between zero and the neutron binding energy of 5-6 MeV. But what is observed is that the total energy of γ emission is between 7-9 MeV. This observed discrepancy is attributed to the large angular momenta of the fission fragments. The average angular momenta of the primary fission products are found to be about 7-8 units of $\hbar$ and also aligned in a plane perpendicular to the fission fragment trajectory. The primary fission product angular momentum distribution is given by [73]

$$P(J) \propto (2J + 1) \exp[-J(J + 1)/B^2] \qquad (21)$$

where B is a parameter which represents the approximate rms value of $J + 1/2$.

In an elegant set of experiments, Wilhelmy, Thompson, Jared, Chiefetz and others [70,74,75,76,77] looked at the prompt γ-ray emission as well as the K x-ray emission in coincidence with pairs of fission fragments from ^{252}Cf. They determined the ground state band transition intensities for 36 even-even primary fission product nuclei and by so doing identified several transitions not previously reported. This work has given experimental evidence for rotation-like behavior in several neutron-rich nuclei in a region of stable deformation, which at the time was not possible from in-beam reactions. The measured intensities of the cascading ground state bands gave the magnitude of the intrinsic angular momenta of the primary products. It was found that the average angular momentum of the primary products from ^{252}Cf spontaneous fission is $\bar{I} \approx (7 \pm 2)\,\hbar$ and that the heavy fission products have approximately 20% more angular momentum than the light products. Also it was found that the more symmetric the mass division the lower the angular momentum.

The important feature of these experiments was that a new method of determining the charge and mass distribution of the primary fission products was developed. The distributions were determined from the experimentally measured intensities of the prompt $2^+ \rightarrow 0^+$ in the ground state bands of even-even nuclei of the fission products. The key assumption to the method is that very little of the de-excitation bypasses the $2^+ \rightarrow 0^+$ ground state band transition and that this reflects to a high degree of accuracy the independent yield of the primary fission products. The results of the experiments that have been performed support this assumption.

The prompt γ-rays were measured in coincidence with the K x-rays which were used to confirm the γ transition assignments to corresponding Z values. The kinetic energies of the fragments were also measured to confirm mass assignments of the γ-ray peaks. Their results showed good agreement with radiochemical results previously reported by others.

While this method was a new and novel approach in determining the charge distribution in fission products, it did not provide an on-line method of particle identification as provided by the various detectors discussed in chapter I. But what this method and the method of using K x-rays did provide was a technique to help measure the performance characteristics of various on-line detectors.

An experiment was performed by Mariolopoulos et al. [78] which measured the K x-rays that were in coincidence with fission fragments from ^{252}Cf which were detected by a ΔE-E_r detector telescope. The ΔE of the fragments were measured using an ionization chamber and the E_r was measured with a 60 μm silicon solid state detector. The x-ray energies were measured using an intrinsic germanium detector. By gating on the emitted x-rays of the heavy fragments that were stopped in the thick nickel backing of the source, the response of the ΔE-Er detector to the complimentary light fragment traveling 180° from the Ge detector was measured. The nuclear charge resolving power $Z/\Delta Z$ of the gas ionization chamber was determined to be about 25 for the light fragment group.

A similar experiment was performed by Yoshida et al. [79] with the exception that the prompt γ-rays from the ^{252}Cf were used to gate on the signals from the gas ionization chamber, which also had the feature of being able to measure the position of the fission fragments. The fragments were stopped in the chamber and with the anode plate divided into two sections, one section was able to measure ΔE of the fragments and the other, the larger of the two sections, was able to measure E_r. The γ-ray energies were measured by a Ge(Li) detector and the nuclear charge resolution for the gas ionization chamber was determined to be about 2.0 for the light fragment group.

Both of these methods are then examples of ways of testing the response of a detector telescope arrangement to typical heavy ions, and in these two cases the ions are fragments from a ^{252}Cf fission source. The latter method was used to test the nuclear charge resolving power of the 3TFD-SBD detector assembly.

Experimental

An experiment was performed at the University of Florida with the purpose of testing the 3TFD-SBD response to the light mass group from ^{252}Cf fission fragments. Two detectors were used for this purpose, the 3TFD-SBD assembly described earlier and an ORTEC n-type intrinsic gamma gauge Ge detector. The four parameters collected were the specific luminescence response of the first TFD, the TOF between the first TFD and the third TFD, the TOF between the first TFD and the second TFD and the energies of the prompt γ de-excitation of the fragments as measured by the Ge detector. A total of 10^6 events were collected with frequent calibrations made to check for long term drifts in the electronic equipment.

The ^{252}Cf source was deposited on a thick nickel backing and had an approximate activity of 4×10^8 disintegrations per second. The source was mounted onto the end of an aluminum cap which in turn was screwed onto one end of a ball valve chamber. By closing the ball valve, the chamber could be isolated from the attached 3TFD-SBD assembly. This chamber also had a separate mechanical vacuum pump attached to it to keep the source under vacuum. The Ge detector was placed next to the nickel backing side of the source, 180° from the path of the fission fragments transiting the 3TFD-SBD assembly. This position was chosen since it has been found the the preferred direction of γ emission is in the direction of the fragment flight [80,81]. A diagram of the experimental set-up along with the electronic set-up is shown in figure 69.

The thin films that were used were the same ones described in the previous chapter, with the luminescence measurements being made on the first TFD having a thickness of 0.337 mg/cm^2. The response of the first TFD was measured by two opposing PM tubes whose pulses were amplified by ORTEC 572 amplifiers (AMP) and then summed to each other using a Canberra 1465A sum/inverter

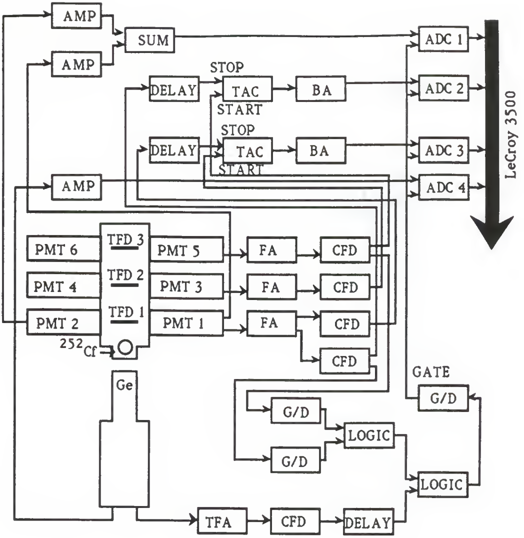

ADC = Analog to Digital Converter
AMP = Amlifier
BA = Biaed Amplifier
CFD = Constant Fraction Discr.
FA = Fast Amplifier
Ge = Germanium Detector

G/D = Gate and Delay Generator
PMT = Photomultiplier Tube
SUM = Sum Amp
TAC = Time to Amplitude Convereter
TFD = Thin Film Detector

Figure 69. Experimental set-up shown with the associated electronics. The Ge detector was positioned 180° to the direction of travel of the fission fragments through the thin film detectors. the abbreviations for the electronics are as described in the text.

(SUM). The output from this went into the first LeCroy 3511 analog-to-digital converter (ADC).

The timing signals from the three PM tubes, one associated with each TFD, were each amplified by an ORTEC 535 quad fast amplifier (FA) with the outputs from each going into an ORTEC 584 constant fraction discriminator (CFD). The two delayed outputs from the CFD associated with the first TFD were used as stop inputs into two ORTEC 566 time-to-amplitude converters (TAC) and the CFD output associated with the third TFD serving as a start for one TAC and the output associated with the second TFD serving as the start for the other. The output from each TAC went to the input of an ORTEC 408A biased amplifier (BA) and the output from each of these went into an ADC. Thus the second ADC recorded the TOF between the first and third TFD and the third recorded the TOF between the first and second TFD.

The energy output from the preamplifier of the Ge detector was amplified by an ORTEC 572 amplifier and this output went to the fourth ADC. The timing output from the Ge detector was amplified by an ORTEC 454 timing filter amplifier (TFA) and this output went to the input of another ORTEC 584 CFD.

The gate to each ADC was generated by requiring the timing signals from the Ge detector to be in coincidence with the timing signals from the first and third TFD's. The CFD outputs associated with these two TFD's each went into the input of a LeCroy 222 gate and delay generator (G/D). The output then went into a Phillips 756 quad logic unit and a coincidence between these two signals was established. A 20 ns wide output pulse went into the input of another quad logic unit along with the delayed signal from the CFD originating from the Ge detector. This established a coincidence between the fragment signals and the γ-ray signals. The output from this logic unit went into an ORTEC 416A gate and delay generator whose output was used as a gate for the ADC's.

The coincidence between the signals from the fission fragments and the γ-rays was set up so that only the γ-rays emitted within a time period of approximately 20 ns after fission were accepted. It has been shown that 96.8% of the γ-rays are emitted within 10 ns after fission of ^{252}Cf [82,83] so there was no need to require a longer time coincidence than about 20 ns.

Results and Discussion

Approximately 10^6 events were collected over a period of about six weeks. A LeCroy 3500 multichannel analyzer was used to collect the data event-by-event. The 3511 ADC's were positioned in a CAMAC mini-crate attached to the 3500 system. A FORTRAN code had been written to do the data collection and the data was stored on magnetic tape for subsequent analysis at the University of Florida using the IBM 3090-600V computer located at the Northeast Regional Data Center. Each 8192 channel spectrum was reduced to 4096 in the analysis for easier storage.

The total TFD luminescence response is shown in figure 70 and the TOF spectra are shown in figures 71 (TFD 1 to 3) and 72 (TFD 1 to 2). the total γ energy spectrum is shown in figure 73 and a particular region of interest located between channels 600 and 1000

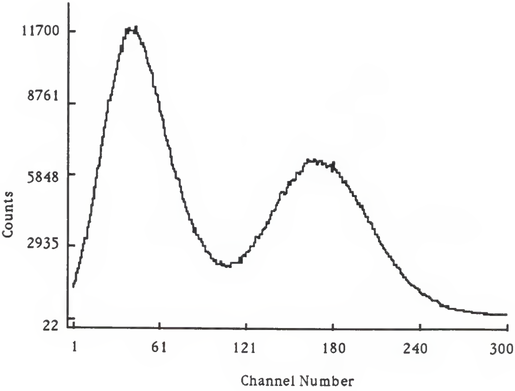

Figure 70. Specific luminescence response of the first TFD to ^{252}Cf fission fragments that were measured in coincidence with the prompt gamma rays.

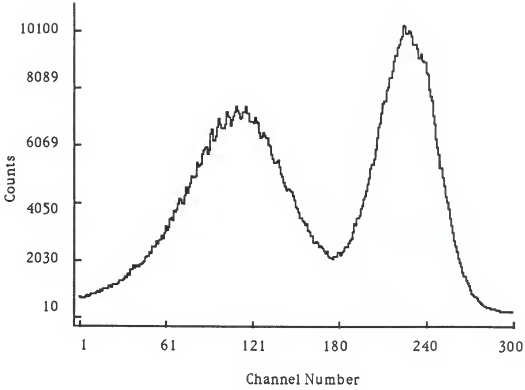

Figure 71. Time of flight spectrum of ^{252}Cf fission fragments that were measured in coincidence with the prompt gamma rays. The figure shown is actually an inverse time of flight since the start signal was from the third TFD while the stop signal was from the delayed signal originating from the first TFD.

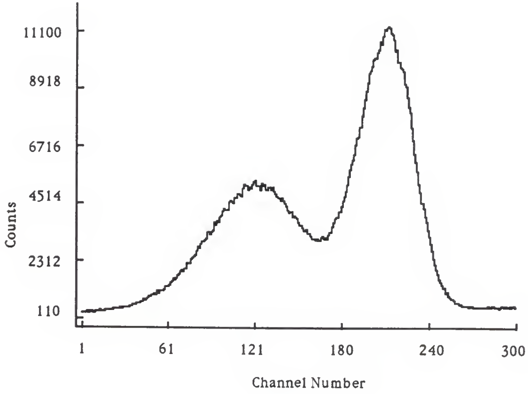

Figure 72. Time of flight spectrum of ^{252}Cf fission fragments measured in coincidence with the prompt gamma rays. Again the figure shown is actually an inverse TOF, but in this case the start signal was from the second TFD and the stop was again the delayed signal from the first TFD.

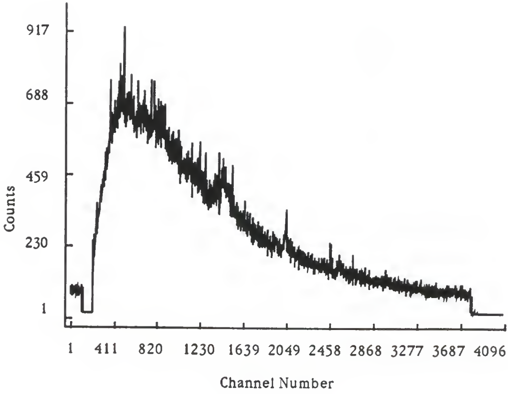

Figure 73. Prompt gamma spectrum from ^{252}Cf fission fragments. The gamma rays were measured in coincidence with the signals from the TFD and were within a 20 ns gate of this signal.

is shown in figure 74. Several peaks have been identified in figure 74 and are labeled along with the location of the peaks in units of keV. Some of the energy assignments of these peaks are somewhat different from their energies assigned in the literature due to Doppler shifting. This will occur for photons from fragments travelling away from the Ge detector as well as for photons from fragments with short lifetimes for γ de-excitation and travelling toward the detector, i. e. into the source backing.

Some γ peaks are not very well defined as can be seen in figure 74, due to both Doppler broadening and low statistics. This is why most of these peaks have not been useful in gating to locate the position of various fragments in the TFD response spectrum.

One exception is the 295.7 keV peak assigned to the 4→2 transition of ^{148}Ce and located in channel 689 of the γ energy spectrum. When gating on this peak and plotting the TFD response associated with this peak, the result is as seen in figure 75 shows a familiar luminescence spectrum with some poorly defined peaks in it. The TFD response spectrum shows the full distribution of fission fragments which correspond to the Compton scattering as is seen in the γ-ray spectrum as the background. The spectrum was also reduced to 256 channels due to the low statistics. The peak of interest in this particular spectrum will turn out to be located in channel 90 and corresponds to the complementary light fragment to Ce which is Zr.

Another very useful γ peak peak is shown in figure 76. The peak is located at 163.6 keV in channel 384 and is from the 2→0 de-excitation of ^{106}Mo. Since the fragment is traveling away from the

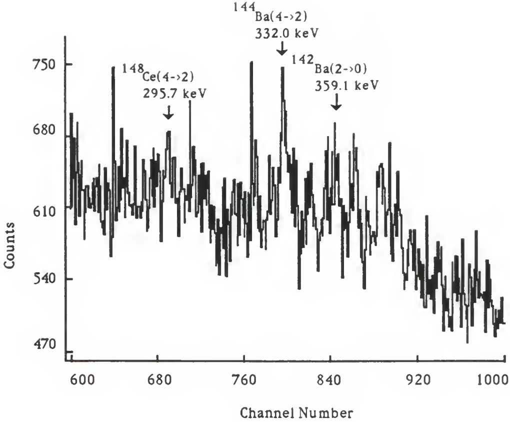

Figure 74. A portion of the gamma spectrum that was recorded in coincidence with the TFD signal. Several prominent peaks are labeled, with the most useful peak being due to the 4->2 transition of ^{148}Ce. The events recorded in the channels corresponding to this peak were used as a gate to plot the coincident TFD response shown in the next figure.

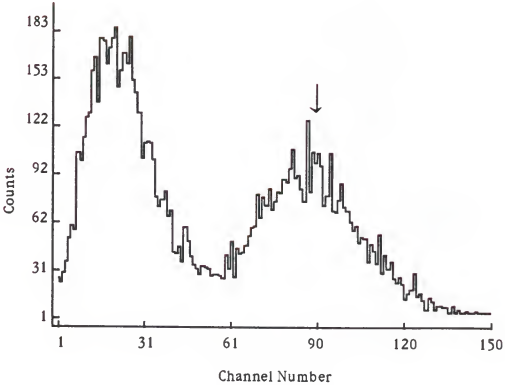

Figure 75. TFD response to ^{252}Cf fission fragments that were in coincidence with the events recorded in the channels of the gamma spectrum corresponding to the 4->2 transition of ^{148}Ce. The peak that shows up in the light mass fragment group is from Zr, the complimentary fragment to Ce.

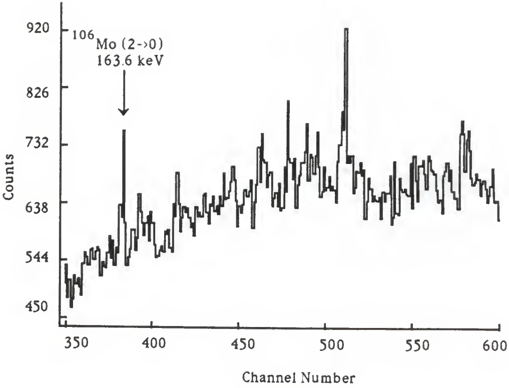

Figure 76. Another portion of the prompt gamma spectrum showing another peak that was used as a gate.

Ge detector and into the 3TFD-SBD detector, the γ peak is downshifted from its assigned value of 171.7 keV and the corresponding peak in the TFD luminescence response will show up in the light fragment group. Since the ^{106}Mo velocity has been reported as being 1.370 cm/ns, this would correspond to a shift of 7.85 keV thus confirming the assignment of the γ peak.

The TFD response corresponding to events occurring in coincidence with this γ peak is shown in figure 77, which again was reduced to 256 channels due to the low statistics. A well defined peak is seen in the light fragment group and thus corresponds to Mo. The TOF spectra whose corresponding events were in coincidence to the same γ peak, showed no significant peaks. This was true of all the cuts made in the γ spectrum where there were no noticeable peaks seen in the corresponding TOF spectra. The two cuts discussed above are also the only two which showed any noticeable peaks in the light fragment groups in the TFD luminescence response.

Thus the spectra shown in figures 75 and 77 were fitted with the spectral fitting code ROBFIT [57]. Of interest in figure 75 is the peak position of the Zr peak and in figure 77 the width of the very well defined Mo peak as well as its position are of interest. In both cases, the background was fitted with 12 constants and the cutoff was taken at 2σ. The fit to figure 77 is shown in figure 78 where the peak as well as the background is shown in the spectrum with the residuals shown above the spectrum. The Mo peak position was found to be 84.504 and its width was found to be 4.784 ± 0.505. This peak width was the used as an input parameter to fit the spectrum of figure 75. The fit can be seen in figure 79 where again the Zr peak

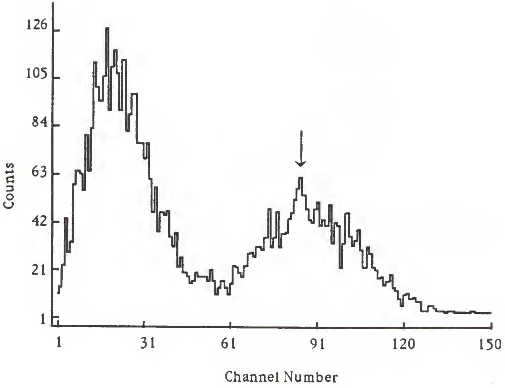

Figure 77. TFD response to the fission fragments which were in coincidence to the peak labeled in the previous figure. The peak due to Mo is very prominent in the light mass fragment group.

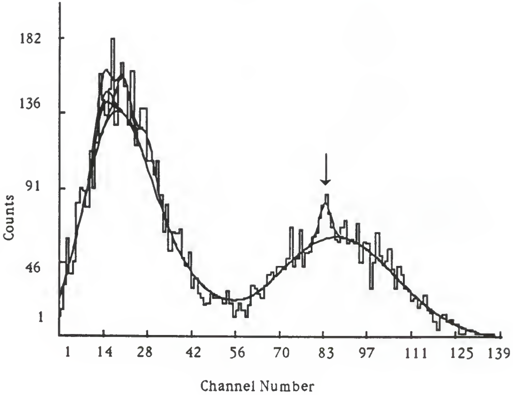

Figure 78. Curve fit to figure 77 using ROBFIT [57]. The peak width and position were determined from the well shaped peak located in the light mass group corresponding to Mo.

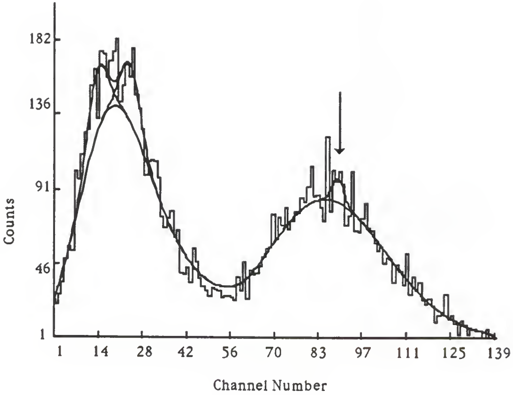

Figure 79. Curve fit to figure 75 again using ROBFIT [57]. The peak position was determined from the peak due to Zr located in the light mass group.

is shown with the background and the residuals. The peak position was found to be in channel 90.245.

Since the difference in nuclear charge between Zr (Z=40) and Mo (Z=42) is two charge units and the distance between the two is 5.741 channels, this would correspond to 2.871 channels per charge unit in the vicinity of Mo giving a width of 1.667 ± 0.176 charge units for the Mo peak. Thus the nuclear charge resolving power of the TFD is found to be 25.2 for the light fragment group. These results will be discussed further in the summary, and along with the results of the previous experiment will be used for comparison with other particle detectors .

CHAPTER 4
CHARGE STATE CHARACTERISTICS OF Ge AND Se IONS INVOLVED IN SMALL IMPACT PARAMETER COLLISIONS WITH A GOLD TARGET

Introduction

For a number of years now, there has been considerable interest in obtaining information regarding the charge states of ions passing through matter. Typical physical information one hopes to obtain includes the average charge state, the distribution of charges, photon emission resulting from inner shell excitation, etc. It has been determined that three mechanisms govern the charge exchange process between an ion and a neutral target [84]: (1) Coulomb capture of one or more electrons from the target to the ion into ground or excited states, (2) radiative capture where the ion captures one or more electrons into ground or excited states accompanied by the emission of a photon, (3) excitation to the continuum where the ion loses one or more electrons leaving the ion in a ground or excited state.

The first experiments performed in this area include the ones by Batho [85] which looked at the ionization and neutralization of Ne, Ar and Kr ions in collisions in the gas phase. Since there already was considerable interest in the 1930s in determining the energy loss of heavy ions passing through matter, there was also a desire to determine a relationship between the energy loss, $\Delta E/\Delta x$, and the charge state. Thus several people studied the charge states of fission fragments passing through various materials [86-93].

With the development of heavy ion accelerators, interest in ionic charge states grew. New information was needed for charge states of various ions passing through different target materials as new sources became available. Predictions of charge state distributions of accelerated ions were needed to obtain the highest possible charge q behind intermediate strippers for further acceleration.

The overwhelming majority of the information concerning the charge state distributions of ions passing through matter is found in terms of the charge state equilibrium of the ions. The idea of charge state equilibrium arose when it was found that there was a minimum thickness of target material, x_{-}, in which the equilibrium charge state fractions, F(q), were found to be independent of the initial charge distribution, $Y_q(0)$. An explanation, first introduced by Bohr [87], was that the net effect of electron capture and loss balanced each other out with a sufficiently thick target. Once charge state equilibrium is achieved, the final distribution varies as a function of penetration depth. Nikolaev and Dmitriev [92] have been able to reproduce experimental data quite well with the empirical relation of $\overline{q}$, the average charge state, as a function of ion energy E

$$\overline{q} = Z_1(1 + X^{-1/0.6})^{-0.6} \qquad (22)$$

where the reduced velocity, X, is given as

$$X = 3.86\sqrt{E/M_1} \; / \; Z_1^{0.45} \qquad (23)$$

where Z_1 is the atomic number of the ion, E is the energy in MeV and M_1 is the ion mass.

Experimentally determined data concerning equilibrium charge state distributions of various ions passing through different target materials have been compiled by Wittkower and Betz [93]. A more recent compilation has been made by Shima, Mikumo and Tawara [94] in which the equilibrium charge state distributions have been listed with respect to the ion energy emerging from the target contrary to the Wittkower and Betz version where the distributions were listed with respect to incident ion energy. The reason is that the distribution of the charges was found to depend on the target thickness and the energy of the emerging ion due to its energy loss going through a foil.

The equilibrium charge state distributions also seem to depend on whether the target material is a solid or a gas. The average charge states were found by many authors to be greater when an ion passed through a solid than through a gas [95-97]. This density effect, more prominent for heavy projectiles, was attributed according to the Bohr-Lindhard model [98] to the influence of excited states of ions which occur during collisions with target atoms. Each subsequent collision inside the solid target occurs before the ion could decay to the ground state, thereby losing the electron from the excited state. Thus a cumulative effect can take place.

While the equilibrium charge state data that has been compiled in the above mentioned tables deal with the experimental situation where the ion examined is detected with 0^o scattering, relatively little experimental data exists for the charge states of ions that are scattered off targets at greater than a 0° angle. There have been many coincidence experiments performed [99] where the charge states of the scattered ion and the recoil were measured in the gas phase. Scattering angles of up to 40° were studied for low energy (< 300 keV) ions.

Others also looked at charge states of ions scattering off various gaseous targets. Bridwell, et al. [100] noted the high charge states of 50 MeV iodine ions scattered at 3°, where electron losses of up to 14 were reported. Others [101-103] also observed high charge states of heavy ions scattering at small angles. From these experiments it was determined that the high charge states could be attributed to a large electron loss from a single violent collision contrasting the single electron loss and capture from multiple collisions which occur in the charge exchange process when observing the ion at 0°. Since the aim of many of these experiments was to relate the dependence of the emerging ion charge state to the impact parameter, it was also determined that the charge states of the scattered ions increased as the distance of closest approach decreased.

These experiments that have been mentioned obviously indicated that the charge exchange process for large angle scattering, where there was considerable overlap of electron clouds belonging to the projectile ion and the neutral target, was different from the 0° scattering case. However, penetration of the projectile never went deeper than the L shell for these low energy and small scattering angle cases.

Among the first to observe a case of K shell penetration were Baron and Delauney [104], who noted high charge states of 495 MeV Kr ions observed at 3° scattering off carbon foils.

A more detailed study was carried out by Rosner, et al. [105] and Rosner and Gur [106] where oxygen beams in the 10-30 MeV range were scattered off gaseous targets and detected at scatter angles between 5° and 9°. One result showed the independence of the outgoing charge distribution to the scattering angle, contrary to previous experiments [99] done at lower energies and therefore larger impact parameters. The insensitivity of the final charge state to the impact parameter in these experiments was explained by noting that at the 5° angle case, there already was penetration of the K shell so scattering beyond 5° would not result in the penetration of any new shells. Thus the charge distribution remained the same as resulting from similar overlap of electronic clouds between the ion and the target atom.

One other significant result was that an "equilibrium charge distribution" was established in the case of high Z targets, i. e. the outgoing charge distribution was independent of the ionic charge of the incoming ion. This was an unusual result since it was confirmed that the scattering was due to single collisions as compared to the multiple collisions found in the equilibrium charge distributions normally observed at 0°. This result, seen for high Z targets, was not observed for cases of low Z targets, inferring that, in the latter case, the ion in some way "remembered" its original charge.

Several more experiments were performed [107-111] with beams of C, N, O and Ne in the 0.5-1 MeV range scattered off various gaseous targets at angles less than 10°. This again corresponded to ions penetrating the K shell with the results again indicating that for ions emerging from a target at angles other than 0°, the charge exchange process is different from the 0° scatter case. The most probable charge exchange process in the large angle scattering case occurs in a single collision where the ion loses multiple electrons and for the 0° scatter case, the most probable type of charge exchange is the single electron capture and loss from multiple collisions between ion and target atoms. Thus a need arose for a model which would predict the average charge state of ions involved in small impact parameter collisions.

Theory

In previously mentioned experiments [99-103] where the trajectories of colliding species penetrated the M or L shells, it was noted that the final charge distribution depended on the impact parameter. The charge exchange process in these low velocity cases, $v \ll 1$ au (Bohr electron velocity), was described by the molecular orbital model [110]. For higher velocity collisions, $v \gg 1$ au, the molecular orbital model cannot be applied to the outer electrons.

One of the first models that attempted to predict experimental results of the average charge states occurring in large angle scattering was published by Rosner and Brandt [111]. The average outgoing charge state of a scattered projectile with atomic number Z_1, initial velocity v_1 and initial charge $q_1(0)$ scattering off a target atom with atomic number Z_2 was given as

$$q_1(Z_2) = q_1(0)\, e^{-\alpha\omega_0 R/v_1} + q_1(\infty)(1 - e^{-\alpha\omega_0 R/v_1}) \qquad (24)$$

where α is a constant of the order 1. The asymptotic mean projectile charge number $q_1(\infty)$ is given as

$$q_1(\infty) \approx Z_1[1 - \exp(-v_1/Z_1^{2/3} v_o)] \qquad (25).$$

In the above equations, the statistical distribution of overlapping spherical electron clouds with radius R is given as

$$R = 2.455\, Z_2^{-1/3}\, a_o \qquad (26)$$

where a_o is the Bohr radius and v_o is the Bohr velocity. The mean electron density ρ_o is given as

$$\rho_o = 1.61 * 10^{-2}\, Z_2^2\, a_o^{-3} \qquad (27)$$

and the eigenfrequency given as

$$\omega_o \approx 0.45\, Z_2 \text{ au} \qquad (28).$$

A more recent model published by Meron and Rosner [112] was developed to treat the charge exchange process quantitatively. The assumption made in this model was that in a close collision, the outer electrons which are not lost from the common electron cloud are redistributed between the nuclei as they move away from each other. The inner shell electrons remain relatively inert and do not take place in the redistribution process. A cutoff electronic velocity, $u_c(v)$ is defined where outer electrons are those with velocity $u < u_c$. This boundary between inner and outer electrons is not well defined but the authors estimate it at a point where

$$u_c \equiv 2v, \qquad (29)$$

where v is the collision velocity.

A function Z(u) is defined as the number of electrons in an atom of atomic number Z whose velocities are smaller than u and is given as

$$Z(u) \approx \frac{Z\ u}{\left[\ u^{2} + \left(\frac{2}{3} Z^{2}\right)^{2/3}\ \right]^{1/2}} \tag{30}$$

The final average charge state is then given as

$$\langle q \rangle_1 = Z_1(u_c) - N_1 \tag{31}$$

where N_1 is the average number of electrons caught into Z_1 (the projectile ion) as it moves away from the target Z_2 and is given as

$$N_1 = \frac{N + Z_1(u_c)}{Z_1(u_c) + Z_2(u_c)} \left[1 - \frac{v_1}{u_c} \right] \tag{32}$$

where v_1 is the is the velocity of Z_1 in the center of mass coordinate system and N is the total number of electrons involved and is given as

$$N = Z_1(u_c) + Z_2(u_c) - q_i \tag{33}$$

where q_i is the initial positive charge of the projectile. This compound-atom model has been shown to reproduce the limited experimental data [112].

Experimental

The experiment that was performed has been described in detail in chapter 2. The 3 TFD-SBD assembly was mounted onto a 1.6 m diameter scatter chamber at a detector port located at a 150° angle from the entrance of the beam. The target located at the center of the scatter chamber was a gold foil of approximately 1.0 mg/cm^2 thickness. Various accelerated ion beams of Ge and Se isotopes in the 53 - 169 MeV range were scattered and the response of the detector to these scattered ions was observed. Twelve parameters of event-by-event data were recorded as described previously.

Three different isotopes of Ge, each at three different beam energies, and two isotopes of Se, each at five different beam energies, were analyzed. These experimental runs have been listed in table 1 and the runs of interest are the following pairs: 4 and 7, 5 and 8, 6 and 9, 12 and 14, and 13 and 15. These runs correspond to different sets of isotopes at energies of 1.0 and 0.75 MeV/amu after 30° scattering. For example, run number 12 corresponds to ^{74}Se having a most probable energy of 1.0 MeV/amu after scattering and run number 14 corresponds to ^{74}Se ions having a most probable energy of 0.75 MeV/amu after scattering. The results of these experimental runs and subsequent analysis as they relate to the previous discussion of charge state distributions will be discussed.

Results and Discussion

Chapter 2 described the response of the TFD to accelerated Ge and Se isotopes of various energies. The TFD was located near the entrance of the 3 TFD-SBD assembly, i. e. it was the first of three thin films encountered by an ion entering the detector assembly. The specific luminescence of all three films as well as the time response between various PM tubes was also measured. Figure 32 of chapter 2 showed the response of the first TFD to 154 MeV ^{70}Ge ions scattered off the gold foil. The width of this peak was made narrower and the shape was more gaussian (figure 35) when a selection for the corresponding TOF, between PM tubes 1 and 5 (figure 30), was made. Figures 37-41 plotted the TFD response to a number of these TOF selections in terms of the velocities of the various ions. Figure 40, which plotted the TFD response to ^{74}Se as a function of velocity of the ions, shows two different TFD responses for one particular velocity (~1.27 cm/ns). This can be seen in the TFD response to all the ions (figures 37-41) but ^{74}Se will be used as an example in the following discussion.

It should be remembered that the points appearing in the above mentioned plots originated from data obtained from different experimental runs, where for each ion species, a different run meant both a different energy and charge state before scattering. Figure 80 shows the TFD response to scattered ^{74}Se ions that had two different incident energy values. The lower response corresponds to ions with initial energy of 61.4 MeV and the higher response corresponds to ions with initial energy of 81.9 MeV. Since the two responses were due to two ion species with the same atomic number and mass, the difference in the responses could be attributed to the different velocities. But there turns out to be another difference in the two species, namely that the ions from the two different experimental runs possessed different charge states before and after scattering.

To show this, a velocity selection was made. Figure 81 shows the TOF of the two different species as measured between PM tubes 1 and 5. There can be seen a small region of overlap located between about channels 225 and 234 caused by the scattered ions passing through different thicknesses of gold foil. A three channel wide cut was selected for the events occurring between channels 227 and 229 in this TOF response and the coincident TFD events were plotted. Figure 82 shows this plot and the two different TFD

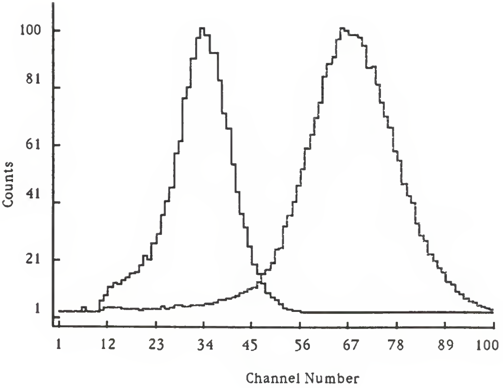

Figure 80. TFD response to ^{74}Se ions scattered at 30° off a gold target. The peak to the left was due to ions having initial beam energy of 61.4 MeV and the one to the right was due to ions with 81.9 MeV initial energy.

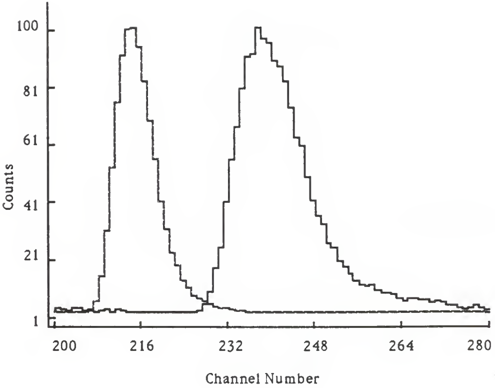

Figure 81. Time of flight spectrum of ^{74}Se ions as measured between PM tubes 1 and 5 as described in detail in chapter 2. The peak to the left represents 81.9 MeV ions and the right one represents 61.4 MeV ions.

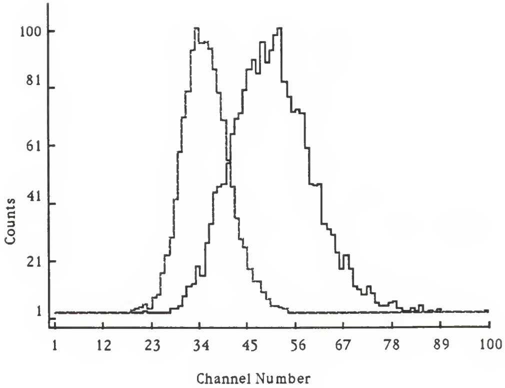

Figure 82. Spectrum representing the charge distribution of ^{74}Se ions scattered 30° off a gold target and into the 3TFD-SBD assembly. The TFD response is gated by a velocity selection from the previous spectrum as described in the text. The 61.4 MeV ions are shown again to the left of the 81.9 MeV ions.

responses. Since now the ions possess the same atomic number, the same mass and the same velocity going through the detector assembly, the difference in the responses must be due to the difference in the charge state distribution after scattering. This difference in the responses, as was mentioned previously, was seen for each isotope when examined at the same corresponding energy values found at the pairs of experimental runs mentioned in the experimental section above.

To further confirm that there is indeed a difference in the charge state distributions, figure 83 shows the response of the second TFD to ^{74}Se ions that were plotted with the same velocity selection that was mentioned above. As would be expected, the peaks of the response are closer to each other when compared to the distance between the two peaks in figure 82. This is explained by the fact that the two ion species with two different charge state distributions are approaching an equilibrium charge state. Figure 84 shows the response of the third TFD to the same two ions with the same velocity selection as before. Here the peaks completely overlap indicating that charge state equilibrium has been established. This result also suggests that for ions having masses near the lower end of the fission fragment mass curve and comparable energies to fission fragments, charge state equilibrium does not occur until passing through approximately 700 $\mu g/cm^2$ of NE-102A.

This difference in charge state distributions seems strange at first glance since previous experiments [105,106] had shown that when scattering off high Z targets, an equilibrium charge distribution was achieved which was independent of the charge

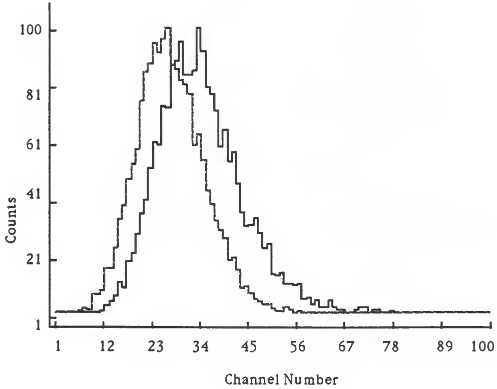

Figure 83. Charge distribution of ^{74}Se ions after scattering and after passing through the first TFD. This response is from the second TFD showing the peaks coming closer together when compared to the previous spectrum. The 61.4 MeV ions are again shown to the left.

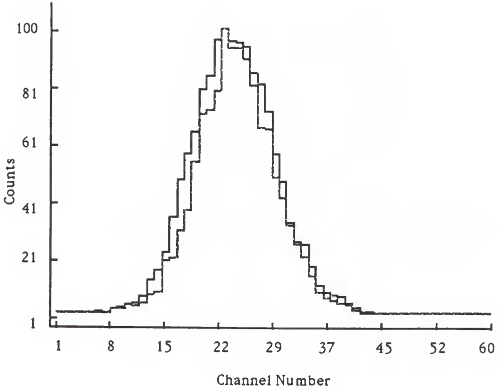

Figure 84. Charge distribution of the ^{74}Se ions shown after scattering and after passing through the first two TFD's. The response, as measured by the third TFD with the velocity selection mentioned in the text, shows the peaks overlapping indicating that the ions have achieved an equilibrium charge state.

state of the incoming ion. It was also shown that once the K shell was penetrated, the outgoing charge was independent of the impact parameter.

The results of this experiment, however can be qualitatively explained using the dynamic screening model [111] and the compound atom model [112]. It should be remembered that the TFD cannot make a precise measurement of the charge state of an ion as is usually done with analyzing magnets. Therefore such information cannot be derived from this experiment for direct comparison to theory, but the difference that is seen in the charge state distributions is readily apparent.

First a calculation was made using simple Rutherford scattering to determine the impact parameter and confirm that the K electron shell was penetrated. Using a screened potential would have been better but a simple calculation gave a rough approximation for the confirmation. The distance of closest approach was found to be 210 fm for the low energy case whereas the K shell radius of the gold target was found to be 1409 fm. Thus K shell penetration was confirmed. Table 2 lists the impact parameters and distances of closest approach for each experimental run that was performed as mentioned in chapter 2.

When using the dynamic screening model to calculate the average charge states of the 81.9 MeV and the 61.4 MeV ^{74}Se ion scattered off gold, values of 15.5 and 14.1 are obtained, respectively. What was interesting in the calculation using this model was that the first term in equation 24 was a number much less than one. This first term includes a factor $q_1(0)$, which is the

Table 2. The impact parameter (b) and distance of closest approach (d) is listed for each experimental run performed in the experiment described in chapter 2 using the Rutherford scattering equations.

Run Number	Ion	Energy (MeV)	b (fm)	d (fm)
1	^{70}Ge	154.1	59.75	77.87
2	^{74}Ge	163.8	57.03	74.32
3	^{76}Ge	168.7	55.83	72.76
4	^{70}Ge	77.05	119.5	155.7
5	^{74}Ge	81.90	114.1	148.7
6	^{76}Ge	84.40	111.6	145.4
7	^{70}Ge	57.80	159.3	207.6
8	^{74}Ge	61.43	152.1	198.2
9	^{76}Ge	63.26	148.8	193.9
10	^{74}Se	163.8	60.61	78.99
11	^{76}Se	168.7	95.30	77.28
12	^{74}Se	81.90	121.2	158.0
13	^{76}Se	84.40	118.5	154.4
14	^{74}Se	61.43	161.6	210.6
15	^{76}Se	63.26	158.1	206.0
16	^{74}Se	122.86	80.80	105.3
17	^{76}Se	126.53	79.04	103.0
18	^{74}Se	53.24	186.5	243.0
19	^{76}Se	54.83	182.4	237.7

original charge state of the ion before scattering, so this model would seem to indicate the unimportance of $q_1(0)$ to the final charge distribution.

Using the compound atom model, the average charge states were found to be 19.6 and 17.7 for 81.9 MeV and 61.4 MeV ^{74}Se , respectively. Here there was a slight change made in the calculations from that of the original model. In the model, the cutoff velocity u_c was taken as 2v (equation 29), or twice the collision velocity. The authors pointed out that this cutoff velocity could be left as a free parameter [113]. It was also easier to define a cutoff for second row elements where there is a big gap between K and L shell energy values, as was the case when modeling the previous experiments [105-112].

In this experiment, the energy levels of the electrons are much more closely spaced since the species in question are heavier projectiles and targets. That's why the cutoff velocity, u_c was taken as being equal to v, the collision velocity. This gave a more reasonable value of $Z(u_c)$ in the subsequent calculation.

Nevertheless, the calculations did reveal two important points. The first was that a difference in charge states was predicted and as was seen in the experiment. The second was the dependence of the final average charge to the collision velocity. The dominant term of equation 31 is $Z_1(u_c)$, which turned out to be two orders of magnitude greater than the other term, N_1. This shows the importance of being able to define a cutoff velocity, u_c, with much better accuracy.

Since the original goal of this experiment was to test the response of the 3TFD-SBD assembly to selected accelerated heavy ions, it is unfortunate that actual values of the charge state distributions of the ions were not made. This seems to be the first experiment that has been done that has some charge state information for heavy ions scattered off a solid target. There is a general lack of experimental information concerning charge states of ions scattered at large angles. Such information would help in providing tests for the few models which are available.

CHAPTER 5
SUMMARY

The characteristics of the charge state distributions of Se and Ge ions scattered at large angles were examined. The instrument used was a 3 TFD-SBD assembly. While precise values of the charge states were not measured, some information was possible to obtain.

The experiment that was performed was actually for the purpose of testing the 3TFD-SBD assembly for use as a nuclear charged particle detector. The charge state information came out of the analysis of these tests. Therefore the material that was presented in chapter 4 was an extension of the results of the tests which were presented in chapter 2.

Chapter 1 was a review of the state of charged particle detectors in general and also a review of past performances of thin film detectors. While the TFD has been previously used, mainly for timing information, little quantitative information exists as to its performance as a nuclear Z detector, and no information exists as to its performance with a stack of other TFD's. Chapter two examined the 3TFD-SBD performance to various accelerated ions while chapter 3 examined the response to fission fragments.

The response characteristics of the 3TFD-SBD detector to low energy Ge and Se ions as well as to ^{252}Cf fission fragments has been examined. The energy range of interest was that below 2 MeV/amu and especially below 1 MeV/amu. These are the typical energies that fission fragments possess and Ge and Se ions lie at the low mass end of a typical fission product distribution. An energy of 1 MeV/amu is also at the energy range that is expected of typical reaction products in deep inelastic reactions. The knowledge of the TFD-SBD performance at the low energies examined in the experiments discussed in the previous two chapters will be of use should it be used for particle identification for an in-beam experiment.

It was found that it was difficult to distinguish between the various Ge and Se isotopes studied in the experiment. Thus it was clearly indicated that the mass of the ion shows no effect on the scintillation process of the TFD. The Ge ions varied by as much as six mass units in the experiment described in chapter 2. Thus velocity and nuclear charge of the ion are the only two parameters which will determine the response of a particular TFD.

The charge state of the ion seems to play a significant role on the TFD response at low energies. At energies below 1 MeV/amu, the energy loss experienced by adjacent Z ions are nearly equal. As was pointed out in chapter 4, with two ions of the same atomic number, the same mass and velocity but different charge states, the TFD response was significantly different.

What is interesting to note is that the Se ions at the extreme low energy (0.75 MeV/amu) were of also low charge state (+4) passing through the accelerator magnets. It was surprising the ions that were scattered 30° into the detector assembly passed through the first two films before charge equilibrium was established. The thickness of the first TFD was found to be 0.337 mg/cm^2, and the the second TFD was found to be 0.367 mg/cm^2 thick. The sum of these two thicknesses, approximately 0.700 mg/cm^2, gives an approximate value for the equilibrium thickness of NE-102A for the conditions mentioned.

It was also shown that width of the response of the TFD could not be reduced significantly by selecting on the ion velocity. It was however possible to create a peak whose shape was more that of a gaussian distribution when making a velocity selection. Narrow gates of about 600 ps in width were chosen in the TOF response and the corresponding TFD response was plotted. It was shown that in this manner, the width of the TFD response was about the same compared to the original response. This was probably due to the fact that the time resolution of the detector was greater than the time cut used. Thus it would be very difficult to select events based on the time response with the present design.

This response was however further narrowed by using the response of each successive TFD to reject events in the first TFD response if that response deviated from the corresponding response of each of the other two TFD's. In one case, events were selected from the first TFD only if they corresponded to no more than a 10% variance in the relative responses from the other two TFD's. In the other case, events were selected from the first TFD only if they corresponded to no more than a 5% variance in the corresponding response from the other two TFD's. Thus events that created large variances between the relative pulse heights from the three detectors were eliminated. For ^{70}Ge at 2.0 MeV/amu, a reduction of 54% in the peak width at FWHM is seen when using all three TFD's and rejecting events outside a 10% variance in the response. For ^{74}Se at 1.0 MeV/amu, a reduction by 40% is seen when rejecting events outside a 5% variance in all three TFD's. Thus while a single TFD may not show the best resolution, using the combination of three TFD's to reject large variances in the response can improve the resolution using the scheme described or using a similar one.

Values of $\Delta L/L$ could also be determined from the results. For the ^{70}Ge ions having initial beam energy of 154 MeV, $\Delta L/L$ for the first TFD was found to be 30.96%. With the above mentioned reduction in the width (using all three TFD's), $\Delta L/L$ was 14.16%. For the ^{74}Se ions at initial beam energy of 81.9 Me, $\Delta L/L$ was determined to be 32.91% and with the reduced width it was found to be 19.31%. These values can be compared to the value of 12% obtained from a particular gas detector [113] whose response to 30 MeV ^{16}O was measured.

The time resolution of the detector for the TOF as measured between the first TFD and third TFD was found to be 807 ps. While this is a relatively high value when compared to typical time responses of carbon foils (95 ps [114]) and gas ionization chambers (with responses as low as 135 ps [16]) with closely spaced electrode plates, this compares to large solid angle gas ionization chambers having typical time resolutions on the order of 1 ns. Time resolution could conceivably be improved somewhat by using faster scintillator foils and faster PM tubes. NE-111 scintillators show a faster decay time compared to NE-102A and time resolutions of 300 ps have been observed [115, 116]. Smaller PM tubes also show faster response compared to RCA 8850 but their ability to collect light is not as good as that of the RCA 8850. Therefore a large reduction in time resolution with this particular design is not probable.

The best way to improve the time resolution is to improve the light collection characteristics with a better design. Some possibilities include larger films, possibly tilted at an angle to the faces of the two opposing PM tubes. Another possibility would be a different surface of the surrounding chamber. Improvements are possible since faster time responses have been reported [116]. Improved light collection would also improve the $\Delta L/\Delta x$ response thereby improving the capability of Z determination.

The experiment described in chapter 3 directly compares the performance of a single TFD to that of other particle detectors. The response of the TFD to ^{252}Cf fission fragments was examined in coincidence with the prompt fragment γ-rays. This technique and a similar technique have been used to determine the nuclear charge resolving power ($Z/\Delta Z$) of various detectors. The detector response that was in coincidence with particular γ peaks was examined to determine the position and width of particular fragments. The resolving power of the TFD was found to be about 25.2 which again compares to a gas ionization chamber tested in the same manner [79]. Due to the low statistics involved in the data, only two fragment peaks were able to be identified, but they were sufficient to determine $Z/\Delta Z$ within an error of ± 4.4. No information was able to be obtained from the TOF data mainly due to the low statistics and possibly also due to the relatively poor time resolution of the detector found in the previous experiment.

Chapter 4 examined the cause of the result of having two different charge states for scattered ions that had the same atomic number, mass and same velocity after scattering. This was qualitatively explained using both the dynamic screening model (DSM) and the compound atom model (CAM). The calculations done using the DSM showed the independence of the final average charge state to the initial ion charge state. The CAM best explained the experimental results by showing the strong dependence of the collision velocity to the final average charge state. The difference between the values of the final average charge states that were derived using the two different models (15.5 for 81.9 MeV 74Se and 14.1 for 61.4 MeV 74Se using DSM and 19.6 and 17.7 using CAM) shows that there is not a complete understanding of the situation when it comes to charge exchange in small impact parameter collisions. Both models were developed from information based upon experiments done with lighter ions such as carbon and nitrogen scattering off low Z targets and both models reproduced the data quite well. But the heavy ion case, as shown in this experiment, shows a discrepancy between the two models. There indeed is a need for more information that can only be obtained by further experimentation.

APPENDIX A
GUIDE TO THE USER OF A TFD

This appendix is meant to serve as a guide for any reader wanting to use a TFD as a particle identifier. It will include conclusions drawn from the results presented in this text as well as thoughts from the author with some suggestions about how to proceed with any experiments.

There are two main conclusions that were presented in this text. The first conclusion was that the TFD can be used as a detector whose purpose is to identify the nuclear charge Z of an ion. The experimental results showed that the nuclear charge resolving power $\Delta Z/Z$ was about as good as most average gas ionization chambers that are routinely used as Z detectors. The second conclusion was that the design of the 3TFD-SBD can be improved since the time response of the TFDs was not as good as reported by others who have studied the time resolution of TFDs. With these conclusions in mind, the following are some suggestions on proceeding should one become interested in using a TFD.

First one should browse through pertinent literature material that has been listed in the reference chapter. One of the first references to read would be the one describing the fabrication of a TFD [33] while remembering the description in this text on modifications in the method of fabrication. This reading material is important since anyone wanting to use a TFD should be able to make one with whatever thickness one chooses. This should be easy once one becomes familiar with the art of making a thin film.

To choose a thickness for a specific purpose, one would have to first read about experiments that were performed that measured the response of the TFD as a function of the thickness [45,117]. Also of importance in both choosing a thickness and comparing experimental results with other published work is the luminescence efficiency $\Delta L/\Delta E$. This was also shown to vary with detector thickness [117] so this parameter must be kept in mind. To obtain values of luminescence efficiency, the experimental energy loss should be measured with any experiment performed. This unfortunately was not done for the experiments described in this text. There could have been some very useful information obtained in the case of the experiment described in chapter 2.

Once one has made a few TFDs, they may be tested using a ^{252}Cf fission fragment source. This will serve two purposes. The first purpose would be for one to become familiar with the use of the electonics and experimental set-up involved with a particle identifier (should one not be already familiar with this) and specifically with a TFD. The second purpose would be for a quick confirmation of the above mentioned characteristics of the light output and luminescence efficiency varying with detector thickness. These are simple experiments that can be performed "in house" where no accelerator site is needed and much useful information can be obtained on the expected performance of the TFD. Should one have a sufficiently strong ^{252}Cf source and a Ge detector, the experiment described in chapter 3 can be performed to obtain the nuclear charge resolving power of a particular TFD. The data is best recorded event-by-event on magnetic tape for the purpose of becoming familiar with the data analysis that needs to be performed with an experiment involving a particle detector (again for someone unfamiliar with these types of detectors).

The advantage of a multiple TFD design has been shown in this text so the testing of any TFD should be done with a design similar to the one described for the 3TFD-SBD. The relatively poor time resolution obtained for the 3TFD-SBD design suggests that improvements are possible since better values of time resolution have been obtained by others [118]. An improvement in the time resolution would seem possible with an improvement in the efficiency of the collection of photons at the photocathode. This would also improve the nuclear charge resolving power simply from the statistical considerations of collecting more photons per scintillation.

Some possible suggestions for improving the light collection include trying a mirrored surface inside the detector chamber as opposed to painting the surface with white reflective paint as was done with the 3TFD-SBD. The information available in the literature on the subject would be the best source for choosing a surface. Another suggestion would be to eliminate the quartz window between the TFD and the face of the PM tube to decrease the distance and thus the solid angle of the path of light travel. This however, might only show a minor improvement. Another possible improvement would be to change the angle between the face of the

TFD and the face of the PM tube from 90° to 45°. This might increase the error in the trajectory of the fragment path but it would increase the TFD area exposed directly to the face of the PM tube thus increasing the number of photons striking the photocathode. One might also consider a detector incorporating TFDs with a larger surface area coupled to larger PM tubes. Such a design has shown to give satisfactory results for use in-beam [119].

Another improvement that has been suggested by M. L. Muga would be to increase the light output of the detector itself. It has been suggested that since the TFD is so thin, the scinillation process involving the solute of a scintillator such as NE-102A, would not be the same as with the bulk material where a saturation level is reached in terms of light output as a function of solute concentration [120]. The thought is that if the solute concentration is increased, the TFD light output would also increase. One possible method to increase solute concentration (that has yet to be tried) would be to use a different solute. There has been much work performed in studying the properties of various scintillators in terms of their light output efficiency and resistance to radiation damage [121,122]. Thus a compound such as "F15" (which has the molecular structure of p-terphenyl with a methyl group attached to the two terminal phenyl groups) could conceivably be dissolved in a solution containing dissolved NE-102A and the resulting solution could then be irradiated and used for making TFDs. The light output from these TFDs could then be experimentally compared to the light output from ones of comparable thickness made by the standard method.

While these thoughts and comments have concentrated on improving a detector incorporating TFDs, it should also be remembered that the TFD is a particle detector and should be treated as such. Any method of analysis or experimental set-up that appears in the literature that involves a gas ionization chamber or any other particle detector can also be incorporated with a TFD. An example would be the use of two energy signals, one at high gain and one at low gain, that are used for gas ionization chambers. This method could have been used in the experiment described in chapter 2, where each PM tube would have had the slow response branched into two signals (high gain and low gain). This would have done away with the need for gain changes between experimental runs. Therefore anyone choosing to use a TFD should also be familiar with techniques for other detectors written in the literature. The interested reader should not only read material concerning detector development but should also read material concerning particle detector application to in-beam experiments. This would most certainly involve gas ionization detectors since they are the most commonly used detectors, but the applications would be the same for the TFD.

The reader should also keep in mind that while the results presented in this text might seem somewhat negative (especially in chapter 2), it should be remembered that the experiments were performed in an energy range that is difficult for any detector to distinguish between heavy ions with a two Z unit difference. Many applications involving particle detectors used in-beam involve light ions at a higher energy range, and in many cases the TFD would have an advantage over gas ionization detectors where high count rates are involved. With a particular application in mind, it should be possible to design a particle detector using TFDs that will perform as good as many other commonly used detectors.

APPENDIX B
PERTINENT CODES

The following is a FORTRAN code written by R. L. Coldwell to read data tapes from the experiment undertaken at HHIRF. This code was written to run on the IBM 3090-600J located at the NERDC in the University of Florida. The code was written assuming 14 parameters.

```
      CHARACTER*6 NAT(11)
      CHARACTER*30 NA
C*** 14 DATA PARAMETER INPUT TO IDOUT
      DIMENSION IDOUT(14)
C*** 11 PARAMETERS OUTPUT
      DIMENSION IMAX(11)
C*** DATA TO BE REDUCED TO 512 CHANNELS
      DIMENSION IMAT(11,512),IZM(52,52)
      DATA IZM/2704*0/
      DATA IMAX/11*512/,IMAT/5632*0/
      DATA NAT/'E SSDE','F TFDA','G TFDB','H TFDC',
     # 'I TIM1','J TIM2','K TIM3','L TIM4','M TIM5','N TIM6','O TIM7'/
      COMMON/MAXL/XA,XB,XC,PROBC,WAI,WBI,WCI
C*** RSEED SUBROUTINE LOCATED IN RANDOM FORTRAN
      CALL RSEED(2219681,62819691)
      WRITE(*,102)
102   FORMAT(' ENTER THE NUMBER OF EVENTS TO BE READ ',
     # 'OR -1 FOR ALL OF THEM')
      READ(*,*)NMEV
      IF(NMEV.LT.0)NMEV=200000000
      WRITE(*,107)
107   FORMAT(' ENTER THE BEGINNING TIME, ENDING TIME')
C***THE FIRST INPUT PARAMETER IS FOR TIME CUTS, THE SECOND
C*** FOR SSD CUTS AND THIRD FOR CUTS IN TFD RESPONSE
```

```
      READ(*,*)NBT,NET
      READ(*,*)AM1,AM2
      READ(*,*)ITFD1,ITFD2
      XMIN=0
      XMAX=512
      YMIN=0
      YMAX=512
      DO 100 I=1,NMEV
      CALL GEVENT(IDOUT,NDET,ISTOP)
C      WRITE(*,1999)(IDOUT(L),L=1,14),ISTOP
1999   FORMAT(' IDOUT,ISTOP',6I6)
      IF(ISTOP.EQ.1)GOTO 110
C*** IDOUT(12) WAS THE TIME RESPONSE BETWEEN
C*** PM 1 AND 5
      TTEST=(IDOUT(12)+RNDMF(1.))*.25
      ITEST=TTEST
      IF(ITEST.LT.NBT.OR.ITEST.GT.NET)GOTO 100
C*** IDOUT(1) WAS SSD
      SSDE=(IDOUT(1)+RNDMF(1.))*.0625
      IF(AM2.LT.0.)GOTO 25
      AM=SSDE
      IF(AM.LT.AM1.OR.AM.GT.AM2)GOTO 100
      ITFD=0.0625*IDOUT(2)
      IF(ITFD.LT.ITFD1.OR.ITFD.GT.ITFD2)GOTO 100
25     CONTINUE
      IM=AMIN1(512.,AMAX1(1.001,SSDE))
      IMAT(1,IM)=IMAT(1,IM)+1
C*** IDOUT(2-7) WERE PM RESPONSES FROM TFD'S WHICH
C*** HAD SIGNALS FROM OPPOSING PM TUBES SUMMED
C*** AND REDUCED FROMM 8192 CHANNELS TO 512
      DO 75 J=2,4
      JS=2*(J-1)
      JT=JS+1
      IF(J.EQ.15)JS=18
      CT=(IDOUT(JS)+IDOUT(JT)+RNDMF(1.))*.5
      IF(CT.GT.8193.)PRINT*,J,I,CT
      CT=CT/2048.
1183   IF(CT.GT.1.)GOTO 75
      IM=AMAX1(1.01,CT*IMAX(J))
      IF(CT.GT.512)GOTO 75
      IMAT(J,IM)=IMAT(J,IM)+1
75     CONTINUE
C*** IDOUT(8-13) WERE TIME RESPONSES FROM PMT'S
```

```
C*** WHICH WERE REDUCED FROM 4096 TO 512 CHANNELS
      DO 775 J=5,11
      JS=J+3
      IF(J.EQ.15)JS=18
      CT=IDOUT(JS)+RNDMF(1.)
      IF(CT.GT.8193.)PRINT*,J,I,CT
      CT=CT/2048.
      IF(CT.GT.1.)GOTO 775
      IM=AMAX1(1.01,CT*IMAX(J))
      IF(CT.GT.512)GOTO 775
      IMAT(J,IM)=IMAT(J,IM)+1
775   CONTINUE
C     WRITE(*,1234).0625*IDOUT(4),.0625*IDOUT(3),.0625*IDOUT(2)
1234   FORMAT(' DEBUG C1,C2,C3',3E14.6)
100   CONTINUE
110   CONTINUE
      DO 2020 JSPECT=1,11
      NA=NAT(JSPECT)//'.LEO'
      WRITE(*,'(1X,A)')NAT(JSPECT)
     IOUT=7+JSPECT
     IF(IOUT.EQ.11)IOUT=19
     INOUT=IMAX(JSPECT)
      WRITE(IOUT,'(20Z4)')(IMAT(JSPECT,I),I=1,INOUT)
2020   CONTINUE
      STOP
      END
      SUBROUTINE GEVENT(IDOUT,NDET,ISTOP)
      CHARACTER*1 CTEMP(8192),ANS
      INTEGER*2 ITEMP(4096),IHEAD,IMNUM
      DIMENSION IDOUT(10)
      CHARACTER*2 ITIT(64),IB(256),ICODE(160)
      EQUIVALENCE (ITEMP(1),CTEMP(1))
      DATA NC/0/,IEVFL/0/,IHEAD/Z8001/,
     # IMNUM/ZFFFF/,N1600/5/
C *** THE FIRST TAPE BLOCK IS 256, SECOND 5 ARE 1600, REST ARE
C*** 8192
C *** THESE FACTS MUST BE ESTABLISHED BY RUNNING DUMPTAPE
C*** ON THE FILES
C *** OF INTEREST
      IF(NC.GT.0)GOTO 1010
      ISTOP=0
      NC=1
     READ(11,101)(IB(I),I=1,128)
```

```
101  FORMAT(32A2)
   DO 10 I=1,64
10   ITIT(I)=IB(I)
   CALL TRAN(ITIT,128)
   DO 15 I=1,N1600
   DO 15 J=1,5
   READ(11,101)ICODE
15   CALL TRAN(ICODE,320)
55   READ(11,'(64A1)',END=600,ERR=550)CTEMP
     IIN=0
    ICOUNT=4096
C *** LOOKING FOR THE BEGINNING OF AN EVENT
     IF(IEVFL.EQ.1)GOTO 1040
1010   IIN=IIN+1
     IF(IIN.GT.ICOUNT)GOTO 55
C     WRITE(*,104)IIN,ITEMP(IIN)
104    FORMAT(I5,Z8)
     IF(ITEMP(IIN).NE.IHEAD)GOTO 1010
     IEVFL=1
     NDET=0
1040   IIN=IIN+1
     IF(IIN.GT.ICOUNT)GOTO 55
     IF(ITEMP(IIN).EQ.IMNUM)THEN
     IEVFL=0
     RETURN
     ENDIF
     NDET=NDET+1
     IDOUT(NDET)=ITEMP(IIN)
     GOTO 1040
550    WRITE(*,123)
123    FORMAT(' ABNORMAL STATUS ON TAPE INPUT')
600    WRITE(*,124)
124    FORMAT(' POSSIBLE END OF FILE'/' DO YOU WANT TO STOP?')
C     READ(*,107)ANS
     ANS='Y'
107    FORMAT(A1)
     IF(ANS.NE.'Y'.AND.ANS.NE.'Y')GOTO 55
     ISTOP=1
     RETURN
     END
    SUBROUTINE TRAN(IR,N)
    LOGICAL*1 IR(N),MASK(4)
    EQUIVALENCE (MA,MASK(1))
```

```
      DATA MA/0/
      DO 101 I=1,N
      MASK(4)=IR(I)
      IF(MA.LT.97.OR.MA.GT.122)GOTO 30
      IF(MA.GT.105)GOTO 10
      MA=MA+32
      GOTO 100
10    IF(MA.GT.114)GOTO 20
      MA=MA+39
      GOTO 100
20    MA=MA+47
      GOTO 100
30    IF(MA.LT.65.OR.MA.GT.90)GOTO 60
      IF(MA.GT.73)GOTO 40
      MA=MA+128
      GOTO 100
40    IF(MA.GT.82)GOTO 50
      MA=MA+135
      GOTO 100
50    MA=MA+143
      GOTO 100
60    IF(MA.LT.48.OR.MA.GT.57)GOTO 70
      MA=MA+192
      GOTO 100
70    IF(MA.LT.40.OR.MA.GT.43)GOTO 80
      IF(MA.EQ.41)MA=93
      IF(MA.EQ.42)MA=92
      IF(MA.EQ.43)MA=78
      GOTO 100
80    IF(MA.NE.47)GOTO 85
      MA=97
      GOTO 100
85    IF(MA.LT.58.OR.MA.GT.59)GOTO 99
      IF(MA.EQ.58)MA=122
      IF(MA.EQ.59)MA=94
      GOTO 100
99    MA=64
100   IR(I)=MASK(4)
101   CONTINUE
      WRITE(6,106)(IR(I),I=1,N)
106   FORMAT(1X,80A1)
      RETURN
      END
```

The following is a FORTRAN code written by R. L. Coldwell for the purpose of reading data tapes on the IBM 3090-600J that were written from the LeCroy 3500. Four data parameters are assumed

```
      CHARACTER*6 NAT(11)
      CHARACTER*30 NA
      CHARACTER*1 CTEMP(2048),C1,ANS
      CHARACTER*2 ITIT(64),IB(1024)
      INTEGER ITEMP(2048)
      INTEGER*2 IHEAD,IMNUM
      INTEGER BLOCKSIZE
      DIMENSION IDOUT(4,164)
      DIMENSION IBGC(4),IEGC(4)
      DIMENSION IDID(656)
      DIMENSION IMAX(4),A(4),B(4)
      DIMENSION IMAT(3,512),IIMAT(1,4096)
      DATA IMAX/3*512/,IMAT/8192*0/
      DATA IIMAX/1*4096/,IIMAT/4096*0/
      DATA NAT/'E TFD1','F TIM1','G TIM2','H GAMM'/
      COMMON/MAXL/XA,XB,XC,PROBC,WAI,WBI,WCI
      EQUIVALENCE (ITEMP(1),CTEMP(1))
      CALL ERRSET(212,255,255)
      CALL RSEED(2219681,62819691)
      WRITE(*,102)
102     FORMAT(' ENTER THE NUMBER OF BLOCKS TO BE READ ',
     # ' OR -1 FOR ALL OF THEM')
      READ(*,*)NMBL
      IF(NMBL.LT.0)NMBL=200000000
      WRITE(*,107)
107     FORMAT(' ENTER THE BEGINNING GAMMA CUT, ',
     # ' ENDING GAMMA CUT')
      READ(*,*)IBGC(1),IEGC(1)
      XMIN=0
      XMAX=512
      YMIN=0
      YMAX=512
      NBL=0
      BLOCKSIZE=2061
      READ(11,'(32A2)')(IB(I),I=1,512)
      DO 18 I=1,64
18      ITIT(I)=IB(I)
      CALL TRAN(ITIT,512)
55      READ(11,'(16(128A1))',END=600,ERR=550)CTEMP
      NBL=NBL+1
C      PRINT*,NBL
453     FORMAT(' NBL=')
      CALL CONV(ITEMP,IDOUT)
C      WRITE(6,'(32Z2)')IDOUT
C      PRINT*, IDOUT
      DO 775 J=1,164
      DO 75 K=1,4
      CT=(IDOUT(K,J)+RNDMF(1.))*.0625
C      WRITE(6,*)K,J,CT
      IF(CT.GT.512)PRINT*,K,J,CT
      IM=CT
C      CT=CT/2048
1183    IF(IM.EQ.0.OR.IM.GT.512)GOTO 75
      IF(K.EQ.1)ITFD=CT
      IF(K.EQ.2)ITMA=CT
      IF(K.EQ.3)ITMB=CT
      IF(K.EQ.4)THEN
        IGAM=CT*8
      ENDIF
      IMAT(K,IM)=IMAT(K,IM)+1
      IIMAT(1,IGAM)=IIMAT(1,IGAM)+1
75      CONTINUE
775     CONTINUE
      IF(NBL.EQ.NMBL)GOTO 600
      GOTO 55
550     WRITE(*,123)
123     FORMAT(' ABNORMAL STATUS ON TAPE INPUT')
600     WRITE(*,124)
124     FORMAT(' POSSIBLE END OF FILE'/' DO YOU WANT TO STOP?')
      ANS='Y'
      WRITE(6,*)NBL
      IF(ANS.NE.'Y'.AND.ANS.NE.'Y')GOTO 55
      DO 2020 JSPECT=5,8
      NA=NAT(JSPECT)//'.LEO'
      WRITE(*,'(1X,A)')NAT(JSPECT)
     IOUT=3+JSPECT
     IF(IOUT.GE.11)IOUT=4+JSPECT
     INOUT=IMAX(JSPECT)
     WRITE(IOUT,'(20Z4)')(IMAT(JSPECT,I),I=1,INOUT)
2020  CONTINUE
     INOUT=IIMAX(1)
     WRITE(13,'(20Z4)')(IIMAT(1,I),I=1,IIMAX)
     STOP
     END
    SUBROUTINE TRAN(IR,N)
    LOGICAL*1 IR(N),MASK(4)
    EQUIVALENCE (MA,MASK(1))
    DATA MA/0/
    DO 101 I=1,N
    MASK(4)=IR(I)
    IF(MA.LT.97.OR.MA.GT.122)GOTO 30
    IF(MA.GT.105)GOTO 10
    MA=MA+32
    GOTO 100
10   IF(MA.GT.114)GOTO 20
    MA=MA+39
    GOTO 100
20   MA=MA+47
    GOTO 100
30   IF(MA.LT.65.OR.MA.GT.90)GOTO 60
    IF(MA.GT.73)GOTO 40
    MA=MA+128
    GOTO 100
40   IF(MA.GT.82)GOTO 50
    MA=MA+135
    GOTO 100
50   MA=MA+143
    GOTO 100
60   IF(MA.LT.48.OR.MA.GT.57)GOTO 70
    MA=MA+192
    GOTO 100
70   IF(MA.LT.40.OR.MA.GT.43)GOTO 80
    IF(MA.EQ.41)MA=93
    IF(MA.EQ.42)MA=92
    IF(MA.EQ.43)MA=78
    GOTO 100
80   IF(MA.NE.47)GOTO 85
    MA=97
    GOTO 100
85   IF(MA.LT.58.OR.MA.GT.59)GOTO 99
    IF(MA.EQ.58)MA=122
```

```
      IF(MA.EQ.59)MA=94
      GOTO 100
99    MA=64
100   IR(I)=MASK(4)
101   CONTINUE
      WRITE(6,106)(IR(I),I=1,N)
106   FORMAT(1X,80A1)
      RETURN
      END
      SUBROUTINE CONV(ITRED,IDOUT)
      LOGICAL*1 ITRED(2048)
      LOGICAL*4 LBYTE
      EQUIVALENCE (LBYTE,IBBYTE)
      INTEGER IDOUT(656),IBYTE(3)
      ICOUNT=1
      IB=1
      IOUT=1
25    LBYTE=ITRED(ICOUNT)
      IBYTE(IB)=IBBYTE
      IF(IBYTE(IB).LT.0)IBYTE(IB)=256+IBYTE(IB)
      IB=IB+1
      IF(IB.LE.2)GOTO 28
      ITEMP=IBYTE(2)
      ITEMP=IBYTE(1)+256*ITEMP
      IDOUT(IOUT)=ITEMP
      IOUT=IOUT+1
      IF(IOUT.GE.656)GOTO 75
      IB=1
28    ICOUNT=ICOUNT+1
      N20=ICOUNT/512
      ICM=ICOUNT-184*N20
      IF(ICM.EQ.328*(ICM/328))ICOUNT=ICOUNT+184
      IF(ICOUNT.LE.2048)GOTO 25
75    CONTINUE
      RETURN
      END
```

The following is a FORTRAN code similar to the first one found in this Appendix except that the purpose of this one is to reduce the TFD response from the first film by using the responses from the other films.

```
      CHARACTER*6 NAT(11)
      CHARACTER*30 NA
      DIMENSION IDOUT(14)
      DIMENSION IMAX(11)
      DIMENSION IMAT(11,512),IZM(52,52)
      DATA IZM/2704*0/
      DATA IMAX/11*512/,IMAT/5632*0/
      DATA NAT/'E SSDE','F TFDA','G TFDB','H TFDC',
     # 'I TIM1','J TIM2','K TIM3','L TIM4','M TIM5','N TIM6','O TIM7'/
      COMMON/MAXL/XA,XB,XC,PROBC,WAI,WBI,WCI
      CALL RSEED(2219681,62819691)
      WRITE(*,102)
102    FORMAT(' ENTER THE NUMBER OF EVENTS TO BE READ ',
     # 'OR -1 FOR ALL OF THEM')
      READ(*,*)NMEV
      IF(NMEV.LT.0)NMEV=200000000
      WRITE(*,107)
107    FORMAT(' ENTER THE BEGINNING TIME, ENDING TIME')
      READ(*,*)NBT,NET
      READ(*,*)AM1,AM2
      READ(*,*)ITFD1,ITFD2
C*** THE CHANNEL NUMBERS OF THE LOWEST AND HIGHEST
C*** RESPONSE FROM EACH TFD IS ENTERED TO NORMALIZE
C*** THE PEAK WIDTH
      READ(*,*)LTFA,HTFA,LTFB,HTFB,LTFC,HTFC
C*** TWO VALUES FOR PERCENT DIFFERENCES IN THE RESPONSE
C*** BETWEEN TFD'S
      READ(*,*)TOL1,TOL2
      XMIN=0
      XMAX=512
      YMIN=0
      YMAX=512
      DO 100 I=1,NMEV
      CALL GEVENT(IDOUT,NDET,ISTOP)
```

```
C     WRITE(*,1999)(IDOUT(L),L=1,14),ISTOP
1999  FORMAT(' IDOUT,ISTOP',6I6)
      IF(ISTOP.EQ.1)GOTO 110
      TTEST=(IDOUT(12)+RNDMF(1.))*.25
      ITEST=TTEST
      IF(ITEST.LT.NBT.OR.ITEST.GT.NET)GOTO 100
      TFIVE=(IDOUT(12)+RNDMF(1.))
      TSIX=(IDOUT(13)+RNDMF(1.))+60
      IF(TFIVE.GT.TSIX)DFFVSX=TFIVE-TSIX
      IF(TFIVE.LE.TSIX)DFFVSX=TSIX-TFIVE
      IF(DFFVSX.GT.5)GOTO 100
      SSDE=(IDOUT(1)+RNDMF(1.))*.0625
      IF(AM2.LT.0.)GOTO 25
      AM=SSDE
      IF(AM.LT.AM1.OR.AM.GT.AM2)GOTO 100
      ITFD=0.0625*IDOUT(2)
      IF(ITFD.LT.ITFD1.OR.ITFD.GT.ITFD2)GOTO 100
25     CONTINUE
C      IM=AMIN1(512.,AMAX1(1.001,SSDE))
C      IMAT(1,IM)=IMAT(1,IM)+1
      DO 75 J=2,7
C      JS=2*(J-1)
C      JT=JS+1
C      IF(J.EQ.15)JS=18
C      CT=(IDOUT(JS)+IDOUT(JT)+RNDMF(1.))*.5
      CT=(IDOUT(J)+RNDMF(1.))
      IF(CT.GT.8193.)PRINT*,J,I,CT
      CT=CT/2048.
1183  IF(CT.GT.1.)GOTO 75
      IM=AMAX1(1.01,CT*IMAX(J))
      IF(CT.GT.512)GOTO 75
      K=J-1
      IMAT(K,IM)=IMAT(K,IM)+1
75     CONTINUE
      DO 775 J=1,3
      JS=2*J
      JT=JS+1
C      IF(J.EQ.15)JS=18
      CT=(IDOUT(JS)+IDOUT(JT)+RNDMF(1.))*.5
C      IF(J.EQ.2)CT=CT*0.8667+13.8*4
C      IF(J.EQ.3)CT=CT*0.8553+6.684*4
C *** THE FOLLOWING FACTORS NORMALIZE THE WIDTH OF THE
C*** PEAKS
```

```
      IF(J.EQ.2)CT=CT*0.84615+23.4615*4
      IF(J.EQ.3)CT=CT*1.0476+17.095*4
      IF(CT.GT.8193.)PRINT*,J,I,CT
      CT=CT/2048.
      IF(CT.GT.1.)GOTO 775
      IM=AMAX1(1.01,CT*IMAX(J))
      IF(CT.GT.512)GOTO 775
C      IMAT(J,IM)=IMAT(J,IM)+1
      IF(J.EQ.1)THEN
        TFA=IM
        IMAT(7,TFA)=IMAT(7,TFA)+1
      ENDIF
      IF(J.EQ.2)TFB=IM
      IF(J.EQ.3)TFC=IM
775     CONTINUE
      IF(TFA.LT.LTFA.OR.TFA.GT.HTFA)GOTO 100
      IF(TFB.LT.LTFB.OR.TFB.GT.HTFB)GOTO 100
      IF(TFC.LT.LTFC.OR.TFC.GT.HTFC)GOTO 100
      PNTA=(TFA-LTFA)/(HTFA-LTFA)
      PNTB=(TFB-LTFB)/(HTFB-LTFB)
      PNTC=(TFC-LTFC)/(HTFC-LTFC)
      IF(PNTA.GE.PNTB)DIFFA=PNTA-PNTB
      IF(PNTA.LT.PNTB)DIFFA=PNTB-PNTA
      IF(PNTA.GE.PNTC)DIFFC=PNTA-PNTC
      IF(PNTA.LT.PNTC)DIFFC=PNTC-PNTA
      PERA=DIFFA
      PERC=DIFFC
C *** THE FOLLOWING IS THE PROCESS OF REJECTING EVENTS
C *** THAT FALL OUTSIDE THE YSER SPECIFIED LIMITS
      IF(PERA.LE.TOL1)THEN
        IMAT(8,TFA)=IMAT(8,TFA)+1
        IF(PERC.LE.TOL1)IMAT(10,TFA)=IMAT(10,TFA)+1
      ENDIF
      IF(PERA.LE.TOL2)THEN
        IMAT(9,TFA)=IMAT(9,TFA)+1
        IF(PERC.LE.TOL2)IMAT(11,TFA)=IMAT(11,TFA)+1
      ENDIF
C      WRITE(*,1234).0625*IDOUT(4),.0625*IDOUT(3),.0625*IDOUT(2)
1234    FORMAT(' DEBUG C1,C2,C3',3E14.6)
100     CONTINUE
110     CONTINUE
      DO 2020 JSPECT=1,11
      NA=NAT(JSPECT)//'.LEO'
      WRITE(*,'(1X,A)')NAT(JSPECT)
     IOUT=7+JSPECT
     IF(IOUT.EQ.11)IOUT=19
     INOUT=IMAX(JSPECT)
      WRITE(IOUT,'(20Z4)')(IMAT(JSPECT,I),I=1,INOUT)
2020  CONTINUE
      STOP
      END
      SUBROUTINE GEVENT(IDOUT,NDET,ISTOP)
      CHARACTER*1 CTEMP(8192),ANS
      INTEGER*2 ITEMP(4096),IHEAD,IMNUM
      DIMENSION IDOUT(10)
      CHARACTER*2 ITIT(64),IB(256),ICODE(160)
      EQUIVALENCE (ITEMP(1),CTEMP(1))
      DATA NC/0/,IEVFL/0/,IHEAD/Z8001/,
     # IMNUM/ZFFFF/,N1600/5/
C *** THE FIRST TAPE BLOCK IS 256, SECOND 5 ARE 1600,
C*** REST ARE 8192
C *** THESE FACTS MUST BE ESTABLISHED BY RUNNING
C*** DUMPTAPE ON THE FILES
C *** OF INTEREST
      IF(NC.GT.0)GOTO 1010
      ISTOP=0
      NC=1
     READ(11,101)(IB(I),I=1,128)
101   FORMAT(32A2)
     DO 10 I=1,64
10    ITIT(I)=IB(I)
     CALL TRAN(ITIT,128)
     DO 15 I=1,N1600
     DO 15 J=1,5
     READ(11,101)ICODE
15    CALL TRAN(ICODE,320)
55    READ(11,'(64A1)',END=600,ERR=550)CTEMP
      IIN=0
     ICOUNT=4096
C *** LOOKING FOR THE BEGINNING OF AN EVENT
      IF(IEVFL.EQ.1)GOTO 1040
1010   IIN=IIN+1
      IF(IIN.GT.ICOUNT)GOTO 55
C      WRITE(*,104)IIN,ITEMP(IIN)
104    FORMAT(I5,Z8)
      IF(ITEMP(IIN).NE.IHEAD)GOTO 1010
      IEVFL=1
      NDET=0
 1040   IIN=IIN+1
      IF(IIN.GT.ICOUNT)GOTO 55
      IF(ITEMP(IIN).EQ.IMNUM)THEN
      IEVFL=0
      RETURN
      ENDIF
      NDET=NDET+1
      IDOUT(NDET)=ITEMP(IIN)
      GOTO 1040
550     WRITE(*,123)
123     FORMAT(' ABNORMAL STATUS ON TAPE INPUT')
600     WRITE(*,124)
124     FORMAT(' POSSIBLE END OF FILE'/' DO YOU WANT TO STOP?')
C     READ(*,107)ANS
      ANS='Y'
107     FORMAT(A1)
      IF(ANS.NE.'Y'.AND.ANS.NE.'Y')GOTO 55
      ISTOP=1
      RETURN
      END
    SUBROUTINE TRAN(IR,N)
    LOGICAL*1 IR(N),MASK(4)
    EQUIVALENCE (MA,MASK(1))
    DATA MA/0/
    DO 101 I=1,N
    MASK(4)=IR(I)
    IF(MA.LT.97.OR.MA.GT.122)GOTO 30
    IF(MA.GT.105)GOTO 10
    MA=MA+32
    GOTO 100
10    IF(MA.GT.114)GOTO 20
    MA=MA+39
    GOTO 100
20    MA=MA+47
    GOTO 100
30    IF(MA.LT.65.OR.MA.GT.90)GOTO 60
    IF(MA.GT.73)GOTO 40
    MA=MA+128
    GOTO 100
40    IF(MA.GT.82)GOTO 50
    MA=MA+135
```

```
      GOTO 100
50    MA=MA+143
      GOTO 100
60    IF(MA.LT.48.OR.MA.GT.57)GOTO 70
      MA=MA+192
      GOTO 100
70    IF(MA.LT.40.OR.MA.GT.43)GOTO 80
      IF(MA.EQ.41)MA=93
      IF(MA.EQ.42)MA=92
      IF(MA.EQ.43)MA=78
      GOTO 100
80    IF(MA.NE.47)GOTO 85
      MA=97
      GOTO 100
85    IF(MA.LT.58.OR.MA.GT.59)GOTO 99
      IF(MA.EQ.58)MA=122
      IF(MA.EQ.59)MA=94
      GOTO 100
99    MA=64
100   IR(I)=MASK(4)
101   CONTINUE
      WRITE(6,106)(IR(I),I=1,N)
106   FORMAT(1X,80A1)
      RETURN
      END
```

The following is a FORTRAN code written for the purpose of calculating initial velocities of ^{74}Se ions before impinging the the first TFD. The code was written for running on a VAX.

```
C *** THE FUNCTIONS FUNC AND FUNCTOO ARE POLYNOMIAL
C *** FITS TO THE DATA OF NORTHCLIFFE AND SCHILLING
C *** FOR ENERGY LOSS SE IONS GOING THROUGH NE 102 PLASTIC
      EXTERNAL FUNC,FUNCTOO
      WRITE(6,106)
106     FORMAT(' ENTER THE TOF CHANNEL NUMBER.')
      READ(*,*)CHAN
C *** THE FOLLOWING EQUATION WAS DERIVED FROM THE
C *** TOF CALIBRATION OF THE EXPERIMENT
      TIME=.204*CHAN-27.405
      WRITE(6,126)
126     FORMAT(' ENTER A TOLERANCE VALUE')
      READ(*,*)TOL
C *** THE INITIAL GUESS MADE TO THE TOF
      GTIME=TIME/2
      ATIME=GTIME
C *** VELOCITY BASED ON A FLIGHT DISTANCE OF 8.255 CM
343     AVEL=8.255/ATIME
C *** ENERGY CALCULATED IN MEV
      AENERG=(((1.228696E-25)/2)*((1.0E7)*AVEL)**2)/1.6021E-13
C *** THE ENERGY RANGE OF THE FITTED FUNCTIONS
      AHI=128.1281
      ALO=0.4256525
      IF(AENERG.GT.AHI.OR.AENERG.LT.ALO)WRITE(6,350)AENERG
350     FORMAT(' ENERGY IS OUT OF BOUNDS',F12.8)
      CALL FUNC(AENERG,BENERG)
      BHI=167.7276
      BLO=3.372861
      IF(BENERG.GT.BHI.OR.BENERG.LT.BLO)WRITE(6,350)BENERG
      BVEL=SQRT(2*BENERG*(1.6021E-13)/(1.228696E-25))
      BVEL=(1.0E-7)*BVEL
      BTIME=8.255/BVEL
      ATCALC=ATIME+BTIME
      WRITE(6,*)ATCALC,BTIME
      IF(TIME.LT.ATCALC)ERR=2*(ATCALC-TIME)/(ATCALC+TIME)
      IF(TIME.GT.ATCALC)ERR=2*(TIME-ATCALC)/(ATCALC+TIME)
      IF(ERR.LT.TOL)GOTO 600
      IF(ATCALC.LT.TIME)ATIME=(TIME-ATCALC)/2+ATIME
      IF(ATCALC.GT.TIME)ATIME=ATIME-(ATCALC-TIME)/2
      GOTO 343
600     WRITE(6,*)TIME,ATCALC,ERR
      WRITE(6,*)AENERG,BTIME,BVEL
      CALL FUNCTOO(BENERG,AINITEN)
      AINITVEL=SQRT(2*AINITEN*(1.6021E-13)/(1.228696E-25))
      AINITVEL=(1.0E-7)*AINITVEL
      WRITE(6,614)AENERG,AVEL,BVEL
614     FORMAT(' ENERGY OUT OF FILM B IS ',F12.8/
     # ' VELOCITY OUT OF FILM B IS',F12.8/
     # ' VELOCITY OUT OF FILM A IS',F12.8)
      WRITE(6,624)BENERG,AINITEN,AINITVEL
624     FORMAT(' ENERGY OUT OF FILM A IS ',F12.8/
     # ' ENERGY INTO FILM A IS    ',F12.8/
     # ' VELOCITY INTO FILM A IS  ',F12.8)
      STOP
      END
      SUBROUTINE FUNC(D,E)
      REAL D,E
      AA=8.44775449
      AB=2.81568855
      AC=-1.19476235E-1
      AD=4.54142168E-3
      AE=-9.927191178E-5
      AF=1.206508744E-6
      AG=-7.502298397E-9
      AH=1.84746235E-11
      E=AA+AB*D+AC*D**2+AD*D**3+AE*D**4+,
     # AF*D**5+AG*D**6+AH*D**7
      WRITE(6,*)E
      RETURN
      END
      SUBROUTINE FUNCTOO(X,Y)
      REAL X,Y
      CA=7.80278339
      CB=2.27482937
      CC=-5.977592583E-2
      CD=1.66918997E-3
      CE=-2.89068381E-5
      CF=2.97598941E-7
```

```
CG=-1.64517867E-9
CH=3.72161496E-12
Y=CA+CB*X+CC*X**2+CD*X**3+CE*X**4+CF*X**5+CG*X**6+CH*X**7
WRITE(6,*)Y
RETURN
END
```

REFERENCES

1. H. Bequerel, Comp. Rend. 122 (1896) 501.

2. C. T. R. Wilson, Proc. Roy. Soc. A85 (1911) 285.

3. E. Ruthorford, *Radioactive Sustances and their Radiations,* Cambridge University Press, Cambridge, Great Britain (1913).

4. E. Rutherford and W. Geiger, Proc. Roy. Soc. A81 (1908) 141.

5. J. M. McKenzie and D. A. Bromley, Phys. Rev. Lett. 2 (1959) 303.

6. J. M. McKenzie, Nucl. Instrum. and Meth. 162 (1979) 49.

7. W. L. Brown, IRE Trans. Nucl. Sci. NS-8 (1961) 2.

8. J. L. Blankenship and C. J. Borlowski, IRE Trans. Nucl. Sci. NS-8 (1961) 17.

9. G. Charpek, R. Bonclier, T. Bressam, J. Farier and C. Zupancic, Nucl. Instrum. and Meth. 62 (1968) 262.

10. G. Hempel, F. Hopkins and G. Schatz, Nucl. Instrum. and Meth. 131 (1975) 445.

11. H. Selzer, Nucl. Instrum. and Meth. 133 (1976) 409.

12. H. Stelzer, Lecture Notes in Physics 178 (1982) 25.

13. A. Breskin, Nucl. Instrum and Meth. 141 (1977) 505.

14. A. Breskin, R. Chechik and N. Zwang, IEEE Trans. Nucl. Sci. NS-27 (1980) 133.

15. A. Breskin, R. Chechik and N. Zwang, Nucl. Instrum. and Meth. 165 (1979) 125.

16. A. Breskin, Nucl. Instrum. and Meth. 196 (1982) 4.

17. W. E. Stein and R. B. Leachman, Rev. Sci. Instrum. 27 (1956) 1049.

18. J. S. Fraser and J. C. D. Milton, Nucl. Instrum. and Meth. 2 (1958) 275.

19. E. Dietz, R. Bass, A. Reiter, U. Friedland and B. Hubert, Nucl. Instrum and Meth. 97 (1971) 581.

20. W. F. W. Schneider, B. Kohlmeyer and R. Bock, Nucl. Instrum. and Meth. 87 (1970) 253.

21. H. G. Clerc, H. J. Gehrhardt, L. Richter and K. H. Schmidt, Nucl. Instrum. and Meth. 113 (1973) 325.

22. F. Busch, W. Pfeffer, B. Kohlmeyer, D. Schull and F. Puhlhoffer, Nucl. Instrum. and Meth. 171 (1980) 71

23. W. Crookes, Proc. Roy. Soc., A71 (1903) 405.

24. J. B. A. England, *Techniques in Nuclear Structure Physics*, John Wiley and Sons, New York, NY (1972).

25. F. S. Goulding, D. A. Landis, J. Cerny and R. H. Pendl, Nucl. Instrum. and Meth. 31 (1964) 1.

26. F. Bloch, Ann. Physik 16 (1933) 285.

27. J. B. Birks, Proc. Phys. Soc. A64 (1951) 874.

28. F. D. Becchetti, C. E. Thorn and M. J. Levine, Nucl. Instrum. and Meth. 138 (1976) 93.

29. M. L. Muga, G. L. Griffith, H. W. Schmitt and H. E. Taylor, Nucl. Instrum. and Meth. 111 (1973) 581.

30. M. L. Muga, D. J. Burnsed and W. E. Steeger, Nucl. Instrum. and Meth. 83 (1970) 135.

31. Table of Physical Constants, NE Technology, Inc., Edinburgh, Scotland 1990.

32. RCA Products Guide, RCA Corp., Lancaster, PA. 1980.

33. M. L. Muga, D. J. Burnsed and W. E. Steeger, Nucl. Instrum. and Meth. 104 (1972) 605.

34. N. N. Ajitanand and K. N. Iyengar Nucl. Instrum. and Meth., 133 (1976) 71.

35. M. L. Muga, Nucl. Instrum. and Meth. 95 (1971) 349.

36. L. Muga and G. Griffith, Nucl. Instrum. and Meth. 109 (1973) 289.

37. M. L. Muga and J. D. Bridges, Nucl. Instrum. and Meth. 134 (1976) 143.

38. L. Muga and A. Clem, Phys. Rev. C 11 (1975) 1287.

39. L. Muga, A. Clem, G. Griffith, H. S. Plendl, R. Eaker and R. Holub, Nucl. Instrum. and Meth. 119 (1974) 255.

40. R. K. Batra and A. C. Schotter, Nucl. Instrum. and Meth. in Phys. Res. B5 (1984) 14.

41. P. Plischke, W. Scobel and R. Wien, Nucl. Instrum. and Meth. 203 (1982) 419.

42. L. Muga, Nucl. Instrum. and Meth., 124 (1975)541.

43. C. Manduchi, M. T. Russo-Manduchi and G. F. Segato, Nucl. Instrum. and Meth. in Phys. Res. A243 (1986) 453.

44. F. D. Brooks, W. A. Cilliers and M. S. Allie, Nucl. Instrum. and Meth. in Phys. Res. A240 (1985) 338.

45. C. B. Franklyn, Nucl. Instrum. and Meth. in Phys. Res. B35 (1988) 315.

46. L. Muga and G. Griffith, Phys. Rev. B9 (1974) 3639.

47. L. Muga and M. Diksic, Nucl. Instrum. and Meth. 122 (1974) 553.

48. N. N. Ajitanand, Nucl. Instrum. and Meth. 143 (1977) 345.

49. I. Kanno and Y. Nakagome, Nucl. Instrum. and Meth. in Phys. Res. A244 (1986) 551.

50. H. L. Ravn and B. W. Allardyce, *Treatice on Heavy Ion Science*, ed. D. A. Bromley, Plenum Press, New York, N. Y. (1989).

51. H. A. Enge, *Treatice on Heavy Ion Science*, ed. D. A. Bromley, Plenum Press, New York, N. Y. (1985).

52. D. Schull, Lecture Notes in Physics *178* (1985) 80.

53. S. D. Thompson, Master's Thesis (1987) University of Florida.

54. Z. Milosevich, Master's Thesis (1988) University of Florida.

55. H. W. Schmitt, W. E. Kiker and C. W. Williams, Phys. Rev. B4 (1965) 837

56. L. C. Northcliffe and R. F. Schilling, Nucl. Data A7 (1970) 233

57. R. L. Coldwell, Nucl. Instrum. and Meth in Phys. Res. A242 (1986) 455

58. O. Hahn and F. Strassman, Naturwissenschaften 27 (1939) 11.

59. L. Meitner and O. R. Frisch, Nature 143 (1939) 239.

60. S. M. Polikanov, V. A. Druin, V. A. Karnankhov, V. L. Mikheev, A. A. Pleve, N. K. Skobelev, V. G. Subbotin, G. M. Ter-Akopyan and V. A. Fomichev, Sov. Phys. JETP 15 (1962) 1016.

61. V. M. Strutinsky, Nucl. Phys. A95 (1967) 420.

62. W. D. Meyers and W. J. Swiatecki, Nucl. Phys. 81 (1966) 1.

63. R. Vandenbosch and J. R. Huizenga, *Nuclear Fission*, Academic Press, New York, N. Y. (1973).

64. V. M. Strutinsky and H. C. Paul, *Physics and Chemistry of Fission*, IAEA, Vienna (1969)157.

65. L. E. Glendenin and J. P. Unik, Phys. Rev. B 140 (1965) 1301.

66. S. S. Kapoor, H. R. Bowman and S. G. Thompson, Phys. Rev. B 140 (1965) 1310.

67. R. L. Watson, H. R. Bowman and S. G. Thompson, Phys. Rev. 162 (1967) 1169.

68. R. L. Watson, R. C. Jared and S. G. Thompson, Phys. Rev. C 1 (1970) 1866.

69. R. St. Laurent, G. N. Phillips, P. Richard and C. F. Moore, Phys. Rev. C 4 (1971) 1122.

70. E. Chiefetz, J. B. Wilhelmy, R. C. Jared and S. G. Thompson, Phys. Rev. C 4 (1971) 1913.

71. W. John, F. W. Guy andJ. J. Wesolowski, Phys. Rev. C 2 (1970) 1451.

72. F. F. Hopkins, G. W. Phillips, J. R. White, C. F. More and P. Richard, Phys. Rev. C 4 (1971) 1977.

73. H. Warhanek and R. Vandenbosch, J. Inorg. Nucl. Chem. 26 (1964) 669.

74. J. B. Wilhelmy, E. Chiefetz, R. C. Jared, S. G. Thompson, H. R. Bowman and J. O. Rasmussen, Phys. Rev. C 5 (1972) 2041.

75. E. Chiefetz, R. C. Jared, S. G. Thompson and J. B. Wilhelmy, Phys. Rev. Lett. 25 (1970) 38.

76. J. B. Wilhelmy, S. G. Thompson, R. C. Jared and E. Chiefetz, Phys Rev. Lett. 25 (1970) 1122.

77. R. L. Watson, J. B. Wilhelmy, R. C. Jared, C. Rugge, H. R. Bowman, S. G. Thompson and J. O Rasmussen, Nucl. Phys. A141 (1970) 449.

78. G. Mariolopoulos, J. P. Bocquet, R. Brissot, H. Nifeneccker, Ch. Ristori, A. Pequet and J. Girard, Nucl. Instrum. and Meth. 180 (1981) 141.

79. Y. Yoshida, K. Tsuji, F. Toyofuku and A. Katase, Nucl. Instrum. and Meth. 159 (1979) 125.

80. M. M. Hoffman, Phys. Rev. 133 (1964) B714.

81. K. Skarsvag, Phys. Rev. C 22 (1980) 638.

82. K. Skarsvag, Nucl. Phys. A253 (1975) 274.

83. K. Skarsvag, Nucl. Phys. A153 (1970) 82.

84. H. D. Betz, in *Applied Atomic Collision Physics*, Vol. 4, ed. S. Datz, Academic Press, New York, NY (1984).

85. H. F. Batho, Phys. Rev. 42 (1932) 753.

86. W. E. Lamb, Phys. Rev. 58 (1940) 696.

87. N. Bohr, Phys. Rev. 58 (1940) 654.

88. N. Bohr, Phys. Rev. 59 (1941) 270.

89. N. Bohr, K. Dan. Vidensk. Selsk. Mat.-Fys. Medd. 18 No. 8 (1948) 1.

90. J. Knipp and E. Teller, Phys. Rev. 59 (1941) 659.

91. N. O. Lassen, K. Dan. Vidensk. Selsk. Mat.-Fys. Medd. 26 No. 5 (1956) 1.

92. V. S. Nikolaev and I. S. Dmitriev, Phys. Lett. A 28 (1968) 277.

93. A. B. Wittkower and H. D. Betz, Atomic Data 5 (1973) 113.

94. K. Shima, T. Mikumo and H. Tawara, At. Data and Nucl. Data Tables 34 (1986) 357.

95. A. B. Wittkower and H. D. Betz, Phys. Rev. A7 (1973) 159.

96. G. Ryding, A. B. Wittkower and P. H. Rose, Phys Rev. 185 (1969) 129.

97. A. B. Wittkower and G. Ryding, Phys. Rev A 4 (1971) 226.

98. N. Bohr and J. Lindhard, K. Dan. Vidensk. Selsk. Mat.-Fys. Medd. 28 No. 7 (1954) 1.

99. Q. C. Kessel, Case St. At. Phys. 1 (1969) 399

100. L. B. Bridwell, J. A. Biggerstaff, G. D. Alton, C. M. Tines, P. D. Miller, Q. C. Kessel and B. W. Wehing, in *Beam Foil Spectroscopy*, Vol. 2, ed. I. A. Sellin and D. J. Pegg, Plenum Press , New York, NY (1969) 657.

101. P. D. Miller, IEEE Trans. Nucl. Sci. NS-26 (1979) 1111.

102. H. A. Scott, L. B. Bridwell, C. D. Moak, G. D. Alton, C. M. Jones, P. D. Miller, R. O. Sayer and Q. C. Kessel, Nucl. Instrum and Meth. 124 (1975) 607.

103. A. Anton, Phys. Rev. A18 (1978) 2459.

104. E. Baron and B. Delaunay, Phys. Rev. A 12 (1975) 40.

105. B. Rosner, D. Gur, J. Alessi, K. C. Chan and L. Shabason, Phys. Lett. A 57 (1976) 320.

106. B. Rosner and D. Gur, Phys. Rev A 15 (1977)70.

107. M. Meron, D. Maor and B Rosner, Phys. Lett A 74 (1979) 201.

108. M. Meron, D. Maor and B Rosner, J. Phys. B: AT. Molec. Phys. 16 (1983) 3983.

109. D. Maor and B. Rosner, Phys. Lett. A 69 (1978) 100.

110. Q. C. Kessel and B. Fastrup, Case St. At. Phys. 3 (1973) 137.

111. B. Rosner and W. Brandt, Phys. Lett. A 61 (1977) 97.

112. M. Meron and B. Rosner, Phys Rev. A 30 (1984) 132.

113. A. Breskin, I. Tserruga and N. Zwang, Nucl. Instrum. and Meth. 148 (1978) 275.

114. H. Oeschler, J. P. Coffin, P. Engelstein, A. Gallmann, K. S. Sim and P. Wagner, Phys. Rev. C 18 (1978) 239.

115. T. Batsch and M. Moszynski, Nucl. Instrum. and Meth. 123 (1975) 341.

116. J. Barrette, P. Braun-Murzinger, C. K. Gelbke, H. L. Harney, H. E. Wegner and B. Zeidman, Nucl. Phys. A 299 (1977) 199.

117. M. Moszynski and B. Bengston, Nucl. Instrum. and Meth. 158 (1979) 1.

118. C. K. Gelbke, K. D. Hildenbrand and R. Bock, Nucl. Instrum. and Meth. 95 (1971) 397.

119. R. B. Piercey, P. Agnvall, D. Ely, J. E. McKisson, A. Weisenberger, S. Majewski, Z. Milosevich, M. L. Muga and A. V. Ramayya, IEEE Trans. Nucl. Sci. 37 (1990) 148.

120. J. B. Birks, Theory and Practice of Scintillation Counting, Pergamon Press, Oxford (1964).

121. M. K. Rowen, Master's Thesis (1988) Univesity of Florida.

122. C. Zorn, IEEE Trans. Nucl. Sci. 37 (1990) 504.

BIOGRAPHICAL SKETCH

The author was born in a small village in southeastern Wisconsin called Milwaukee. He graduated from high school in an even smaller village called South Milwaukee and then proceeded on to college. He received a Bachelor's degree from the University of Wisconsin located in Madison. He then chose to leave for graduate school, where he further pursued his studies at the University of Florida. He plans on one day becoming a sumo wrestler.

I certify that I have read this study and that in my opinion it conforms to acceptable standards of scholarly presentation and is fully adequate, in scope and quality, as a dissertation for the degree of Doctor of Philosophy.

M. Luis Muga

M. Luis Muga, Chairman
Professor of Chemistry

I certify that I have read this study and that in my opinion it conforms to acceptable standards of scholarly presentation and is fully adequate, in scope and quality, as a dissertation for the degree of Doctor of Philosophy.

Robert J. Hanrahan

Robert J. Hanrahan
Professor of Chemistry

I certify that I have read this study and that in my opinion it conforms to acceptable standards of scholarly presentation and is fully adequate, in scope and quality, as a dissertation for the degree of Doctor of Philosophy.

Willis B. Person

Willis B. Person
Professor of Chemistry

I certify that I have read this study and that in my opinion it conforms to acceptable standards of scholarly presentation and is fully adequate, in scope and quality, as a dissertation for the degree of Doctor of Philosophy.

F. E. Dunnam

F. Eugene Dunnam
Professor of Physics

I certify that I have read this study and that in my opinion it conforms to acceptable standards of scholarly presentation and is fully adequate, in scope and quality, as a dissertation for the degree of Doctor of Philosophy.

Robert L. Coldwell

Robert L. Coldwell
Associate Professor of Physics

I certify that I have read this study and that in my opinion it conforms to acceptable standards of scholarly presentation and is fully adequate, in scope and quality, as a dissertation for the degree of Doctor of Philosophy.

Z. R. Pop

Zoran R. Pop Stojanovic
Professor of Mathematics

This dissertation was submitted to the Graduate Faculty of the Departmant of Chemistry in the College of Liberal Arts and Sciences and to the Graduate School and was accepted as partial fulfillment of the requirements for the degree of Doctor of Philosophy.

May 1991

Dean, Graduate School